

Regulation and function of Retinol Saturase in brown adipose tissue and thermogenesis

Inaugural-Dissertation

to obtain the academic degree

Doctor rerum naturalium (Dr. rer. nat)

Submitted to the

Department of Biology, Chemistry, Pharmacy

of

Freie Universität Berlin

by

Chen Li

2023

The present doctoral study was carried out from September 2018 to August 2023 at the Institute of Pharmacology at Charité - Universitätsmedizin Berlin under the supervision of Prof. Dr. rer. nat. Michael Schupp.

1st reviewer: Prof. Dr. rer. nat. Michael Schupp

2nd reviewer: Prof. Dr. rer. nat. Nan Ma

Date of defense: March 5th, 2024

Declaration of Independence

Herewith I certify that I have prepared and written my thesis independently and that I have not used any sources and aids other than those indicated by me.

Berlin, November 17, 2023

Table of Contents

Abbreviations	1
Abstract	6
Kurzzusammenfassung	7
1 Introduction	8
1.1 The discovery of RetSat and its catalytic function	8
1.2 Prior findings of RetSat in adipose tissue	8
1.3 Brown, beige, and white adipocytes	10
1.4 The discovery of brown adipose tissue	13
1.5 UCP1-dependent thermogenesis	14
1.6 Pharmacological approaches of brown adipose tissue activation/ recruitment and white adipose tissue browning	17
1.6.1 β 3-adrenergic receptor agonists	17
1.6.2 Thiazolidinediones	19
1.6.3 Retinoids	19
1.7 The regulation of brown adipose tissue in metabolic syndrome	20
1.8 Aim of this project	22
2 Chemicals, reagents, kits	23
2.1 Chemicals and reagents	23
2.2 Buffers and solutions	27
2.3 Kits	29
2.4 Antibodies	29
2.5 Oligonucleotides	30
2.5.1 Primers for real-time quantitative polymerase chain reaction	30
2.5.2 Silencing RNA oligonucleotides	31
2.5.3 Primers for mouse genotyping	32
2.6 Mouse diets	32
2.7 Equipments	33
2.8 Consumables	33
3 Methods	35
3.1 iBACs and 3T3-L1 cell line and culturing	35
3.1.1 Cell passaging	35
3.1.2 Cell thawing	35
3.1.3 Cell cryopreservation	36
3.1.4 Preadipocyte differentiation	36
3.2 Adipose-derived stromal vascular fraction cells isolation	37

3.3 Transfection.....	38
3.3.1 RNA interference mediated gene silencing	38
3.3.1.1 Electroporation	38
3.3.1.2 Lipofection.....	38
3.3.2 Virus transfection.....	39
3.3.2.1 Retrovirus transfection	39
3.3.2.2 Adenovirus transfection	39
3.4 Oil red O staining.....	40
3.5 Seahorse mitochondria stress test	40
3.6 <i>In vivo</i> model and experiments.....	42
3.6.1 Animals housing	42
3.6.2 BAT-specific RetSat knockout mouse model establishment.....	42
3.6.3 BAT-specific RetSat knockout mouse model genotyping	44
3.6.3.1 Genomic DNA isolation.....	44
3.6.3.2 Polymerase chain reaction	45
3.6.3.3 Agarose gel electrophoresis	45
3.6.4 Mice sacrifice and sample collection.....	46
3.6.5 Metabolism phenotype characterization	46
3.6.5.1 Diet challenge, weekly body weight and body composition.....	46
3.6.5.2 Tolerance test.....	46
3.6.5.3 β 3-adrenergic receptor agonist injection.....	46
3.6.5.4 Acute cold exposure	47
3.6.6 Histology	47
3.6.6.1 Tissue fixation, embedding, and sectioning	47
3.6.6.2 Deparaffinization and hematoxylin-eosin staining	47
3.7 Real-time quantitative polymerase chain reaction (RT-qPCR)	47
3.7.1 RNA extraction	48
3.7.1.1 Adipocyte RNA extraction	48
3.7.1.2 Adipose tissue RNA extraction.....	48
3.7.2 cDNA synthesis	48
3.7.3 RT-qPCR process	49
3.8 Immunoblotting.....	50
3.8.1 Protein extraction	50
3.8.1.1 Protein extraction from cultured cells.....	50
3.8.1.2 Protein extraction from frozen tissue	50
3.8.2 Total protein quantification.....	51
3.8.3 Semi-quantitative analysis of immunoblotting signals	51

3.9 RNA-Sequencing.....	52
3.9.1 RNA concentration and purification	52
3.9.2 Sequencing and data analysis.....	53
3.10 Statistics.....	53
4 Results	54
4.1 RetSat is highly expressed in brown adipose tissue	54
4.2 RetSat is induced by β -adrenergic stimulation.....	55
4.3 RetSat is up-regulated during brown adipocyte differentiation	56
4.4 RetSat depletion does not impair brown adipocyte differentiation	57
4.5 RetSat over-expression slightly enhances brown adipocyte differentiation .	58
4.6 RetSat is required for the thermogenic gene expression in immortalized brown adipocytes.....	59
4.7 RetSat is required for thermogenesis gene expression in primary brown adipocytes.....	61
4.8 RetSat ablation reduces mitochondrial respiration in primary brown adipocytes	62
4.9 RetSat is required for 3T3-L1 adipocytes browning	63
4.10 RetSat depletion reduces mitochondrial respiration in 3T3-L1 adipocytes	64
4.11 BAT-specific RetSat deletion mouse model construction and validation....	65
4.12 RetSat deletion in brown adipose tissue of mice impairs acute cold tolerance	66
4.13 RetSat deletion in brown adipose tissue of mice does not promote diet-induced obesity	68
4.14 BAT-specific RetSat deletion mice had slightly weakened glucose disposal capacity.....	69
4.15 RetSat deletion in BAT downregulates mitochondrially encoded and protein-folding associated genes	70
5 Discussion.....	71
5.1 RetSat is highly expressed in adipose tissue and stimulated by β -AR activation	71
5.2 Dynamic expression of RetSat and its action in brown adipocyte differentiation	71
5.3 RetSat is required for thermogenesis gene expression in brown adipocytes and white adipocyte browning	72
5.4 Loss of RetSat function reduces mitochondrial respiration in adipocytes....	72
5.5 The effect of RetSat BAT depletion on metabolic profile of mice	73
5.6 RetSat is necessary for core body temperature maintenance upon acute cold	

exposure	74
5.7 Potential mechanism of RetSat in BAT upon transcriptome analysis	75
Reference.....	76
List of Figures	95
List of Tables	97
Acknowledgement.....	98

Abbreviations

18F-FDG PET-CT	18F-fluorodeoxyglucose positron emission tomography-computed tomography
ADP	adenosine di-phosphate
Adrb3	β 3-adrenergic receptor
ALDH1A1	aldehyde dehydrogenase 1 family member a1
ANOVA	analysis of variance
aP2	adipocyte protein 2
APS	ammonium persulfate
ATGL	adipose triglyceride lipase
ATP	adenosine tri-phosphate
BAT	brown adipose tissue
BCA	bicinchoninic acid assay
BLAST	Basic Local Alignment Search Tool
BMI	body mass index
BP	biological process
BSA	bovine serum albumin
C/EBP	CCAAT/enhancer binding protein
CaCl ₂	calcium chloride
cAMP	cyclic adenosine monophosphate
cDNA	complementary DNA
ChREBP	carbohydrate response element binding protein
Cidea	cell death-inducing DNA fragmentation factor α -like effector A
CNS	central nervous system
Co Q	coenzyme Q

CREB	cAMP response element binding protein
Cyt C	cytochrome c
DAPI	4',6-diamidino-2-phenylindole
ddH2O	double distilled water
DIT	Diet induced thermogenesis
DMEM	dulbecco's modified eagle medium
DMSO	dimethyl sulfoxide
DNA	deoxyribonucleic acid
ECL	enhanced chemiluminescence
EDTA	ethylenediaminetetraacetic acid
ER	endoplasmic reticulum
ETC	electron transport chain
eWAT	epididymal white adipose tissue
FADH2	flavin adenine dinucleotide
FBS	fetal bovine serum
FCCP	trifluoromethoxy carbonylcyanide phenylhydrazone
FDR	false discovery rate
GDP	guanosine diphosphate
GFP	green fluorescent protein
GLUT1	glucose transporter 1
GO	Gene Ontology
Gs	G proteins
GTP	guanosine triphosphate
H&E	hematoxylin & eosin
H2O2	hydrogen peroxide
HEPES	4-(2-hydroxyethyl)-1- piperazineethanesulfonic acid
HFD	high-fat diet

HRP	horseradish peroxidase
HSL	hormone-sensitive lipase
iBACs	immortalized brown adipogenic cells
IBMX	3-isobutyl-1-methylxanthine
ingWAT	inguinal white adipose tissue
ipGTT	intraperitoneal glucose tolerance test
ipITT	intraperitoneal insulin tolerance test
KCl	potassium chloride
KEGG	Kyoto Encyclopedia of Genes and Genomes
KH ₂ PO ₄	potassium dihydrogen phosphate
MAMs	mitochondria-associated membranes
MgSO ₄	magnesium sulfate
mRNA	messenger ribonucleic acid
Myf5	myogenic factor 5
NaCl	sodium chloride
NADH	nicotinamide adenine dinucleotide
NaF	sodium fluoride
NaOH	sodium hydroxide
NCBI	National Center for Biotechnology Information
NE	norepinephrine
NEFA	non-esterified fatty acid
NMR	nuclear magnetic resonance
OCR	oxygen consumption rate
OH-	hydroxyl ions
OXPHOS	oxidative phosphorylation
P/S	penicillin/streptomycin
p38MAPK	p38 mitogen-activated protein kinases

PBS	phosphate-buffered saline
PCR	polymerase chain reaction
pgWAT	perigonadal white adipose tissue
Pi	inorganic phosphate
PKA	protein kinase A
PPAR γ	peroxisome proliferator-activated receptor γ
PRDM16	PR domain containing 16
PVDF	polyvinylidene fluoride
RAN	ras-related nuclear protein
RAR	retinoic acid receptor
RetSat	retinol saturase
RBP4	retinol binding protein 4
RNA	ribonucleic acid
RNase A	ribonuclease A
ROS	reactive oxygen species
RT-qPCR	real-time quantitative polymerase chain reaction
RXR	retinoid X receptor
scRNA-seq	single-cell RNA sequencing
scWAT	subcutaneous white adipose tissue
SDS	sodium dodecyl sulfate
SDS-PAGE	sodium dodecyl sulphate-polyacrylamide gel electrophoresis
sem	standard error of the mean
siRNA	small interfering ribonucleic acid
SNS	sympathetic nervous system
SPF	specific pathogen free
SVF	stromal vascular fraction
T2DM	type 2 diabetes mellitus

T3	3,3',5-Triiod-L-thyronin
TAE	tris acetate EDTA
TCA	tricarboxylic acid
TCA cycle	tricarboxylic acid cycle
TEMED	tetramethyl ethylenediamine
Tris Base	hydroxymethyl aminomethane
Tris HCL	hydroxymethyl aminomethane hydrochloride
TZDs	thiazolidinediones
Ucp1	uncoupling protein 1
upH2O	ultrapure distilled water
UPR	unfolded protein response
UV	ultraviolet
WAT	white adipose tissue
WHO	world health organization
WT	wildtype
β 3-AR	β 3-adrenergic receptor
β A	β -adrenergic receptor agonist

Abstract

Background and objective: Retinol Saturase (RetSat) is an oxidoreductase that was named after its initially identified enzymatic reaction, and is expressed in multiple metabolic organs, especially liver and adipose tissue. In the past decade, brown adipose tissue (BAT) activation and white adipose tissue (WAT) browning have been considered promising approaches to combat metabolic syndrome. In this project, the function of RetSat in thermogenetic fat was investigated.

Method: Since RETSAT protein is strongly induced in the BAT of cold-exposed mice, firstly, the regulation of RetSat in adipose tissue and adipocyte by β -adrenergic receptor stimulation was studied. The RetSat gain and loss of function studies in preadipocytes were conducted to explore its effect on brown adipocyte differentiation. Furthermore, RetSat was depleted in adipocytes to study its effect on thermogenetic gene expression, and mitochondria function was monitored by Seahorse assay. Subsequently, the BAT-specific RetSat deletion mouse model was established by the Cre/LoxP system, and subjected to diet (normal chow and high-fat diet) challenges, and tolerance (glucose, insulin, and cold exposure) tests to study its effect on metabolic profile. Finally, RNA sequencing was employed to explore the potential mechanism.

Results: RetSat expression in adipose tissue and adipocytes was induced by β -adrenergic receptor stimulation. Moreover, RetSat slightly enhanced brown adipocyte differentiation, and was required for thermogenic gene expression in adipocytes, UCP1 induction, and mitochondrial respiration. RetSat deletion in BAT did not alter adiposity, but slightly weakened glucose disposal capacity in mice fed high-fat diet, and impaired cold tolerance upon acute cold exposure. The transcriptome data indicated RetSat down-regulated mitochondrially encoded and protein-folding genes in murine BAT.

Conclusion: RetSat modulates thermogenic capacity of adipocytes and might provide a therapeutic intervention for metabolic disease.

Kurzzusammenfassung

Hintergrund und Ziel: Retinol-Saturase (RetSat) ist eine oxidoreduktase, die nach ihrer ursprünglich identifizierten enzymatischen reaktion benannt wurde und in mehreren stoffwechselorganen, insbesondere in der leber und im fettgewebe, vorkommt. In den vergangenen jahrzehnten galten die aktivierung des braunen Fettgewebes (BAT) und die bräunung des weißen fettgewebes (WAT) als vielversprechende ansätze zur bekämpfung des metabolischen syndroms. In diesem projekt wurde die funktion von RetSat im thermogenetischem fett untersucht.

Methode: Da das RETSAT protein im BAT von kälteexponierten mäusen stark induziert wird, wurde zunächst die regulation von RetSat im fettgewebe und in adipozyten durch stimulation des β -adrenergen rezeptors untersucht. Die studien über den gewinn und verlust der funktion von RetSat in präadipozyten wurden durchgeführt, um seine wirkung auf die differenzierung der braunen adipozyten zu untersuchen. Darüber hinaus wurde RetSat in adipozyten dezimiert, um seine wirkung auf die thermogenetische genexpression zu untersuchen, und die mitochondrienfunktion wurde mittels Seahorse assay überwacht. Anschließend wurde das BAT spezifische RetSat deletions mausmodell durch das Cre/LoxP-System erstellt und einer diät-herausforderungen (normales futter und fettreiche ernährung) sowie toleranztests (glukose, insulin und kälteexposition) unterzogen, um die auswirkungen auf das metabolische profil zu untersuchen. Schließlich wurde eine RNA-sequenzierung eingesetzt, um den möglichen mechanismus zu untersuchen.

Ergebnisse: Die expression von RetSat in fettgewebe und adipozyten wurde durch stimulation des β -adrenergen rezeptors induziert. Darüber hinaus verstärkte RetSat leicht die differenzierung der braunen adipozyten und war für die thermogene genexpression in adipozyten, die UCP1 induktion und die mitochondriale atmung erforderlich. Die RetSat deletion in BAT veränderte die adipositas nicht, schwächte jedoch die glukoseverwertungskapazität von mäusen, die fettreiche nahrung erhielten, leicht und beeinträchtigte die kältetoleranz bei akuter kälteexposition. Die transkriptomdaten zeigten, dass RetSat mitochondrial kodierte und proteinfaltende gene in der BAT der maus herunterreguliert.

Schlussfolgerung: RetSat moduliert die thermogene kapazität von adipozyten und könnte eine therapeutische intervention bei stoffwechselerkrankungen darstellen.

1 Introduction

1.1 The discovery of RetSat and its catalytic function

Retinol Saturase (RetSat) was initially discovered in carotenoid and retinoid metabolism of vertebrates (1). The protein RETSAT was named after its catalytic activity that converts all-*trans* retinol into all-*trans*-13, 14-dihydro retinol by double bond saturation (**Figure 1**) (1, 2).

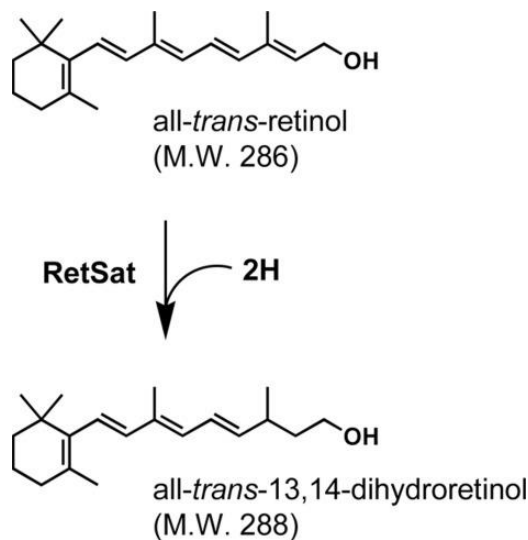


Figure 1. RetSat catalyzed saturation reaction of 13, 14 double bond of all-*trans* retinol. Figure is from (1).

1.2 Prior findings of RetSat in adipose tissue

Given the online mRNA expression profile database BioGPS (3), RetSat has the strongest expression in human adipose tissue, and in mice, it takes the second highest expression just behind the liver. Moreover, RetSat is gradually up-regulated during the murine 3T3-L1 white adipocyte differentiation, similarly, strongly expressed in human adipocytes compared to preadipocytes (4). RetSat in white adipocytes is regulated by peroxisome proliferator-activated receptor γ (PPAR γ), that is, its expression is induced by PPAR γ agonist and suppressed by antagonist (4). Furthermore, PPAR γ depletion results in decreased RetSat expression in adipocytes (4).

As shown in the **top panel of Figure 2**, apart from dynamical expression, RetSat depletion in 3T3-L1 preadipocytes severely impaired the differentiation, and the supply

of PPAR γ agonist but not all-*trans*-13,14-dihydro retinol can rescue this defect (4). Moreover, over-expressed RetSat in preadipocytes enhanced the differentiation and PPAR γ transcriptional level, however, all-*trans*-13, 14-dihydroretinol was undetectable in these adipocytes (4), implying the function of RetSat in 3T3-L1 adipocyte differentiation is independent of 13, 14 dihydro retinol formation. Additionally, RetSat knockdown in 3T3-L1 mature adipocytes did not convert the morphology of cells and even did not effect gene expression of major metabolic pathways (4).

In vivo, RetSat expression is down-regulated in the epididymal white adipose tissue (eWAT) of diet-induced and genetically obese mice, and it is also decreased in the subcutaneous white adipose tissue (scWAT) from obese humans relative to leans. The adipose tissue dysfunction and reduced PPAR γ activity resulting from the infiltration of inflammatory cells may account for this downregulation (4).

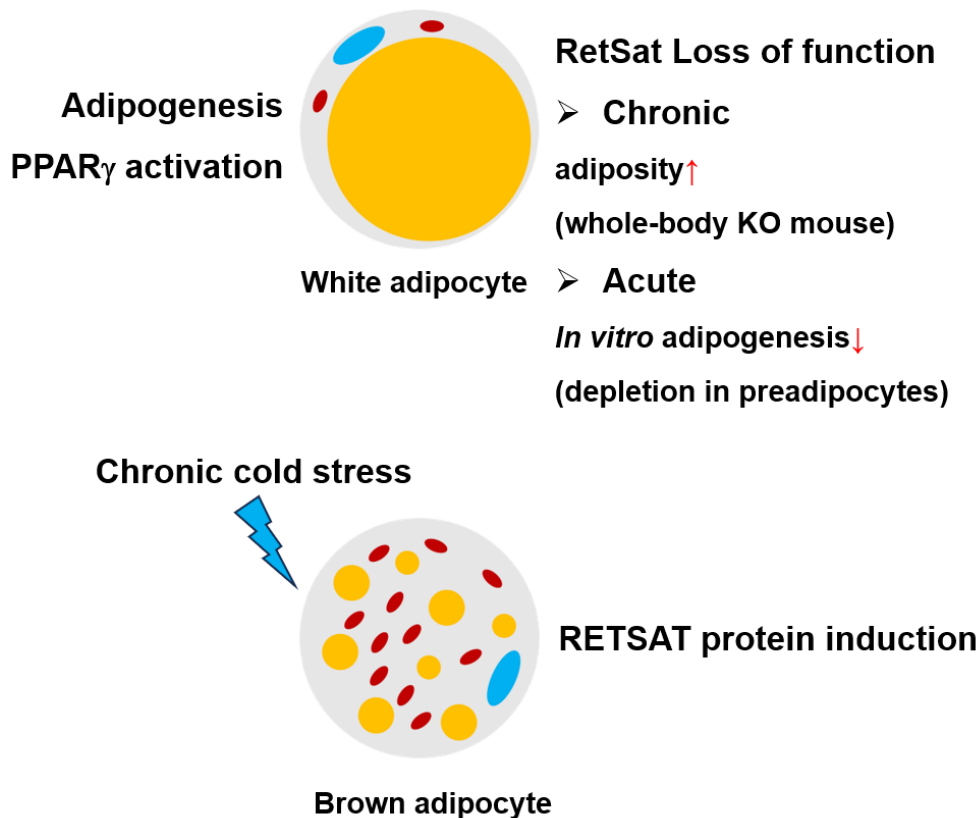


Figure 2. Regulation of RetSat expression and effect of RetSat in adipocytes. In white adipocytes, PPAR γ activation induced RetSat expression. The whole-body RetSat knockout mice had slightly increased adiposity, however, RetSat depletion in white preadipocytes caused impaired adipogenesis, as depicted on the top panel. RETSAT protein was induced in brown adipose tissue (BAT) of chronic cold-exposed

mice, as depicted on the bottom panel. Figure is adapted from (5).

RetSat whole-body knockout mice showed similar food intakes but significantly higher body weight gain upon either normal chow or high-fat diet (HFD) compared to wildtype (WT) mice (6, 7). Furthermore, RetSat-deficiency mice had intact adipose tissue but increased adiposity upon HFD (**Figure 2, top panel**), especially the volume of visceral and inguinal adipose tissue, which can account for increased body weight gain and enhanced *PPAR γ* and Adipocyte protein 2 (*aP2*) expression (8). Histological analysis revealed RetSat whole-body knockout mice have unaltered adipocyte morphology which is in line with the unvaried adipose tissue, verifying the no effect of RetSat on adipocyte differentiation *in vivo* (8). Upon feeding normal chow, RetSat whole-body knockout mice also displayed comparable glucose disposal capacity and insulin sensitivity (8), implicating the role of RetSat in systemic metabolism. However, the more specific tissue or cell-type RetSat knockout mouse model is required to verify the regulation of RetSat in white adipose tissue (WAT).

RETSAT protein in the brown adipose tissue (BAT) of mice was profoundly inducible by cold exposure in the recent mass spectrometry work (**Figure 2, bottom panel**) (9). More importantly, its timely induction was comparable to some thermogenic regulators, especially uncoupling protein 1 (UCP1).

1.3 Brown, beige, and white adipocytes

Adipose tissue is a multifaceted organ and characterized by heterogeneity and plasticity (10). Typically, adipose tissues are classified by white, brown, and beige (also called brite) adipose tissue, and are named by their colors (11). The characteristics of three types of adipocytes are listed in **Table 1**. WAT is the most predominant type of fat in mammals, which is mainly located in subcutaneous and visceral depots with cushioning ability (12). Classical BAT is contained in the interscapular fat depot of mice. While, in humans, BAT scatters the back and neck in newborns and the neck and supraclavicular area in adults (13). Beige adipose tissue is appreciated as an atypical type of thermogenic fat, derived from WAT that received prolongedly external stimulus (14). Metabolically, WAT primarily acts as a site of energy storage in the form of triglycerides. BAT dominantly specializes in energy consumption via non-shivering thermogenesis. Beige adipose tissue dynamically appears and contributes to adaptive thermogenesis. As shown in **Figure 3**, morphologically, white adipocytes contain abundant unilocular lipid droplets and low mitochondria density. Brown adipocytes hold

plenty of mitochondria and small multilocular lipid droplets. Beige adipocytes have fewer mitochondria than brown adipocytes and smaller lipid droplets than white adipocytes. The origin and fate of adipocytes are elucidated by the *in vivo* lineage tracing study among adipose tissues, for instance, classical brown adipocytes in the specialized BAT depots originate from a subpopulation of progenitors with Myogenic factor 5 (Myf5) positive expression, whereas white adipocytes arise from other progenitors with Myf5 negative expression (15). Consistently, earlier transcriptome study indicated that Myf5 expresses uniquely in brown preadipocytes and muscle cells, rather than white preadipocytes (16).

In addition to mature adipocytes, BAT and WAT also harbor diversified cell populations including adipogenic progenitor cells, stem cells, immune cells, endothelial cells, and fibroblasts (17). The specific modifications throughout development might generate distinct cell types with unique expression profiles, even within a given cell population (18). The complicated composition of adipose tissue and heterogeneity of brown adipocytes have been further revealed via single-cell RNA sequencing (scRNA-seq) in recent years. An adipocyte subpopulation with evidently lower UCP1 and Adipoq expression was defined within the mouse BAT, of which morphology and properties are more like white adipocytes, coexisting with the classical high-thermogenic brown adipocytes (19). More interestingly, the interconversion of low- and high- thermogenic brown adipocytes are derived by the temperature of the ambient environment (19). Another rare adipocyte subpopulation was identified to modulate the neighborhood adipocytes activity via acetate signaling in mice and humans, and the abundance is increased by thermoneutral condition (~30°C) in mice (20).

BAT is a highly plastic organ and is remodeled by various conditions in metabolism (21). Cold exposure and β 3-adrenergic stimulants are general approaches to induce thermogenesis, which will be discussed in the following sections. The phenomenon of heat production and increased energy expenditure after eating is referred to as diet-induced thermogenesis (DIT) (22), and the recruitment of DIT is entirely UCP1-dependent in mice at thermoneutrality (23, 24). The moderate-to-vigorous-intensity physical activities are recommended to prevent or treat metabolic syndrome, however, treadmill exercise studies do not affect BAT activity or UCP1 expression (25). Independent from its role in BAT, exercise results in the adaptation of WAT and inducing browning, particularly in inguinal WAT (ingWAT) (26).

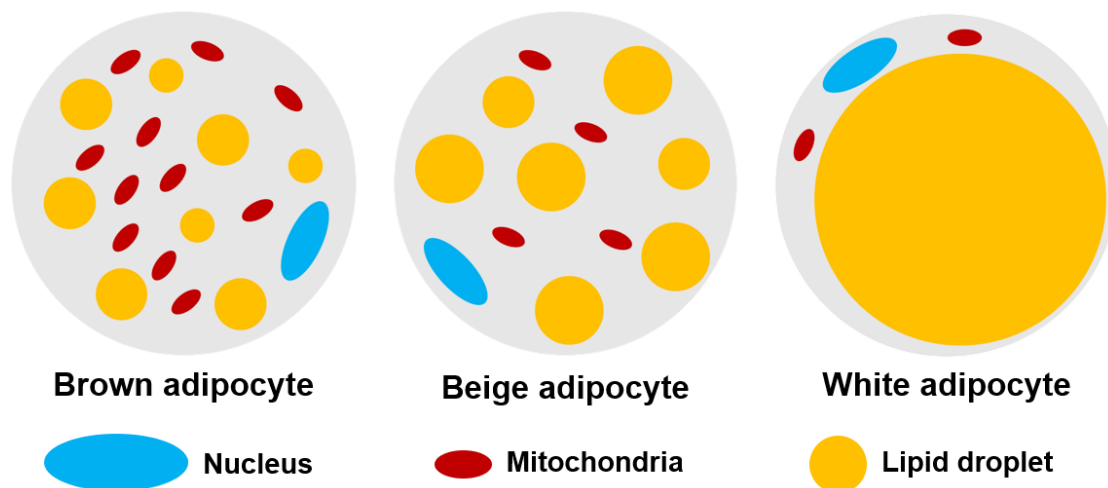


Figure 3. The morphology comparison of brown adipocyte, beige adipocyte, and white adipocyte.

Table 1. Comparison of features among classical brown, white, and beige adipocytes

Property	Classical brown adipocytes	Beige adipocytes	Classical white adipocytes
origin	Myf5+	Myf5-	Myf5-
primary function	energy expenditure	adaptive thermogenesis	excess energy storage
morphology	elliptical and smaller than white	spherical	spherical
mitochondria density	abundant	present upon stimulation	low
lipid droplet morphology	multilocular	paucilocular	unilocular
lipid content	high	high	very high
UCP1 expression	strong	detectable upon stimulation	almost undetectable
location	located in BAT depots	located in WAT depots	located in WAT depots

On the other hand, some factors lead to BAT involution and white-like appearance. The reduced substrate oxidative capacity and increased lipid accumulation are found

in the BAT at thermoneutrality where basal metabolism is sufficient to maintain body temperature (27). The thermoneutral zone for humans and mice is 22°C and 30°C, respectively, most humans spend most of their time in thermoneutral or near-thermoneutral environments (28), which is a chronic exposure factor to promote metabolic diseases. BAT involution is derived by endogenous fatty acid synthesis rather than dietary fatty acids, Carbohydrate response element binding protein (ChREBP) deficiency during thermoneutral adaptation defends mitochondria degradation and BAT loss of function (29). The thermogenic activity of BAT declines during aging, with the features of atrophy morphology and reduced UCP1 expression (30). The examination of BAT and brain activity in young and elderly men after cold exposure indicated lower brain activity in older subjects might partially cause reduced BAT activity (31). In mice, aging decreases the content of β -adrenergic receptor (β -AR) (32) and mitochondrial β -oxidation (33) in BAT.

Obesity contributes to BAT whitening, smaller BAT mass is found in obese humans (34). BAT is a highly vascularized organ, and obesity causes capillary rarefaction and functional hypoxia in BAT, with mitochondria dysfunction and lipid droplet accumulation (35). The obesogenic diet promotes glyceroneogenesis and triacylglycerol synthesis in brown adipocytes through disturbing substrate oxidation and enhancing fatty acid esterification (36).

1.4 The discovery of brown adipose tissue

BAT was initially discovered in hibernating animals, termed as the hibernating gland that adapts to cold environments (37). In the early 20th century, BAT was also found in non-hibernating mammals, especially the neck and scapular regions of human infants (38). Owe to the lack of sufficient skeletal muscle, infants maintain core body temperature by BAT non-shivering thermogenesis (39, 40). The cold-exposed humans were thought to generate heat via shivering thermogenesis, BAT was considered to be of negligible physiologic relevance in adult humans until a series of radiography studies in 2009 (41). The ¹⁸F-fluorodeoxyglucose positron emission tomography-computed tomography (¹⁸F-FDG PET-CT) was employed to identify the functional BAT in adult humans during cold exposure (42). Moreover, metabolically active human BAT has significant negative correlations with body mass index (BMI), fat mass, age, and ambient temperature. Additionally, thermogenesis makers express substantial levels in BAT (43, 44). These reports collectively reveal the importance of BAT in adult

humans.

1.5 UCP1-dependent thermogenesis

According to the well-investigated pathway, the preoptic area of the hypothalamus in the central nervous system (CNS) of endothermy receives the stimuli via cutaneous thermal receptors. Afterward, the norepinephrine controlled by the sympathetic nervous system (SNS) is released from the adrenal medulla to the circulation system (45). As shown in **Figure 4**, upon activation by catecholamine, β -AR on the plasma membrane of brown adipocytes, couple stimulatory G protein (Gs) increasing cyclic adenosine monophosphate (cAMP) level via adenylyl cyclase (46). Subsequently, cAMP binds to protein kinase A (PKA) and thus promotes phosphorylation of lipase, including adipose triglyceride lipase (ATGL), hormone-sensitive lipase (HSL), and Perilipin, mobilizing lipid to provide the substrates for catabolism (47).

Upon the β -adrenergic signaling cascade, PKA phosphorylation leads to UCP1 activation via numerous transcription factors. The CCAAT/enhancer binding protein (C/EBP) and cAMP response element binding protein (CREB) are implicated in the canonical means of triggering UCP1 transcription in brown adipocytes. PKA phosphorylation promotes the translocation of C/EBPs and CREB from the cytoplasm to the nucleus, binding to genomic sites near the *Ucp1* gene (48).

It is widely accepted that UCP1 is inactivated upon the basal state of brown adipocytes, due to exposure to cytosolic purine nucleotides including guanosine triphosphate (GTP), guanosine diphosphate (GDP), adenosine di-phosphate (ADP), and adenosine tri-phosphate (ATP), thus the heat produced by the non-shivering thermogenesis is blocked (49). Apart from oxidation to provide chemical energy, fatty acids, predominantly long-chain fatty acids, are thought to unlock the inhibition of UCP1 (50). Free fatty acids derived from lipolysis appear to occupy the binding site of UCP1 in a competitive manner with purine nucleotide (51). The interaction of purine nucleotides with fatty acids remains further revealed, and the inhibitory effect of purine nucleotides is associated with calcium complex formation, enzymatic nucleotide degradation, and pH (52). On the other hand, adrenergic stimulation results in not merely a decrease in di- and triphosphate purine nucleotides in brown adipocytes, but a smaller total purine nucleotide pool size cellularly (53).

The mitochondrion is a type of membrane-bound cell organelle, that provides

organisms with chemical energy stored in ATP (54). In eukaryotes, ATP synthesis is driven by oxidative phosphorylation (OXPHOS) conducted through the electron transport chain (ETC), which is composed of NADH dehydrogenase (complex I), succinate dehydrogenase (complex II), Cytochrome c reductase (complex III), Cytochrome c oxidase (complex IV), Coenzyme Q (CoQ) and Cytochrome C (Cyt C) (55). The chemiosmotic hypothesis theorized by Peter D. Mitchell accounts for the coupling of electron transportation and ADP phosphorylation in the inner membrane of mitochondria (56). The nutritional substrates (mainly fatty acids and carbohydrates) are oxidized in some catabolic cellular processes, including tricarboxylic acid cycle (TCA cycle), β -oxidation, and glycolysis, to generate energy-rich hydrogen carriers nicotinamide adenine dinucleotide (NADH) and flavin adenine dinucleotide (FADH₂). The electrons are donated by NADH and FADH₂ at either NADH dehydrogenase or succinate dehydrogenase, where succinate is oxidized to fumarate. The protons are pumped by the free energy released during catabolism from the mitochondria matrix out to intermembrane space via complex I, III, and IV, as not enough energy gets released from the redox reaction on complex II (57). Additionally, the oxygen atom is the terminal carrier of electrons and binds with hydrogen ions to produce H₂O via complex IV, this oxygen-consuming process is termed mitochondrial respiration (58).

The electrical potential (increased positively charged hydrogen ions) and chemical potential (decreased pH) outside of the inner membrane transform to proton motive force to promote proton backflow to the matrix via ATP synthase and drive the binding of ADP and inorganic phosphate (Pi) to produce ATP (59).

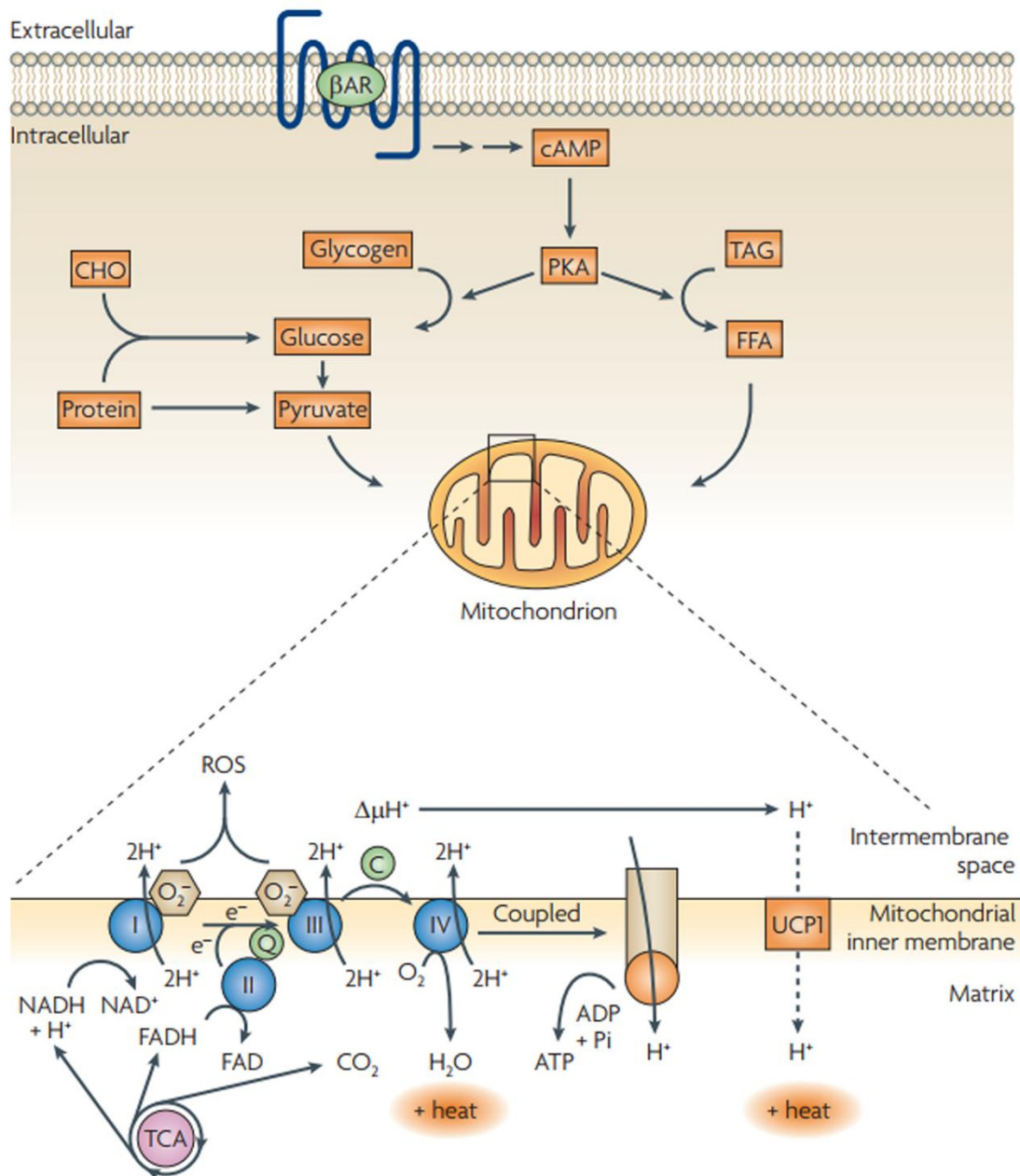


Figure 4. UCP1-mediated uncoupling in mitochondria of brown adipocytes. Briefly, the stimulation of β -adrenergic receptors on brown adipocytes triggers a series of signal transduction cascades, the increased cAMP level stimulates PKA activity, and subsequently, the activated multiple enzymes convert nutritional macromolecules to small molecules that enter into mitochondria as fuel. The protons generated by the TCA cycle are pumped into mitochondrial intermembrane space by ETC complexes to form the electrochemical gradient which is used to synthesize ATP. The protons can go back to the mitochondrial matrix through UCP1, and heat is generated during this process. The details are described in the text. Figure is from (60).

Oligomycin A is a specific ATP synthase inhibitor, however, the electron flow is not absolutely blocked because of a phenomenon termed proton leak, which refers to protons returning back to the mitochondria matrix independent of ATP synthase (61). UCP1 serves as this parallel channel located in the mitochondrial inner membrane, thereby, the proton gradient is dissipated partially and the coupling of mitochondrial respiration and ATP synthesis is not completed (62). As a consequence, the spare energy generated by substrate oxidation is released by mitochondria as heat. Pharmacologically, Trifluoromethoxy carbonylcyanide phenylhydrazone (FCCP) is a proton carrier promoting the electron flow, thus oxygen consumption reaches the maximum (63). Rotenone and Antimycin A bind to complex I and III respectively to disrupt the whole ETC and inhibit oxidative phosphorylation (64, 65). Oligomycin A, FCCP, Rotenone, and Antimycin A are widely applied for cellular respiration study.

Oxidative stress results from excessive oxygen reactive species (ROS) accumulation, but inadequate antioxidants to get rid of them, leading to cell death or tissue damage (66). Mitochondrial ROS is generated during oxidative phosphorylation under physiological conditions in humans, as a byproduct of ATP synthesis inevitably. In return, ROS is harmful to ATP synthase and impairs mitochondrial energy production (67). During the course of electron transport, some unpaired electrons react with oxygen to form superoxide ion ($O_2^{\bullet-}$) at complex I and complex III, this process is termed as electron leak (68). Other unstable molecules include hydroxyl ions (OH^-) and hydrogen peroxide (H_2O_2).

1.6 Pharmacological approaches of brown adipose tissue activation/ recruitment and white adipose tissue browning

β 3-adrenergic receptor agonists (β 3-AR), thiazolidinediones, and retinoids are the well-known small molecules for brown adipose tissue activation/ recruitment and white adipose tissue browning (**Figure 5**).

1.6.1 β 3-adrenergic receptor agonists

Three β -AR subtypes, β 1-, β 2-, and β 3-AR, have been identified so far. β 3-AR, the best-studied thermogenesis target, is found in adipose tissue, cardiovascular system, and urinary bladder, and is known to be responsible for thermoregulation in BAT, and lipolysis in WAT (69). The function of β 3-AR in rodents has been proven by different evidences, however, the role of β 3-AR in the human BAT is disputed (70-72).

Isoproterenol is a non-selective β -AR agonist (β A), and is used to treat bradycardia in the clinic and induction of thermogenesis and lipolysis *in vitro* (73). CL 316,243 is a β 3-AR (β 3A) agonist with high selectivity (74), increasing the body temperature, energy expenditure, and UCP1 content in BAT in rats (75). It can also promote the utilization efficiency of free fatty acids in BAT (76), and induce more beige adipocytes in ingWAT than in perigonadal white adipose tissue (pgWAT) (77).

Mirabegron is approved for overactive bladder treatment by stimulating the β 3-AR that relaxes detrusor muscle (78) and is considered the most promising and safest β 3A currently available that has the potential to be used in the therapeutic treatment of metabolic disorders, although it has unavoidable adverse effects that heart rate and blood pressure increase at relatively small magnitude (79). Multiple trials revealed chronic pharmacological stimulation with Mirabegron promoted BAT metabolic activity and basal energy expenditure, with enhanced insulin sensitivity and secretion in healthy subjects (80, 81). Additionally, in obese humans, Mirabegron administration substantially improved adipose tissue dysfunction and glucose homeostasis, and induced beige adipose tissue recruitment in human ingWAT, however, it did not show any effect on BAT (82, 83).

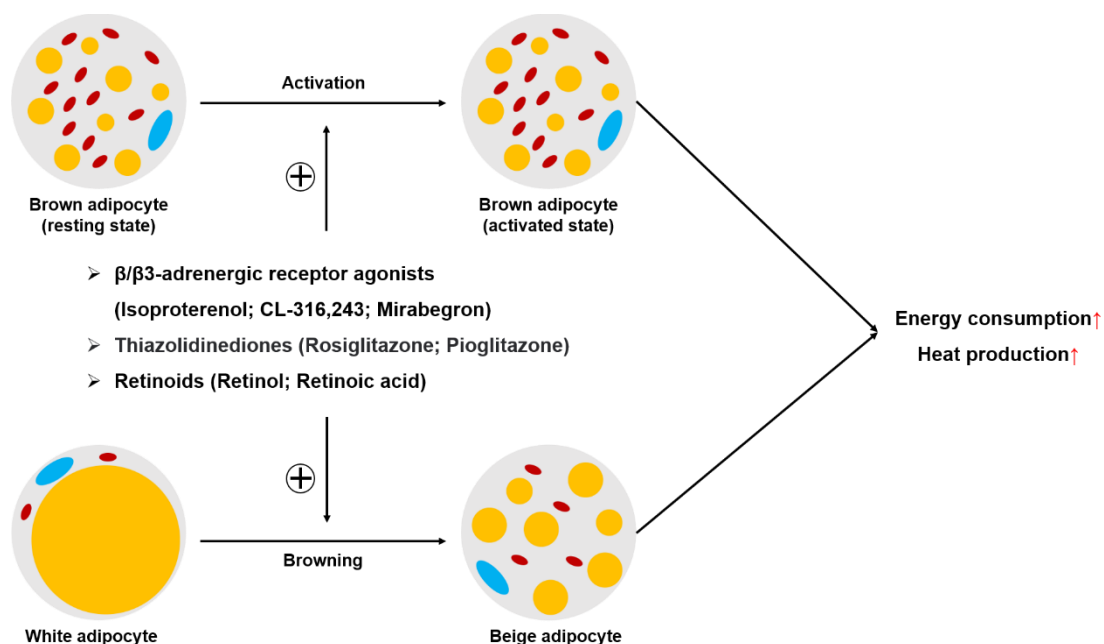


Figure 5. Pharmacological approaches to activate brown adipocytes and induce white adipocyte browning. β/β 3A, Thiazolidinediones, and Retinoids are the small molecules that promote basal state brown adipocytes to the activated state and convert white adipocytes to beige adipocytes, enhancing energy consumption and heat

production.

1.6.2 Thiazolidinediones

Thiazolidinediones (TZDs) are a class of insulin sensitizers and are indicated for the treatment of type 2 diabetes mellitus (T2DM) (84). The specific target of TZDs is PPAR γ , and activation of PPAR γ increases lipid storage in WAT and insulin sensitivity in the liver and muscle (85). PPAR γ is first substantially expressed in the murine interscapular brown adipose tissue (iBAT) during embryonic development (86), and PPAR γ in BAT is indispensable for the insulin-sensitizing action of TZDs (87). TZDs promote the differentiation of brown adipocytes (88) and the browning program in WAT (89), meanwhile, the up-regulated thermogenesis genes were observed (90, 91). Additionally, the PPAR γ agonist, Rosiglitazone increased glycogen mobilization to generate more fatty acids providing the substrates of BAT thermogenesis (92). When activated, PPAR γ binds to retinoic X receptor (RXR) to form a heterodimer complex in a DNA-dependent mechanism (93), directly regulating *Ucp1* gene transcription (94). Furthermore, the deacetylation of SirT1-dependent (95) and synergistic effect of PR domain containing 16 (PRDM16) (96) are involved in the promotion browning program of PPAR γ . In the ingWAT of non-obese T2DM patients with Pioglitazone preclinically, decreased immune cell infiltration and increased UCP1 expression were found (97).

1.6.3 Retinoids

Carotenoids, the common constituents of various vegetables, are dietary supplements, and their oxidative metabolites are important molecules with high antioxidant action. In vertebrates, carotenoids are transformed into retinal by β -carotene-15,15'-dioxygenase, which is further metabolized to retinol or retinoic acid (98).

Retinol, the active form of Vitamin A₁, is used for vitamin A deficiency and skin care and is on the essential medicines list by the World Health Organization (WHO). The 8-week Vitamin A-supplemented diet resulted in unchanged BAT weight in murine, but an induced *Ucp1* mRNA in BAT (99, 100) and increased response capacity to β 3A stimulation (99). In contrast, the mice fed the vitamin A-restricted diet had a lower trend in UCP1 expression of BAT and excess body weight, accompanied by hypertrophy of brown adipocytes implying BAT metabolic dysfunction (101). Furthermore, the retinol binding protein 4 (RBP4)-deficient mice had impaired cold tolerance capacity, and the

defect retinol transport led to a significant decrease in cold-induced thermogenic genes in scWAT, but RBP4 ablation had no alteration in BAT (102).

Retinoic acid is the major active metabolite of Vitamin A, under the retinoids family, mediating embryonic development, and is used to treat certain forms of leukemia. Numerous studies indicated retinoic acid up-regulated the expression of UCP1 *in vivo* and *in vitro* (103-106), even the increase can be observed after retinoic acid administration for 5h in mice (105). It is known that retinoic acid acts to regulate cell fate via the activation of nuclear transcription factors retinoic acid receptor (RAR) and RXR (107). Two active isomers of retinoic acid, *all-trans* retinoic acid and 9-*cis* retinoic acid were both identified as transcriptional activators of the UCP1 gene through the associated responsive region via RAR/RXR heterodimers (108-110). Furthermore, retinoic acid treatment rescued the decreased content of UCP1 and RAR α /RXR α , which were induced by Vitamin A deficient diet in BAT (111).

Mechanistically, retinoic acid caused a decreased membrane potential and increased respiratory rate in the isolated mitochondria from BAT, even with a significantly greater effect than Palmitic acid, the most common saturated fatty acid (112). It was speculated that, apart from adequate lipid solubility, another obligatory requirement of UCP1 ligand is including a free carboxyl group (113) which was interpreted as promoting proton translocation (114), and retinoic acid fulfills these requirements. Additionally, metabolomic analysis indicated glucose metabolism pathway was involved in the action of retinoic acid in brown adipocytes (115). Moreover, the inhibition of the p38 mitogen-activated protein kinases (p38MAPK) pathway suppressed retinoic acid-stimulated UCP1 expression (116).

1.7 The regulation of brown adipose tissue in metabolic syndrome

Due to the capacity to consume nutritional substrates and energy expenditure promotion, the classic BAT activation and recruitment of beige adipocytes in WAT are universally considered to be potential treatment regimens for metabolic diseases, particularly obesity and T2DM (117). Various factors have been identified to cause the degeneration of BAT (118). A large retrospective study indicated that changed ambient temperature led by seasonal variation regulates BAT activity, displaying highest in winter and lowest in summer (119), and a stronger proportion was observed in the subjects with metabolically active BAT (120). The incidence of cold-activated action on BAT decreased following age, which might be due to the accumulation of body fat in

the form of WAT (121), and it appears to be the gender difference existed in BAT activity and mass (122). Metabolic syndrome is known to determine the prevalence and mass of BAT, obese men have less activated BAT than lean men (123). Additionally, diabetic status is the independent factor of detectable BAT in humans (124), and BAT correlates negatively with glucose concentration (125).

Obesity is defined as the BMI over 30 in humans with excessive fat accumulation (126), displaying a risk to health, and it is widely considered that metabolic activity and prevalence of BAT are inversely related to body fatness, particularly visceral fat (127). Non-shivering thermogenesis confers the ability of BAT to promote whole-body energy expenditure, thereby reversing the positive energy balance that is the main cause of obesity. In morbidly obese patients who received gastric banding surgery, increased BAT activity was seen after weight loss (128). The canonical cold exposure chronically resulted in an increase in BAT activity and a concomitant decrease in body fat mass (129). BAT transplantation reversed or prevented genetic (130) and HFD-induced obesity (131), meanwhile, the greater energy expenditure in the Norepinephrine challenge test and higher core temperatures upon cold exposure were found in recipient mice with HFD (132), due to the enhanced sympathetic activity. Another possible mechanism is that the increased fat mass activates endogenous BAT by releasing cytokines (130-132).

The leading reason for high blood glucose levels in the circulation system of T2DM patients is impaired glucose utilization efficiency, which is caused by insulin resistance in the liver, adipose tissue, and muscle (133). The increased plasma glucose disposal, insulin sensitivity, and substrates (glucose and fatty acids) oxidation were found in healthy subjects with more active BAT under both basal and cold exposure conditions (134). Furthermore, glucose uptake in the BAT was directly induced by acute cold exposure, accompanied by increased blood perfusion (135). More importantly, cold acclimation improved insulin sensitivity in the liver and adipose tissue of T2DM subjects (136), and enhanced glucose turnover rate in the mitochondrial TCA cycle (137). The action of BAT in whole-body glucose homeostasis was strengthened by BAT transplantation, and the increased insulin sensitivity was seen in recipient mice under basal and HFD conditions (138). β 3-AR stimulated glucose uptake in BAT is primarily dependent on the transcription and translocation of glucose transporter 1 (GLUT1), rather than the stimulation of insulin (139).

1.8 Aim of this project

RetSat effects the white adipocyte differentiation, and RetSat whole-body knockout impacts the body weight and glucose homeostasis of mice. Additionally, RETSAT protein in mice BAT is induced by cold exposure in a time-dependent manner.

BAT and non-shivering thermogenesis have been thought to have metabolic benefits in the past decade, however, the function of RetSat in BAT has not been well understood. Therefore, the aim of this project was to explore the role of RetSat in BAT and non-shivering thermogenesis, including the browning of white adipocyte.

This project aims to address the following questions:

How about the regulation of RetSat in adipocyte and adipose tissue by β -AR stimulation?

Does RetSat effect brown adipocyte differentiation?

Is RetSat required for the thermogenesis gene expression in adipocytes?

Does RetSat effect mitochondria function in adipocytes?

Is RetSat in BAT required for the cold tolerance of mice?

Does RetSat in BAT effect the metabolic profile of mice?

2 Chemicals, reagents, kits

2.1 Chemicals and reagents

The used chemicals and reagents are listed in **Table 2**.

Table 2. Chemicals and reagents

Substance	Manufacturer
0.05% Trypsin-EDTA (1X)	Gibco, Thermo Fisher Scientific Inc. (Waltham, MA, US)
0.5% Trypsin-EDTA (10X)	Gibco, Thermo Fisher Scientific Inc. (Waltham, MA, US)
0.9% Saline	B. Braun Melsungen AG (Melsungen, DE)
10% Ammonium persulfate (APS) solution	Sigma Aldrich (St. Louis, MO, US)
10% Sodium dodecyl sulfate (SDS)	Carl Roth GmbH & Co. KG (Karlsruhe, DE)
100% Ethanol	EMSURE, Thermo Fisher Scientific Inc. (Waltham, MA, USA)
100% Methanol	EMSURE, Thermo Fisher Scientific Inc. (Waltham, MA, USA)
2 x Fast Start Universal SYBR Green	Eurogentec (Seraing, BE)
2-Propanol	Merck KGaA (Darmstadt, DE)
3,3',5-Triiod-L-thyronin (T3)	Sigma Aldrich (St. Louis, MO, US)
30% Acrylamide	AppliChem GmbH (Darmstadt, DE)
3-isobutyl-1-methylxanthine (IBMX)	Sigma Aldrich (St. Louis, MO, US)
4% Buffered Formaldehyde	Merck KGaA (Darmstadt, DE)
4-(2-hydroxyethyl)-1-piperazineethanesulfonic acid (HEPES) buffer	Gibco, Thermo Fisher Scientific Inc. (Waltham, MA, US)
4',6-diamidino-2-phenylindole (DAPI)	Sigma Aldrich (St. Louis, MO, US)
5 x PCR master mix "ready-to-load"	Bio & Sell (Feucht, DE)
70% Ethanol	Carl Roth GmbH & Co. KG

	(Karlsruhe, DE)
Acetic acid	Carl Roth GmbH & Co. KG (Karlsruhe, DE)
Acetone	Sigma Aldrich (St. Louis, MO, US)
Agarose	Carl Roth GmbH & Co. KG (Karlsruhe, DE)
Antimycin A	Sigma Aldrich (St. Louis, MO, US)
Bovine serum albumin	Biowest (Nuaille, France)
Calcium chloride (CaCl ₂)	Carl Roth GmbH & Co. KG (Karlsruhe, DE)
Chloroform	Merck KGaA (Darmstadt, DE)
CL 316, 243	Sigma Aldrich (St. Louis, MO, US)
Collagenase type II	Worthington Biochemical Corporation (Lakewood, NJ, US)
D-(+)- Glucose	Sigma Aldrich (St. Louis, MO, US)
ddH ₂ O	double distilled water
Dexamethasone	Sigma Aldrich (St. Louis, MO, US)
Dimethyl sulfoxide (DMSO)	Sigma Aldrich (St. Louis, MO, US)
DMEM 25 mM glucose, (+) L-glutamine (-) pyruvate	Gibco, Thermo Fisher Scientific Inc. (Waltham, MA, US)
dNTP mix	Invitrogen, Thermo Fisher Scientific Inc. (Waltham, MA, US)
Eosin	Merck KGaA (Darmstadt, DE)
Fatty Acid Free Bovine serum albumin	Sigma Aldrich (St. Louis, MO, US)
Fetal bovine serum (FBS)	Gibco, Thermo Fisher Scientific Inc. (Waltham, MA, US)
Glycerol	Sigma Aldrich (St. Louis, MO, US)
Glycine	Carl Roth GmbH & Co. KG (Karlsruhe, DE)
hematoxylin	Carl Roth GmbH & Co. KG (Karlsruhe, DE)
Hydroxymethyl Aminomethane (Tris Base)	Merck KGaA (Darmstadt, DE)
Hydroxymethyl Aminomethane	Carl Roth GmbH & Co. KG

Hydrochloride (Tris HCL)	(Karlsruhe, DE)
Indomethacin	Sigma Aldrich (St. Louis, MO, US)
Insulin human rapid	Sanofi (Paris, France)
Insulin solution human	Sigma Aldrich (St. Louis, MO, US)
Isoflurane	AbbVie Inc. (North Chicago, IL, USA)
Isoproterenol	Sigma Aldrich (St. Louis, MO, US)
Lipofectamine 2000	Invitrogen, Thermo Fisher Scientific Inc. (Waltham, MA, US)
Magnesium sulfate (MgSO ₄)	Carl Roth GmbH & Co. KG (Karlsruhe, DE)
M-MLV reaction buffer (5X)	Promega Corporation (Fitchburg, WI, US)
M-MLV reverse transcriptase	Promega Corporation (Fitchburg, WI, US)
NP40 (IGEPAL CA-630)	Sigma Aldrich (St. Louis, MO, US)
Nucleic acid dye	Carl Roth GmbH & Co. KG (Karlsruhe, DE)
Oil red O	Sigma Aldrich (St. Louis, MO, US)
Oligomycin	Sigma Aldrich (St. Louis, MO, US)
OPTI-MEM buffer	Gibco, Thermo Fisher Scientific Inc. (Waltham, MA, US)
Penicillin/Streptomycin (P/S)	Gibco, Thermo Fisher Scientific Inc. (Waltham, MA, US)
Phosphate-buffered saline (PBS)	Gibco, Thermo Fisher Scientific Inc. (Waltham, MA, US)
Pierce ECL immunoblotting substrate	Thermo Fisher Scientific Inc. (Waltham, MA, US)
Pierce non-reducing sample buffer, lane marker	Thermo Fisher Scientific Inc. (Waltham, MA, US)
Pioglitazone hydrochloride	Sigma Aldrich (St. Louis, MO, US)
Polylysine	Sigma Aldrich (St. Louis, MO, US)
Ponceau S	Cayman Chemical Company (Ann Arbor, MI, USA)

Potassium chloride (KCl)	Carl Roth GmbH & Co. KG (Karlsruhe, DE)
Potassium dihydrogen phosphate (KH ₂ PO ₄)	Carl Roth GmbH & Co. KG (Karlsruhe, DE)
Precision Plus Protein Dual Color Standards	Bio-Rad Laboratories (Hercules, CA, US)
Protease inhibitor cocktail tablets, cOmplete Mini EDTA-free	F. Hoffmann-La Roche AG (Basel, CH)
Proteinase K	F. Hoffmann-La Roche AG (Basel, CH)
PVDF	Bio-Rad Laboratories (Hercules, CA, US)
QIAzol lysis reagent	Qiagen GmbH (Hilden, DE)
Random hexamer primer	Invitrogen, Thermo Fisher Scientific Inc. (Waltham, MA, US)
Ribonuclease A (RNaseA)	Thermo Fisher Scientific Inc. (Waltham, MA, US)
Rotenone	Sigma Aldrich (St. Louis, MO, US)
skim milk	Carl Roth GmbH & Co. KG (Karlsruhe, DE)
Sodium chloride (NaCl)	Merck KGaA (Darmstadt, DE)
Sodium deoxycholate	Sigma Aldrich (St. Louis, MO, US)
Sodium fluoride (NaF)	Sigma Aldrich (St. Louis, MO, US)
Sodium hydroxide (NaOH)	Carl Roth GmbH & Co. KG (Karlsruhe, DE)
Tetramethylethylenediamine (TEMED)	Sigma Aldrich (St. Louis, MO, US)
Trifluoromethoxy carbonylcyanide phenylhydrazone (FCCP)	Sigma Aldrich (St. Louis, MO, US)
Tween 20	Merck KGaA (Darmstadt, DE)
Ultrapure distilled water (upH ₂ O) DNase/RNase free	Invitrogen, Thermo Fisher Scientific Inc. (Waltham, MA, US)
XF assay media	Agilent (Santa Clara, USA)
XF calibrant solution	Agilent (Santa Clara, USA)
XF glucose	Agilent (Santa Clara, USA)

XF glutamine	Agilent (Santa Clara, USA)
XF Pyrvate	Agilent (Santa Clara, USA)
Xylene	Carl Roth GmbH & Co. KG (Karlsruhe, DE)
β -mercaptoethanol	Sigma Aldrich (St. Louis, MO, US)

2.2 Buffers and solutions

➤ SVF isolation buffer

20 mM HEPES

5 mM KH_2PO_4

1 mM MgSO_4

1 mM CaCl_2

136 mM NaCl

4.7 mM KCl

1 g/L Glucose

2% BSA

ddH₂O

Set pH to 7.4 by NaOH, add Collagenase II at final concentration 2 mg/ml before use.

➤ Tailcut Buffer

0.1 M Tris (pH 8.5)

0.2 M NaCl

5 mM EDTA

0.2% [w/v] SDS

ddH₂O

➤ TE Buffer

10 mM Tris (pH 7.5)

1 mM EDTA

ddH₂O

➤ 1x (Tris acetate EDTA) TAE electrophoresis running buffer

40 mM Tris Base
20 mM Acetic acid
0.4 mM EDTA
ddH₂O

➤ RIPA buffer

2 mM EDTA (pH 8.0)
150 mM NaCl
50 mM NaF
50 mM Tris-HCl (pH 7.2)
0.5% [w/v] Sodium deoxycholate
1% [v/v] NP40 (IGEPAL CA-630)
0.1% [v/v] SDS
1 tablet of protease inhibitor complete EDTA-free
ddH₂O

➤ Loading buffer

87.5% [w/v] Pierce non-reducing sample buffer, lane marker
12.5% [w/v] β-mercaptoethanol

➤ Electrophoresis buffer

48 mM Tris-Base
192 mM Glycine
0.1% [w/v] SDS
ddH₂O

➤ Transfer buffer

25 mM Tris-base
192 mM NaCl
20% Methanol
0.05% [w/v] SDS
ddH₂O

➤ 10×TBS

0.2 M Tris-Base

0.2 M Tris-HCl

1.36 M NaCl

ddH₂O, adjusted pH 7.6

➤ 1×TBST

1×TBS plus 0.1% [v/v] Tween 20

2.3 Kits

The used kits are listed in **Table 3**.

Table 3. Kits

Kit	Manufacturer
PeqGOLD total RNA kit	VWR International (Radnor, PA, US)
RNeasy mini kit	Qiagen GmbH (Hilden, DE)
Pierce BCA protein assay kit	Thermo Fisher Scientific Inc. (Waltham, MA, US)
RNA clean & concentrator kit	Zymo Research (Irvine, CA, USA)
Amaxa Cell Line Nucleofector Kit V	Lonza (Basel, CH)
Seahorse kit	Agilent (Santa Clara, USA)

2.4 Antibodies

The primary antibodies used for the immunoblotting are listed in **Table 4**. The antibodies were diluted in the indicated ratio in a solution of the corresponding percentage of skim milk powder in a 1:1 TBS/TBST mixture.

Table 4. Primary antibodies for immunoblotting

Antibody	Species	Product	Application
PPAR _γ	Mouse	Santa Cruz, sc-	1:200 in 2.5%

		7273 (E8)	skim milk
UCP1	Rabbit	GeneTex, GTX10983	1:1000 in 4% skim milk
RETSAT	Rabbit	Sigma-Aldrich, HPA046513	1:1000 in 4% skim milk
OXPHOS	Mouse	Abcam, ab110413	1:5000 in 4% skim milk
RAN	Mouse	BD Biosciences, #610341	1:5000 in 4% skim milk
TUBA	Rabbit	Cell Signaling, #2144	1:2000 in 4% skim milk

The horseradish peroxidase (HRP) conjugated secondary antibodies were diluted in a ratio of 1:2000 in a solution of 4% skim milk powder in a 1:1 TBS/TBST mixture. The secondary antibodies used for the immunoblotting are listed in **Table 5**.

Table 5. Secondary antibodies for immunoblotting

Antibody	Species	Product	Application
Anti-mouse; HRP conjugated	Goat	31430, Thermo Fisher Scientific	1:2000 in 4% skim milk
Anti-rabbit; HRP conjugated	Goat	31460, Thermo Fisher Scientific	1:2000 in 4% skim milk

2.5 Oligonucleotides

2.5.1 Primers for real-time quantitative polymerase chain reaction

Primers for real-time quantitative polymerase chain reaction (RT-qPCR) were designed using the National Center for Biotechnology Information (NCBI) genome browser to pick intron-spanning sequences which were then verified by NCBI-Nucleotide Basic Local Alignment Search Tool (BLAST). Primers were synthesized by Thermo Fisher Scientific. The used primers and their sequences (from 5' to 3') are listed in **Table 6**.

Table 6. Primers for real-time quantitative polymerase chain reaction

Gene	Sequence (5' to 3')
<i>mAdrb3</i>	Forward: GGCCCTCTCTAGTTCCCAG
	Reverse: TAGCCATCAAACCTGTTGAGC
<i>mCidea</i>	Forward: AGGGACACCACGCATTTTCAT
	Reverse: CCGATTTCTTTGGTTGCTTG
<i>mCox7a1</i>	Forward: AAAACCGTGTGGCAGAGAAG
	Reverse: CAGCGTCATGGTCAGTCTGT
<i>Cre</i>	Forward: GCTTGCATGATCTCCGGTAT
	Reverse: ATACCTGGCCTGGTCTGGA
<i>mElovl3</i>	Forward: GTGGTCGTCTATCTGTTGCTCA
	Reverse: GCCAGGAAGAAGGACCAGAG
<i>mFabp4</i>	Forward: TGAAGACAGCTCCTCCTCG
	Reverse: AATCCCCATTTACGCTGATGATC
<i>mPparg2</i>	Forward: TGGGTGAACTCTGGGAGATTC
	Reverse: GAGAGGTCCACAGAGCTGATTCC
<i>mPrdm16</i>	Forward: TCTGCCACAAGTCCTACACG
	Reverse: GAACATCTGCCACAGTCCT
<i>mRetSat</i>	Forward: GCGGCTGTTGTCATACCTTT
	Reverse: CCAAGATAAAACGGCCAATG
<i>mRplp0</i>	Forward: TCATCCAGCAGGTGTTTGACA
	Reverse: GGCACCGAGGCAACAGTT
<i>mUcp1</i>	Forward: GGGCCCTTGTAACAACAAA
	Reverse: ACTGGAGAGGCCAGGAGTGT

2.5.2 Silencing RNA oligonucleotides

The small interfering ribonucleic acid (siRNA) used in this project were designed previously (140) and synthesized by Eurogentec and listed in **Table 7**.

Table 7. siRNA oligonucleotides sequences

Target	Sense	Antisense
siControl (non-targeting)	UAGCGACUAAACACAUC AAUU	UUGAUGUGUUUAGUCGCUAU U
siRetSat_1	UCAGCCGAGUACCAGAG AAUU	UUCUCUGGUACUCGGCUGAU U
siRetSat_2	GCUCAAAGGUCAAGGCA CAUU	UGUGCCUUGACCUUUGAGCU U

2.5.3 Primers for mouse genotyping

Primers used for mouse genotyping in this project were synthesized by Thermo Fisher Scientific and their sequences (from 5' to 3') are listed in Table 8.

Table 8. Primers for mouse genotyping

Gene	Sequence (5' to 3')
<i>RetSat flox</i>	Forward: CTCCTTTTCTGAGGCTGGTG
	Reverse: AAGGCAGACCTTTCTTTTAAGG
<i>Ucp1-Cre</i>	Forward: CGATGCAACGAGTGATGAGGTTC
	Reverse: GCACGTTCACCGGCATCAAC
<i>Myogenin</i> (internal control)	Forward: TTACGTCCATCGTGGACAGC
	Reverse: TGGGCTGGGTGTTAGCCTTA

2.6 Mouse diets

Table 9. List of mouse diets

Diet	Manufacturer
Normal chow, standard diet V 1523-0	ssniff-Spezialdiäten (Soest, D)
High-fat diet, 60% kcal/fat, D12492	Research Diets (New Brunswick, US)

2.7 Equipments

Table 10. Main equipments

Equipment	Manufacturer
CFX384 real time PCR system	Bio-Rad Laboratories (Hercules, CA, USA)
CFX96 real time PCR system	Bio-Rad Laboratories (Hercules, CA, USA)
Chemidoc™ XRS+ imaging system	Bio-Rad Laboratories (Hercules, CA, USA)
climate chamber	Weiss Technik GmbH (Balingen, DE)
CO2 Incubator	Heraeus (Berlin, DE)
ContourXT glucose meter	Ascensia Diabetes Care Holdings AG (Basel, CH)
Electrophoresis Chambers and Power Supplies	Bio-Rad Laboratories (Hercules, CA, USA)
Homogenizator Tissue Tearor	Biospec Products, Inc. (Breda, NL)
microscope Leica DM IL LED	Leica Mikrosysteme Vertrieb GmbH (Wetzlar, DE)
Mikroprozessor-pH-meter 743	Knick Elektronische Messgeräte GmbH & Co. KG (Berlin, DE)
Minispec LF50, NMR	Bruker (Billerica, US)
NanoDrop® ND-1000 photometer	PEQLAB Biotechnologie GmbH (Erlangen, DE)
Nucleofector	amaxa GmbH (Koeln, DE)
PTC-200 Peltier Thermal Cycler	Bio-Rad Laboratories (Hercules, CA, USA)

2.8 Consumables

Table 11. Consumables

Item	Manufacturers
1, 5, 10, 20 ml syringe	B. Braun Melsungen (Melsungen, DE)
1.5, 2 ml safe seal tube	SARSTEDT (Nümbrecht, DE)

10 cm cell culture dish	Corning Inc. (Corning, US)
10, 200, 1000 µl pipet tips	SARSTEDT (Nümbrecht, DE)
12-well cell culture dish	SARSTEDT (Nümbrecht, DE)
15, 50 ml Falcon conical tube	Corning Inc. (Corning, US)
200 µl 8-tube PCR strip	neoLabMigge (Heidelberg, DE)
5, 10, 25 ml serological pipets	SARSTEDT (Nümbrecht, DE)
96, 384-well qPCR plate	Bio-Rad Laboratories (München, DE)
Cannula Sterican	B. Braun Melsungen (Melsungen, DE)
Cell scraper	Sarstedt AG & Co. KG (Nümbrecht, DE)
CONTOUR®NEXT glucose strips	Bayer Vital (Leverkusen, DE)
Cryogenic vial	Thermo Fisher Scientific Inc. (Waltham, MA, US)
Disposable scalpel	Feather Safety Razor Co., Ltd (Osaka, JP)
Liquid nitrogen	Sol Group (Berlin, DE)
microplate, 96-well, flat-bottom	Greiner Bio-One GmbH (Kremsmünster, AT)
Microseal qPCR plate sealing film	Bio-Rad Laboratories (München, DE)
Nylon sieve 250µM pores	Klein & Wieler (Königswinter, DE)
Omnican® 50 U100-insulin syringe	B. Braun Melsungen (Melsungen, DE)
Parafilm	Carl Roth (Karlsruhe, DE)
PVDF membrane	Bio-Rad Laboratories (München, DE)
Syringe filter, Minisart NML, CA, 28 mm, 0,2 µm, sterile	Sartorius AG (Göttingen, DE)
Whatman filter paper	Thermo Fisher Scientific Inc. (Waltham, MA, US)

3 Methods

3.1 iBACs and 3T3-L1 cell line and culturing

Immortalized brown adipogenic cells (iBACs) (141) were provided by Prof. Dr. Andreas Prokesch (Medical University of Graz, Austria) and Prof. Dr. Patrick Seale (University of Pennsylvania, USA). Briefly, primary brown preadipocytes were isolated from iBAT of newborn mice, immortalized by retroviral SV40T antigen, and selected by Puromycin.

3T3-L1 is a clonal production of 3T3 isolated from mouse embryos with fibroblast-like morphology and is widely applied to study basic cellular mechanisms associated with obesity (142).

3.1.1 Cell passaging

The iBACs and 3T3-L1 preadipocytes are adherent cells, the cells toward the end of the logarithmic growth phase, which means 80–90% confluence, are taken for passaging. The old media was removed by aspiration from the 10 cm dish, preadipocytes were washed once with pre-warmed PBS, and then were trypsinized by 1 ml 0.05% trypsin-EDTA incubating at 37°C for 5 min. The preadipocytes were observed under the microscope to confirm completed detachment, and 3 ml of complete media was added immediately to prevent over-trypsinization. The preadipocytes resuspend solution was pipetted thoroughly to obtain single cell suspension, and seeding cells into another 10 cm dish at 1:10 ratio.

3.1.2 Cell thawing

The cryogenic vial containing frozen preadipocytes was taken from liquid nitrogen storage and immediately thawed vial by quick shaking in the 37°C water bath, until there was just a small bit of ice left. The thawed preadipocytes were seeded evenly into 10 cm dish with pre-warmed growth media. The state of preadipocytes was observed under microscope the next day and the media was aspirated, subsequently, preadipocytes were washed with pre-warmed PBS to remove residual DMSO, finally, fresh growth media was added.

3.1.3 Cell cryopreservation

Preadipocytes in the logarithmic growth phase were trypsinized from dishes and poured together, centrifuged at 300g for 10 min to remove growth media. The cell pellet was re-suspended by freeze media, which was comprised of 40% DMEM, 50% FBS, and 10% DMSO. The mixture was aliquoted into the cryogenic vials, preadipocytes should be frozen slowly at 1 °C/min. Thus, the cryogenic vials were placed into CryoBox filled with 2-Propanol. Finally, CryoBox was kept at -80°C overnight.

3.1.4 Preadipocyte differentiation

iBACs and 3T3-L1 preadipocytes were induced to adipose-like phenotype by the cocktail mixtures (143, 144) described in **Table 12**, **Table 13**, and **Table 14**.

Table 12. Growth media composition

	Substance	iBACs	3T3-L1
Growth media	Dulbecco's Modified Eagle Medium	Glucose C_{final} = 25 mM	Glucose C_{final} = 25 mM
	Fetal bovine serum	P_{final} = 10%	P_{final} = 10%
	Penicillin/ Streptomycin	P_{final} = 1%	P_{final} = 1%
	HEPES	C_{final} = 20 mM	-

Table 13. Maintenance media composition

	Substance	iBACs	3T3-L1
Based on growth media, and supply	insulin	C_{final} = 20 nM	C_{final} = 1.7 μ M
	3,3',5-Triiod-L-thyronin	C_{final} = 1 nM	-

Table 14. Induction media composition

	Substance	iBACs	3T3-L1
--	-----------	-------	--------

Based on maintenance media, and supply	Dexamethasone	$C_{\text{final}} = 5 \mu\text{M}$	$C_{\text{final}} = 1 \mu\text{M}$
	3-isobutyl-1-methylxanthine	$C_{\text{final}} = 0.5 \text{ mM}$	$C_{\text{final}} = 0.5 \text{ mM}$
	Pioglitazone	$C_{\text{final}} = 5 \mu\text{M}$	$C_{\text{final}} = 5 \mu\text{M}$
	Indomethacin	$C_{\text{final}} = 0.125 \text{ mM}$	-

The process of preadipocyte differentiation is illustrated in **Figure 6**. During the whole process, cells were cultured in the incubator with 37°C and 5% CO₂. The adipocytes with a degree of differentiation of at least 90% were considered mature and applied for subsequent experiments.

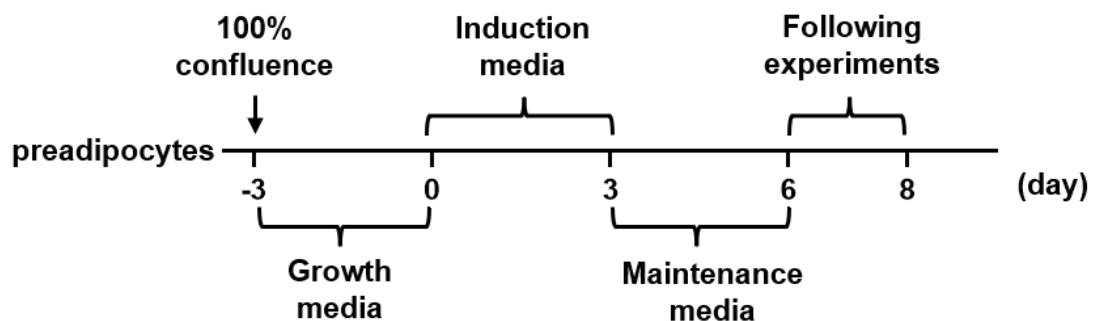


Figure 6. Preadipocyte differentiation process.

3.2 Adipose-derived stromal vascular fraction cells isolation

Adipose tissue is comprised of mature adipocytes and stromal vascular fraction (SVF) (145), which includes preadipocytes. Preadipocytes take the highest percentage within SVF and are induced into mature adipocytes for further applications. To further investigate RetSat function in a more physiologically relevant cellular model, primary brown preadipocytes were isolated and differentiated. The iBAT was dissected and minced with scissors, all pieces were moved and incubated in isolation buffer for 30 min at 37 °C shaking. After digestion, the solution was filtered through 250 μM nylon membrane. The filtrate was centrifuged at 300g for 10 min, and SVF was pelleted. The SVF pellet was resuspended by growth media, and seeded in 12-well plates. The following expansion and differentiation methods are the same as iBACs in 3.1.4.

3.3 Transfection

Transfection is a method that introduces exogenous genetic material into eukaryotic cells and is widely applied in biomedical research (146).

3.3.1 RNA interference mediated gene silencing

RNA interference (RNAi) is a post-transcriptional gene silencing response in eukaryotes and is applied to reduce specific gene expression in organisms (147). Small interfering RNA (siRNA) (148) intracellularly delivered by electroporation or lipofection degrades related mRNA after transcription to silence the singular gene of interest.

3.3.1.1 Electroporation

Electroporation (149) is an efficient approach that introduces siRNA into the cells by utilizing a brief pulse of a high-voltage electric field to increase cell membrane permeability. Mature adipocytes were washed with pre-warmed PBS to remove media, and incubated with 4 g/l trypsin plus 0.5 mg/ml Collagenase P at 37 °C for 10 min. After detachment, adipocytes were re-suspended in PBS, aliquoted into tubes, and centrifuged at 300 g for 3 min. Aspirated media, adipocytes were gently re-suspended in 90 µl electroporation buffer, then 3 nmol siRNA oligonucleotides, and transferred into the cuvette, electroporation was performed at the Amaxa device. Finally, adipocytes were re-suspended in media, and loaded into 12-well plates dropwise.

3.3.1.2 Lipofection

In order to efficiently knock down RetSat in adipocytes from multiple wells of the Seahorse cell culture plate, Lipofectamine 2000 was chosen as the reagent. Lipofectamine is a vesicle that easily merges with cell membrane and delivers siRNA into cells by endocytosis (150). Reverse transfection was applied in a Seahorse cell culture plate (151), and all amounts and volumes were given on a per-well basis. Lipofectamine-siRNA complex was prepared first, 1 nmol siRNA and 4 µl Lipofectamine® 2000 were diluted in 4.75 µl and 4 µl OPTI-MEM buffer, respectively, and incubated at hood for 5 min. After mixing diluted lipofectamine and siRNA, the complex was loaded into the plate and incubated for another 25 min. Meanwhile, mature adipocytes were trypsinized, properly diluted, and seeded into a Seahorse cell culture plate. After waiting for 3 days, the plate was used for Seahorse assay.

3.3.2 Virus transfection

3.3.2.1 Retrovirus transfection

Virus is used as a vector to deliver genetic materials into host cells (152). After invading host cells, retrovirus adversely produces DNA from its RNA genome, and integrates it into the genome of host cells to achieve stable integration (153). The retrovirus production was performed as previously described (4). Briefly, BOSC23 cells were transfected with empty or RetSat retroviral construct by Lipofectamine 2000. The supernatant was harvested after 72h and mixed with 10 g/mL Polybrene. The pre-confluent iBACs preadipocytes were infected by retrovirus-rich media and changed the media to regular growth media. During immortalization, iBACs had been drug selected after SV40 large-T antigen retrovirus transduction, so this cell line has Puromycin resistance (141). The stable expression was obtained after 1-2 passages.

3.3.2.2 Adenovirus transfection

Cre Recombinase is a type I topoisomerase from bacteriophage P1 that is applied to delete a segment of DNA flanked by LoxP sites in cells or experimental animals (154). Since recombinant GFP adenovirus expresses green fluorescent protein under the control of CMV promoter, which is easily visualized under fluorescence microscopy, it serves as a control for other recombinant adenoviruses (155). The adenovirus GFP and Cre were prepared in the research group previously, briefly, GFP or Cre gene was inserted into the shuttle plasmid, and the entire sequence of recombinant virus was reconstituted in cosmid. Subsequently, recombinant adenovirus was generated by infection HEK293 cells and supernatant collection. Finally, virus titer was determined.

To delete RetSat in primary brown adipocytes, adenovirus Cre was taken to infect primary brown adipocytes from newborn mice with RetSat flox/flox. The DMEM with 0.5 µg/ml polylysine, 0.5% BSA, and 1% P/S were prepared (156), adenovirus was added to this mixture, and incubated at room temperature for at least 100 min. Subsequently, adipocytes were washed with PBS, and incubated with above virus media for at least 100 min in incubator. The equivalent amount of DMEM with BSA and P/S was supplemented to adipocytes, and incubated in incubator overnight. The virus media was replaced by growth media the next day, the subsequent experiments were conducted after infected 4 days. For Cre-mediated deletion, 4.2×10^8 infectious units were used in 100 µl media per well of the Seahorse cell culture plate, and 1.4×10^9

infectious units were used in 600 µl media per well of the 12-well plate. The adenovirus GFP infected cells were the control to determine transfection efficiency (4), and the amount was adjusted by titer.

3.4 Oil red O staining

Oil red O staining is used to specifically visualize neutral lipids in adipocytes, thereby indicating lipid accumulation (157). The 0.5% stock solution was prepared by dissolving Oil Red O powder in 100% 2-Propanol. The working solution was freshly diluted from stock solution in a ratio of 3:5 by ddH₂O and filtered through Whatman filter paper. The living adipocytes in the 12-well plate were washed with PBS to remove FBS and then fixed with 4% buffered Formaldehyde at room temperature for 20 min. The fixed adipocytes were incubated with working solution on shaker for 1h, washed 3 times by PBS again until no excess dyestuff, and finally observed and photographed.

3.5 Seahorse mitochondria stress test

Seahorse Cell mitochondria stress test is a gold standard assay to measure mitochondria function in cells (158). Mitochondrial oxidative phosphorylation is the main process to generate ATP in mammals. Oxygen concentration in living cells supernatant is monitored by Seahorse XF96 Extracellular Flux Analyzer in real time and converted to oxygen consumption rate (OCR) value, one of the key mitochondria function parameters. The adipocytes were seeded in the Seahorse cell culture plate priorly and the sensor cartridge was activated by calibrant solution before assay. The respiratory baseline was measured without any injection initially, followed by Oligomycin, FCCP, and Rotenone/Antimycin A injection according to standard protocol. The detailed steps are described in **Table 15**. After running, cells were fixed with 4% buffered Formaldehyde, and stained by DAPI, fluorescence was recorded (159). Finally, OCR values were normalized by the staining of nuclei, and respiratory parameters were calculated as illustrated in **Figure 7**.

Table 15. Mitochondria stress test stepped commands

Command	Time	Cycle
Calibrate	-	-
Equilibrate	12 min	-

Mix	2 min	4x
Wait	0.5 min	
Measure	2 min	
Port A injection (Oligomycin)	-	-
Mix	2 min	4x
Wait	0.5 min	
Measure	2 min	
Port B injection (FCCP)		-
Mix	2 min	4x
Wait	0.5 min	
Measure	2 min	
Port C injection (Rotenone and Antimycin A)	-	-
Mix	2 min	4x
Wait	0.5 min	
Measure	2 min	
Program end	-	-

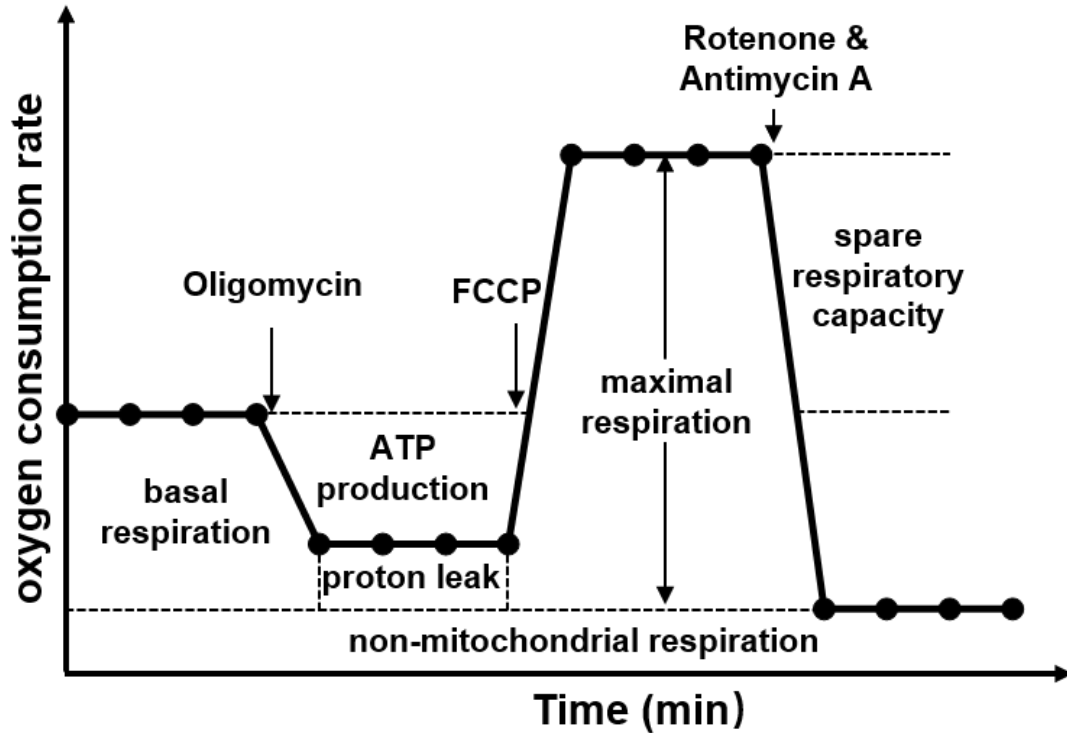


Figure 7. Seahorse mitochondria stress test profile.

3.6 *In vivo* model and experiments

3.6.1 Animals housing

All experimental procedures were approved under number G 0130/17, and followed by national and European guidelines for proper conduct of animal experiments. The mice were bred in FEM-Buch and transferred to the animal facility of Max Rubner Center (MRC) for Cardiovascular Metabolic Renal Research. The housing conditions are room temperature of $23 \pm 1^\circ\text{C}$, with 12h light/12h dark with specific pathogen-free (SPF) condition. Mice had free access to drinking and food, except where stated otherwise.

3.6.2 BAT-specific RetSat knockout mouse model establishment

C57BL/6J background mice with flox/flox alleles were generated previously in research group. In brief, to insert LoxP sites into the mouse genome flanking exon 2 and exon 3 of RetSat, the targeting RetSat vector was introduced in mouse embryonic stem cells by electroporation. The selected heterozygous knockout embryonic stem cells were

injected into a developing embryo which was transferred into a mouse afterward. The heterozygous floxed mice were mated with C57BL/6J mice to yield homozygous RetSat flox/flox mice. The male mice on C57BL/6J background with UCP1 Cre recombinase (160) (provided by Prof. Dr. Tim Schulz, German Institute of Human Nutrition Potsdam) were crossed with female RetSat flox/flox mice to generate RetSat flox/flox mice with UCP1 Cre that termed as Cre⁺ mice, and the littermates without the Cre expression as the controls, Cre⁻ mice.

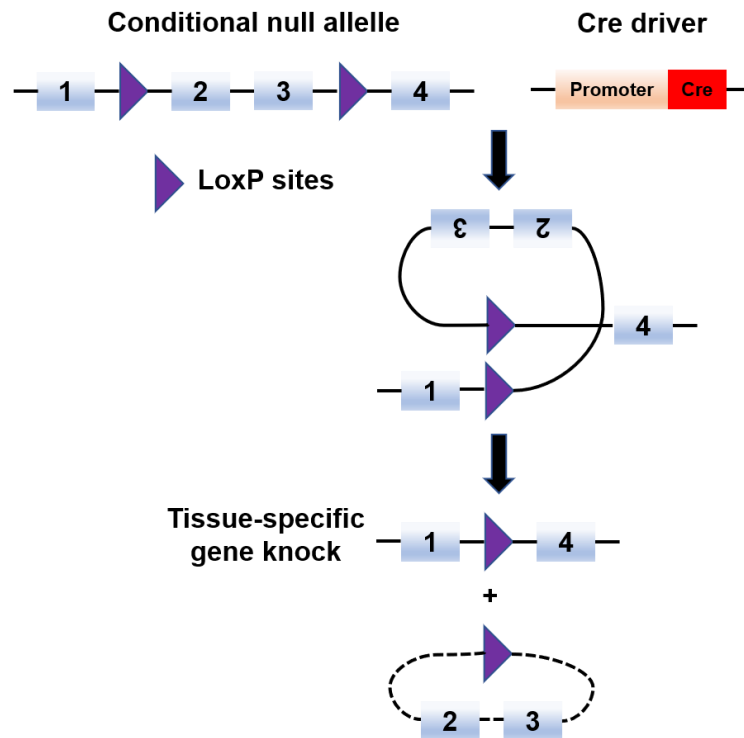


Figure 8. Cre-induced recombination of floxed allele. Cre recombinase recognizes two loxP sites and excises the loxP flanked (floxed) DNA, finally generating the DNA with inactivated gene RetSat.

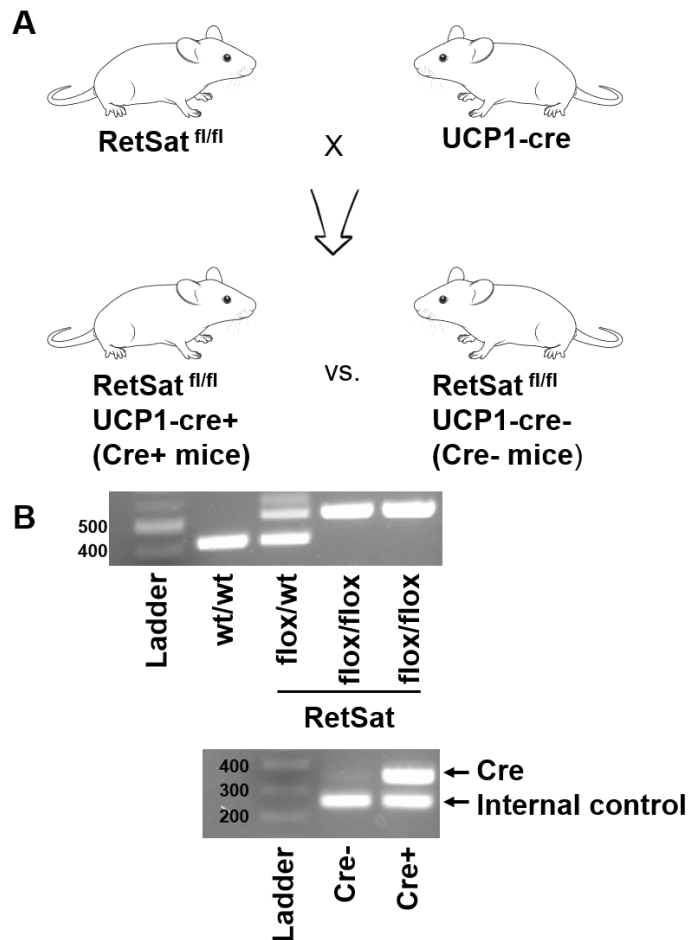


Figure 9. Experimental scheme for establishing RetSat flox/flox UCP1 Cre mice. (A) Mice breeding strategy. (B) Genotyping PCR results of wt/wt, RetSat flox/wt, RetSat flox/flox mice (upper panel), and Cre-, Cre+ mice (lower panel).

3.6.3 BAT-specific RetSat knockout mouse model genotyping

3.6.3.1 Genomic DNA isolation

The ear biopsy from the weaned mouse was placed in a tube with DNA isolation mix including tailcut buffer with 0.6 mg/ml proteinase K, and heated at 55°C overnight. The next day, sample was heated at 95°C for an additional 10 min and cooled down at -20°C for 10 min. Finally, TE buffer with RNaseA 1.3 µ/ml was added to the sample to promote RNA denaturing, after centrifugation at 16,000g for 3 min, the DNA in the supernatant was ready for the polymerase chain reaction (PCR) reaction.

3.6.3.2 Polymerase chain reaction

The PCR allows DNA fragments *in vitro* amplification rapidly with primers and DNA polymerase on thermal cycling. For each mouse, 1 μ l DNA template was mixed with a 19 μ l mix including primer, 5 x PCR master mix “ready-to-load”, and ultrapure distilled water (upH₂O) as indicated in **Table 16**. The mixture was placed in the thermal cycler, and the program is indicated in **Table 17**.

Table 16. PCR mastermix

Reagent	Volume	Final Concentration
DNA template	1 μ l	-
Forward primer (10 μ M)	0.8 μ l	200 nM
Reverse primer (10 μ M)	0.8 μ l	200 nM
5 x PCR master mix “ready-to-load”	4 μ l	1x
upH ₂ O	13.4 μ l	-
Total volume	20 μ l	-

Table 17. PCR program

Program	Temperature	Time	Cycle
Initial denaturation	94°C	2 min	-
Amplification	94°C	15 s	36
	59.5°C	1 min	
	72°C	1 min	
Primer annealing	72°C	5 min	-

3.6.3.3 Agarose gel electrophoresis

Agarose gel electrophoresis is used to separate DNA fragments based on size. The prepared agarose gel with nucleic acid dye was placed in an electrophoresis tank, and samples mixed with loading dye were loaded in one end of the gel which was immersed

in TAE buffer. DNA migrated through pores of gel to the positively charged electrode when electrical current was applied. The resulting bands were visualized under ultraviolet (UV) light.

3.6.4 Mice sacrifice and sample collection

The mice were anesthetized deeply by Isoflurane and then sacrificed by cervical dislocation. The whole blood was drawn out by cardiac puncture immediately and allowed to clot for 30 min at room temperature on benchtop, followed by centrifugation at 16,000 g for 15 min at 4°C, serum on the top was collected. After serum collection, the tissues were weighed and immediately frozen in liquid nitrogen, and all samples were stored at -80°C until analysis.

3.6.5 Metabolism phenotype characterization

3.6.5.1 Diet challenge, weekly body weight and body composition

In the indicated cohorts, the 10-week age mice were challenged by high-fat diet for 12 weeks, and body weight was monitored weekly. Nuclear Magnetic Resonance (NMR) analysis was taken to determine mouse body composition in the time-domain nuclear magnetic resonance (TD-NMR) system.

3.6.5.2 Tolerance test

The fed blood glucose level was recorded, and then mice were transferred into the single cages and free to water without food. For the intraperitoneal glucose tolerance test (ipGTT), after 16 h fasting, the lean and obese mice received 2 g/kg or 0.5 g/kg glucose intraperitoneal injection, respectively. For the intraperitoneal insulin tolerance test (ipITT), after 4 h fasting, the lean and obese mice received 0.5 U/kg or 0.75 U/kg glucose intraperitoneal injection, respectively. The blood glucose from the tail vein was monitored before injection and 15 min, 30 min, 60 min, 90 min after injection by CONTOUR®NEXT glucose strips.

3.6.5.3 β 3-adrenergic receptor agonist injection

Mice were intraperitoneally injected with CL 316, 243 (1 mg/kg body weight), a potent and highly selective β 3A for 10 consecutive days. While control mice were intraperitoneally injected with a vehicle of sterile PBS. All mice were sacrificed on the

last day and samples were collected.

3.6.5.4 Acute cold exposure

The core body temperature of mice was measured by the rectal probe thermometer at room temperature. Subsequently, each mouse was placed alone in the climate chamber at 4°C for 3h, rectal temperature was monitored every hour. After cold exposure, mice were sacrificed immediately and samples were collected.

3.6.6 Histology

3.6.6.1 Tissue fixation, embedding, and sectioning

The iBAT was harvested from mice, placed into cassette, and immediately submerged in 4% buffered Formaldehyde at 4°C overnight for fixation. Subsequently, the tissue underwent a series of gradient ascent Ethanol (70%, 96%, 100%) and Acetone in incubator at 60°C for dehydration, and embedded in paraffin by paraffin wax machine. After solidification, the tissue is sectioned into 5 µm using a microtome, and stored at room temperature until staining.

3.6.6.2 Deparaffinization and hematoxylin-eosin staining

The size of individual adipocytes in adipose tissue can be investigated by Hematoxylin and Eosin (H&E) staining. The section was rehydrated by passing Xylene and gradually decreased Ethanol (100%, 96%, 80%, 70%) to ddH₂O, then dipped in Hematoxylin for nuclear staining. Subsequently, the section was rinsed with tap water for 5 min, and dipped in Eosin for counterstain, rinsed with tap water again. Finally, the section was dehydrated in increasing concentrations of Ethanol (70%, 80%, 96%, and 100%) and Xylene, mounted in DPX media for observation under the microscope. Since the lipids are extracted by Ethanol in dehydration, the vacuoles appear to be empty.

3.7 Real-time quantitative polymerase chain reaction (RT-qPCR)

Real-time quantitative polymerase chain reaction (RT-qPCR) is a universally quantitative method to monitor DNA amplification in real-time, based on the polymerase chain reaction principle. The double-stranded DNA was labeled with non-specific fluorescent dyes, and gene expression was detected by complementary DNA

(cDNA) copy number sensitively.

3.7.1 RNA extraction

3.7.1.1 Adipocyte RNA extraction

The adipocyte RNA extraction is followed by the manufacturer's instruction of PeqGOLD total RNA kit (13-6834-02P, VWR). Cell harvesting was conducted by rinsing the bottom of the plate with TRK Lysis Buffer and homogenizing cells in the homogenizer column. The filtrate was mixed thoroughly with the same amount of 70% Ethanol to precipitate RNA, then the RNA bound to silica-based matrix was rinsed by Wash Buffer I and 80% Ethanol in Mini Column to dissolve residual salt, finally RNA was eluted in 30 μ l RNase-free water and transferred to a 1.5 ml tube.

3.7.1.2 Adipose tissue RNA extraction

In the 1.5 ml tube, approximately 50 mg of frozen brown adipose tissue was homogenized in 400 μ l QIAzol reagent sufficiently. Additional 600 μ l QIAzol reagent was added and placed at room temperature for 5 min. Subsequently, added 200 μ l Chloroform, and vortex the mixture for 15 s vigorously, followed by staying at room temperature for 5 min and centrifuging at 16,000 g for 15 min under 4°C. The RNA-rich upper aquatic phase was transferred into another 1.5 ml tube. The following steps were according to the manufacturer's instruction of kit. The aqueous phase was mixed with the same volume of 70 % Ethanol to precipitate RNA, transferred the solution to RNeasy Spin column, centrifuged the column, and discarded the filtrate. The RNA bound to the silica-based matrix was rinsed by RW1 and RPE buffer. Finally, RNA was eluted in 30 μ l RNase-free water and transferred to a 1.5 ml tube.

All RNA samples were kept at -80°C and concentration was measured by NanoDrop ND-1000 spectrometer.

3.7.2 cDNA synthesis

To synthesize first-strand cDNA from RNA, based on the concentration, the same amount of RNA (0.1-1 μ g) from each sample of the same set was mixed with 100 ng random hexamer primer and upH₂O, to the volume of 15 μ l. The mixture was heated at 70°C for 5 min to melt the secondary structure and then immediately cooled at 4°C for 15 min. After that, the RNA sample was complemented with Master Mix including

M-MLV reaction buffer, dNTP mix, M-MLV reverse transcriptase, upH₂O, and reverse transcription at 37°C for 1 h, as shown in **Table 18**. The synthesized cDNA was applied for the following RT-qPCR.

Table 18. Reverse transcriptase master mix

Reagent	Volume	Final Concentration
M-MLV Reaction Buffer (5x)	5 µl	1x
dNTPmix (10 mM)	1.25 µl	0.5 mM
upH ₂ O	2.75 µl	-
M-MLV Reverse Transcriptase	1 µl	200 U
Total volume	10 µl	-

3.7.3 RT-qPCR process

To obtain a standard curve, 5 µl cDNA from each sample of a set was mixed and then diluted consecutively to 10%, 1%, and 0.1%. The remaining cDNA was diluted 1:10 with upH₂O. 2 µl diluted cDNA template was loaded in the 96- or 384- well qPCR plate with duplicated wells, and the prepared master mix (**Table 19**) was loaded into the according wells. The RT-qPCR program was run in CFX Connect Real-Time System (**Table 20**). Finally, the gene expression was calculated with reference to the standard curve, and the relative mRNA level was quantified in relation to the housekeeping gene.

Table 19. RT-qPCR master mix

Reagent	Volume	Final Concentration
Forward primer (5 µM)	0.1 µl	200 nM
Reverse primer (5 µM)	0.1 µl	200 nM
2 x Fast Start Universal SYBR Green	2.5 µl	1x
upH ₂ O	0.3 µl	-
Total volume	3 µl	-

Table 20. RT-qPCR program

Program	Temperature	Time	Cycle
Initial denaturation	95°C	10 min	-
DNA denaturing, primer hybridization and amplification	95°C	10 s	40
Primer annealing	60°C	1 min	
Melting curve	95°C	30 s	-
	70°C→90°C	5 s	

3.8 Immunoblotting

Immunoblotting is a regular method to identify the abundance of the specific target protein within a complex mixture of proteins isolated from tissue homogenate or cell lysate.

3.8.1 Protein extraction

3.8.1.1 Protein extraction from cultured cells

After media collection, the cells in the 12-well plate were washed with pre-chilled PBS, then scraped from the well bottom gently and collected into the 1.5 ml tube with PBS. Mixture was centrifuged at 16,000 g for 3 min. The supernatant was removed and loaded with adequate RIPA buffer to reconstitute the cell pellet. For sonication, the cells were lysed by sound energy, and the cell lysate was centrifuged at 16,000 g and for at least 40 min. The supernatant was collected carefully, that is cell protein, was kept at -80°C.

3.8.1.2 Protein extraction from frozen tissue

Approximately 50 mg of frozen tissue in the 1.5 ml tube on ice was homogenized with 400 µl RIPA buffer by the micro pestle. The subsequent centrifugation is the same with 3.8.1.1 protein extraction from cultured cells.

3.8.2 Total protein quantification

The Pierce™ BCA Protein Assay Kit (23225, Thermo Scientific) was applied for total protein concentration measurement. The working solution was mixed with reagents A and B (50:1) freshly. 5 µl BCA standard provided in the kit and protein were loaded into 96-well plate, and then 95 µl working solution was loaded. The plate was horizontally shaken and incubated at 37 °C for 30 min. The absorbance was measured at 562 nm using spectrophotometer. Finally, the protein concentration of the sample was calculated with reference to the stand curve.

3.8.3 Semi-quantitative analysis of immunoblotting signals

Sodium Dodecyl Sulfate-Polyacrylamide Gel Electrophoresis (SDS-PAGE) is a method to separate proteins based on their molecular weight. SDS-PAGE Gel was prepared according to the interested protein molecular weight to allow for proper protein separation (**Figure 21**).

Table 21. Sodium Dodecyl Sulfate-Polyacrylamide 1.5 mm thick gel composition

Reagent	10% resolving gel	12% resolving gel	stacking gel
ddH ₂ O	4.1 ml	3.4 ml	3.05 ml
1.5 M TRIS HCL buffer (pH 8.8)	2.5 ml	2.5 ml	-
0.5 M TRIS HCL buffer (pH 6.8)	-	-	1.25 ml
10% SDS	100 µl	100 µl	50 µl
30% Acrylamide	3.3 ml	4 ml	0.65 ml
10% APS	75 µl	75 µl	50 µl
TEMED	7.5 µl	7.5 µl	6 µl

Loading the prepared resolving gel mix into the assembled gel solidification, gently added a layer of 2-Propanol on the top to remove bubbles and prevent drying, and let the resolving gel stay at room temperature for 45 min until polymerized stably. After pouring out the 2-Propanol and drying the space, overlaid the stacking gel mix and inserted the 15-well comb on the top, waiting another 45 min at room temperature. The

gel was wrapped in wet tissue and stabilized overnight at 4°C for next-day electrophoresis.

After adjusting the protein amount of a set of samples by the concentration, 10-20 µg protein and proper volume RIPA buffer were mixed with 5x loading buffer adequately. The protein mixture was denatured at 95 °C for 10 min, and centrifuged at 16,000 g for 30 min. Gel was placed inside the holder of the electrophoresis which was filled with electrophoresis buffer. 20 µl sample mix was loaded into each well of gel, started electrophoresis at 80V, and turn the voltage to 120 V when the dye front reached the dissolving gel. When the protein separated adequately, the electrotransfer was performed immediately. The order of the stuff in the cassette is bottom sponge, 2 layers of Whatman filter paper, activated PVDF membrane, SDS-PAGE, another 2 layers of Whatman filter paper, and top sponge. The electrotransfer ran at 4°C overnight with 29 V in the transfer apparatus filled with transfer buffer.

The Ponceau S staining was conducted first next day, the PVDF membrane was dehydrated in 100% Methanol for 15 s and air-dried totally, then reactivated again, stained by 0.1% Ponceau S stain with 1% Acetic acid for 10 min, and scanned. The remaining traces of Ponceau S was washed out by 0.1 M NaOH solution, and the PVDF membrane was blocked by 4% skim milk immediately at room temperature for 1h. Subsequently, the membrane was incubated in the primary antibody diluted in 4% skim milk overnight at 4 °C, followed by the proper horseradish peroxidase (HRP) conjugated secondary antibody for 1 h at room temperature. The results were detected and imaged by the Bio-rad ChemiDoc imaging system after enhanced chemiluminescence (ECL) substrate solution incubation. Densitometric analyses were performed by ImageJ (161).

3.9 RNA-Sequencing

The iBAT of five Cre- mice and another five Cre+ mice under normal chow at room temperature were taken to the RNA sequencing. The total RNA isolation was described as 3.7.1.2.

3.9.1 RNA concentration and purification

In order to apply the high-quality RNA to the sequencing, the RNA was highly concentrated and purified by the RNA Clean & Concentrator kit (R1014, Zymo

Research). The process was followed by the instruction of the manufacturer. The 15 μ l total RNA from each mouse was mixed with 30 μ l RNA Binding Buffer, and then mixed with additional 45 μ l 100% Ethanol. The mixture was transferred to Zymo-Spin™ IC Column with collection tube, and centrifuge at 16,000 g for 3 min, the flow-through was discarded. To do the DNase I treatment, 40 μ l DNase I reaction mix (**Table 22**) was added to the column matrix and incubated at room temperature for 15 min. Subsequently, the RNA bound to the column matrix was washed by 400 μ l RNA Prep Buffer and 2 rounds of 700 μ l RNA Wash Buffer, finally, 15 μ l DNase/RNase-free Water was loaded and centrifuged to elute the RNA. The ultra-pure RNA was purity checked again and kept at -80°C until further analysis.

Table 22. DNase I reaction mix

Reagent	Volume
DNase I (1 U/ μ l)	5 μ l
DNA Digestion Buffer	35 μ l
Total volume	40 μ l

3.9.2 Sequencing and data analysis

The RNA sequencing process was performed by Core Unit Genomics, Berlin Institute of Health at Charité. Briefly, the purity and integrity of RNA were assessed, mature mRNA was selected, library was prepared, and sequencing was performed. The DESeq2 package was employed to identify the differentially expressed genes with Ensembl annotation, gene symbol, log₂ FC, P-value, and false discovery rate (FDR). Subsequently, the data was corrected for multiple testing via default parameters by Benjamini–Hochberg method. Pathway and gene ontology enrichment were analyzed by DAVID (162).

3.10 Statistics

All data were expressed as mean \pm standard error of mean (SEM). The *in vitro* experiments were performed at least three times with similar results, and a representative result was selected. Unpaired two-tailed Student's t-test was applied to test the significance between two groups, one-way or two-way Analysis of Variance

(ANOVA) was applied to test the significance among more than two groups. $P < 0.05$ were considered statistically significant.

4 Results

4.1 RetSat is highly expressed in brown adipose tissue

To investigate the function of RetSat, its expression across tissues and cells was analyzed thoroughly by BioGPS, an online database that collects microarray data from Gene Expression Omnibus (163). By searching, *RetSat* is widely distributed and **Figure 10A** displays the top 10 high-expression tissues or cells in mice. Specifically, RetSat is highest expressed in the liver, followed by kidney or BAT. The immunoblotting results confirmed the strong expression of RETSAT protein in iBAT, which also showed the highest UCP1 abundance as known (**Figure 10B**), implying RetSat might serve a prominent role in the BAT function in mice.

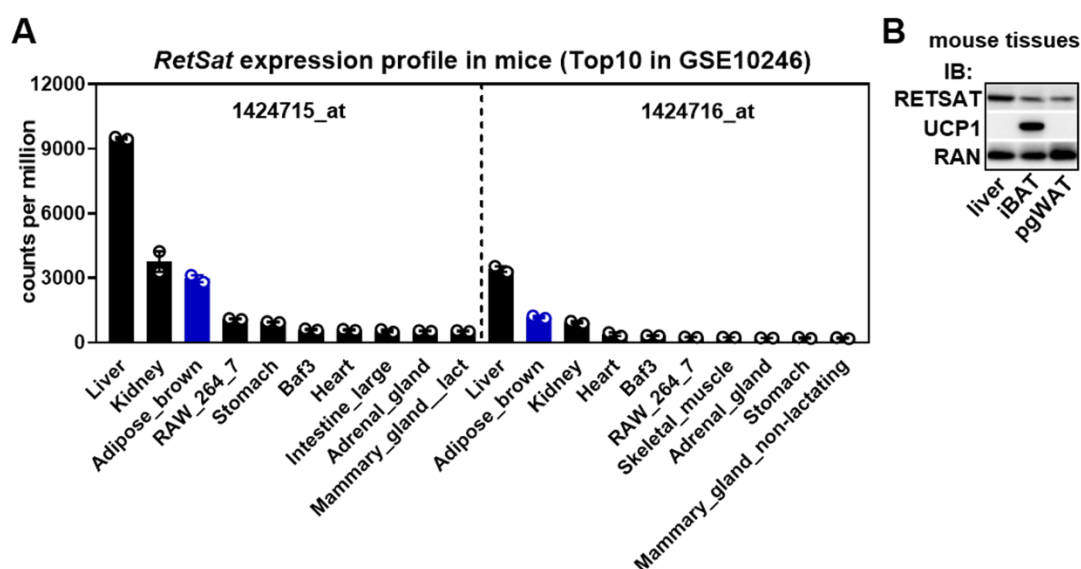


Figure 10. RetSat is highly expressed in brown adipose tissue. A) *RetSat* expression profile in mice. Gene expression profile of murine *RetSat* from BioGPS (probesets 1424715_at and 1424716_at). B) Protein expression of RETSAT and UCP1 in murine liver, BAT, and pgWAT was analyzed by immunoblotting. RAN protein served as loading control.

4.2 RetSat is induced by β -adrenergic stimulation

Since RETSAT protein was robustly induced in iBAT of cold-acclimated mice, and the β -AR of brown adipocytes is activated by Norepinephrine released from sympathetic nerve when cold exposure, whether β -AR stimulation induces RetSat was investigated. To study the *in vitro* effect, differentiated primary preadipocytes from SVF isolated from iBAT and ingWAT of wild-type mice, and iBACs and 3T3-L1 adipocytes were stimulated by Isoproterenol, non-selective β A, for 24-48h. As expected, *RetSat* mRNA expression was elevated in above stimulated adipocytes at different magnitudes (**Figure 11A**). C57BL/6J male mice were intraperitoneally injected with CL 316, 243, a specific β 3A, or vehicle PBS for consecutive 10 days upon normal chow. In line with *in vitro* results, RETSAT protein expression was induced by β 3-adrenergic stimulation in iBAT in a similar manner to UCP1 (**Figure 11B, upper panel**), even a stronger induction was detected in ingWAT (**Figure 11B, lower panel**), where is known to have significant thermogenic capacity upon appropriate stimulations. These findings further confirmed that RetSat is induced by β -adrenergic stimulation.

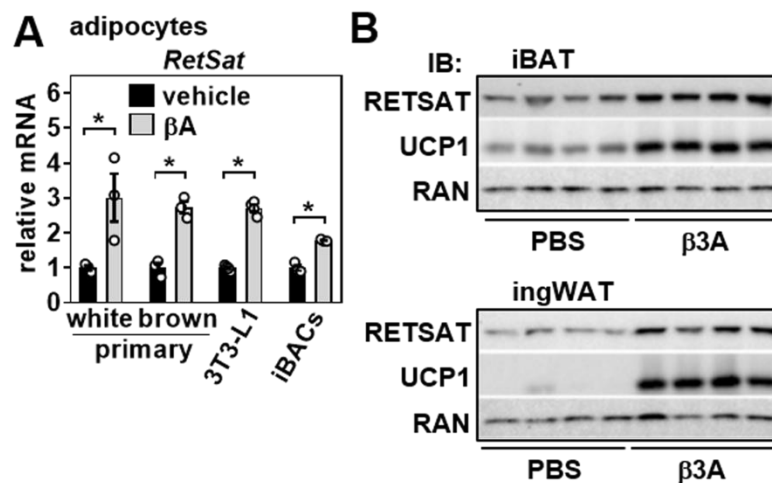


Figure 11. RetSat is induced by β -adrenergic stimulation. A) Differentiated primary white and brown adipocytes were incubated with pan- β -AR agonist Isoproterenol for 24 (primary adipocytes, 3T3-L1) or 48 hours (iBACs) and mRNA expression of *RetSat* determined by qPCR. B) protein expression of RETSAT and UCP1 determined. RAN protein served as loading control. The data are presented as individual data points and mean \pm sem, * P <0.05.

4.3 RetSat is up-regulated during brown adipocyte differentiation

It was reported that RetSat is induced during the differentiation of white 3T3-L1 adipocytes. To analyze whether RetSat is regulated during the differentiation of brown adipocytes, iBACs preadipocytes (day 0) and adipocytes (day 7) were compared. The degree of differentiation was directly observed by Oil red O staining, as shown in **top panel of Figure 12A**, iBACs adipocytes were full of lipid droplets, indicating preadipocytes were adequately differentiated into mature adipocytes by adipogenic induction cocktail. The robust adipogenesis marker PPAR γ and thermogenesis maker UCP1 protein expression in the iBACs adipocytes validated the differentiation (**Figure 12A, bottom panel**), As expected, RETSAT protein was strongly expressed in the iBACs adipocytes compared to preadipocytes. Moreover, the different expressed pattern of RetSat was confirmed by the indicated gene expression in **Figure 12B**. These results suggest RetSat is up-regulated during brown adipocyte differentiation, in a similar manner to the differentiation of white 3T3-L1 adipocytes.

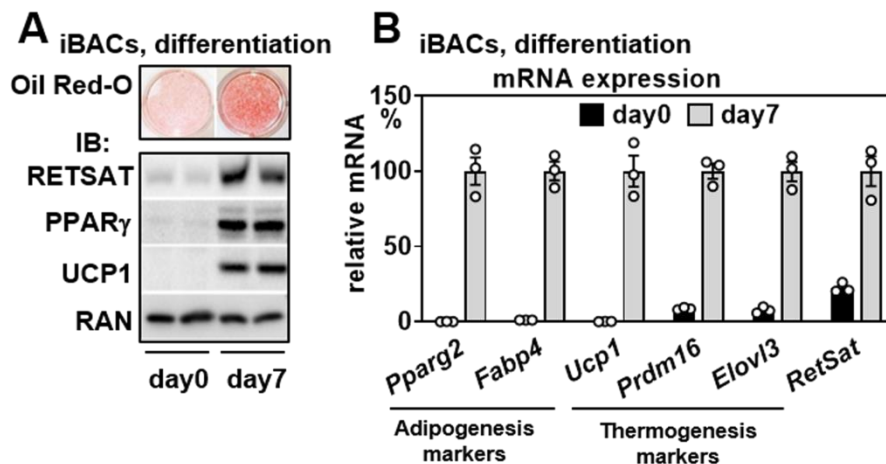


Figure 12. RetSat is up-regulated during differentiation of brown adipocytes.

Immortalized brown adipocytes (iBACs) were analyzed for A) intracellular lipids by Oil Red-O staining (top panel) and protein expression of RETSAT, PPAR γ , and UCP1 before (day 0) and after (day 7) differentiation (bottom panel). RAN protein served as loading control. B) Cells described in A) were analyzed for mRNA expression of the indicated genes. The data are presented as individual data points and mean \pm sem, * P <0.05

4.4 RetSat depletion does not impair brown adipocyte differentiation

The previous study showed RetSat is required for 3T3-L1 adipocyte differentiation, and whether the effect is present in iBACs was investigated. RetSat siRNA delivered into iBACs preadipocytes by electroporation led to depletion, and nontargeted oligo was as control, two independent RetSat oligos were used to double exam the effect (**Figure 13A**). Since RetSat is controlled by PPAR γ , which plays dominant role in adipogenesis, electroporated iBACs preadipocytes were differentiated by suboptimal condition, that is without PPAR γ agonist Pioglitazone, until day 7. The effect of RetSat depletion in iBACs differentiation was assessed by phase-contrast microscopy and known adipogenesis and thermogenesis makers. The iBACs adipocytes with either of RetSat siRNA both showed mildly less extent of differentiation compared to the adipocytes with control oligo under microscope (**Figure 13B**). *Pparg2*, *Fabp4*, and *Elovl3* mRNA were not strongly changed during the iBACs differentiation, whereas *Ucp1* mRNA was significantly down-regulated in the differentiated adipocytes with one of the RetSat siRNAs (**Figure 13C**).

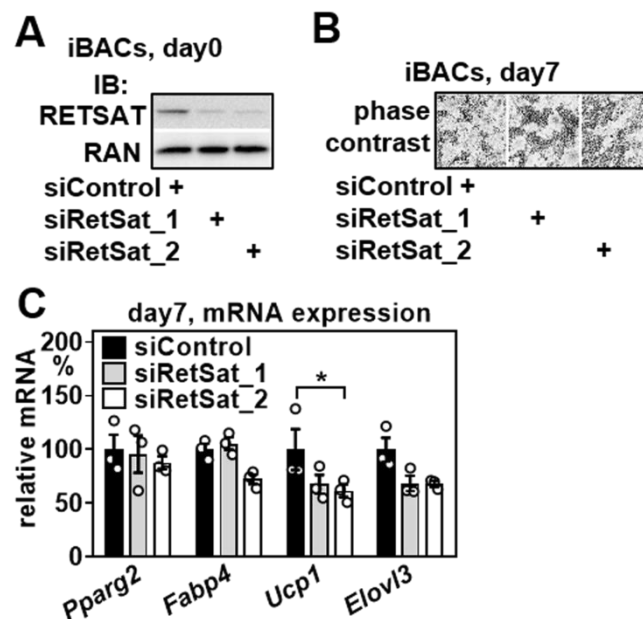


Figure 13. RetSat depletion does not impair brown adipocyte differentiation. A) Undifferentiated iBACs were electroporated with indicated siRNA and protein expression of RETSAT was analyzed, RAN protein served as loading control. Cells were differentiated and adipocytic conversion was assessed by B) phase contrast microscopy and C) mRNA expression of the indicated genes. The data are presented

as individual data points and mean±sem, * P <0.05.

4.5 RetSat over-expression slightly enhances brown adipocyte differentiation

Since RetSat was also reported to increase PPAR γ transcriptional activity and adipogenesis in 3T3-L1 cells, to study the hypothesis that RetSat enhances the adipogenesis in brown adipocytes, its expression was overexpressed in iBACs preadipocytes. Specifically, pre-confluent iBACs preadipocytes were infected with retrovirus-RetSat, which was generated as previously, to overexpress RetSat expression, and retrovirus-empty infection as control. The ectopic expression efficiency was validated by immunoblotting before starting differentiation, as shown in **Figure 14A**, RETSAT protein was robustly induced by retrovirus in preadipocytes. The infected iBACs preadipocytes underwent suboptimal differentiation condition without Pioglitazone and the effect of RetSat overexpression in differentiation was determined by phase-contrast microscopy and known adipogenesis and thermogenesis makers. The stronger degree of differentiation was observed in the differentiated iBACs adipocytes with retrovirus-RetSat upon microscope (**Figure 14B**). The RetSat overexpressed in iBACs preadipocytes led to significantly induced *Fabp4* and *Elovl3* mRNA expression during differentiation, and an increased trend in *Pparg2* and *Ucp1* mRNA (**Figure 14C**), suggesting RetSat slightly promotes brown adipocytes adipogenesis and concomitant thermogenesis genes.

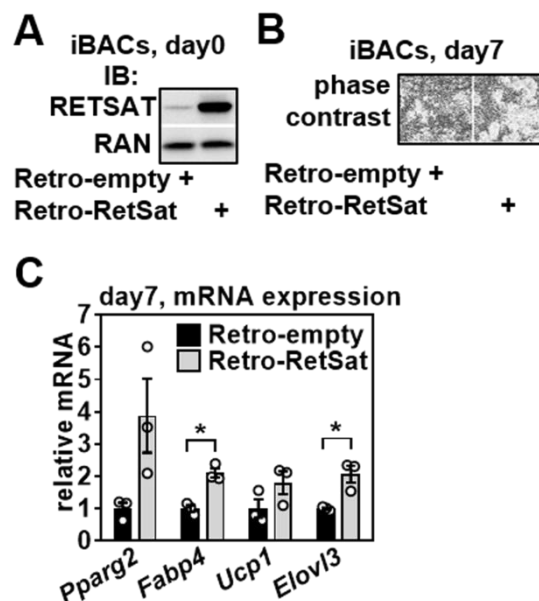


Figure 14. RetSat over-expression slightly enhances brown adipocyte differentiation. A) Undifferentiated iBACs were infected with empty or RetSat-encoding retroviruses and protein expression of RETSAT was analyzed, RAN protein served as loading control. Cells were differentiated in the absence of the PPAR γ agonist Pioglitazone and adipocytic conversion was assessed by B) phase contrast microscopy and C) mRNA expression of the indicated genes. The data are presented as individual data points and mean \pm sem, * P <0.05.

4.6 RetSat is required for the thermogenic gene expression in immortalized brown adipocytes

Thermogenesis is the primary characteristic of brown adipocytes, and RetSat mildly enhances thermogenesis gene expression, the hypothesis that whether RetSat is required for the thermogenic gene expression in iBACs adipocytes was explored. To this end, RetSat was knocked down in iBACs adipocytes by electroporation with two different oligos, 72h later, cells received the β A Isoproterenol stimulation for 4h, finally gene expression was compared. Although, *Pparg2* mRNA showed comparable expression when *RetSat* was depleted by 70~80% (**Figure 15A**), strikingly, thermogenesis genes *Ucp1*, *Cidea*, *Elovl3*, and *Adrb3* expression were reduced by RetSat depletion. Moreover, the reduction was observed in iBACs adipocytes with either of two RetSat siRNA oligos. More importantly, this reduction was reproduced in the β A Isoproterenol stimulated iBACs adipocytes, that is activated brown adipocytes (**Figure 15B**). Furthermore, the effect of RetSat depletion was validated by down-regulation of the most important mitochondrial uncoupling protein, UCP1 (**Figure 15C and D**), and the reduced UCP1 protein in the iBACs was sustained for at least 7 days (**Figure 15E**). The mRNA expression of mitochondria gene cytochrome c oxidase subunit 7a1 (*Cox7a1*), which is a cold-responsive protein (164), also reduced in the RetSat depleted iBACs adipocytes (**Figure 15F**). These findings demonstrate RetSat is required for thermogenic gene expression in both basal and activated immortalized brown adipocytes.

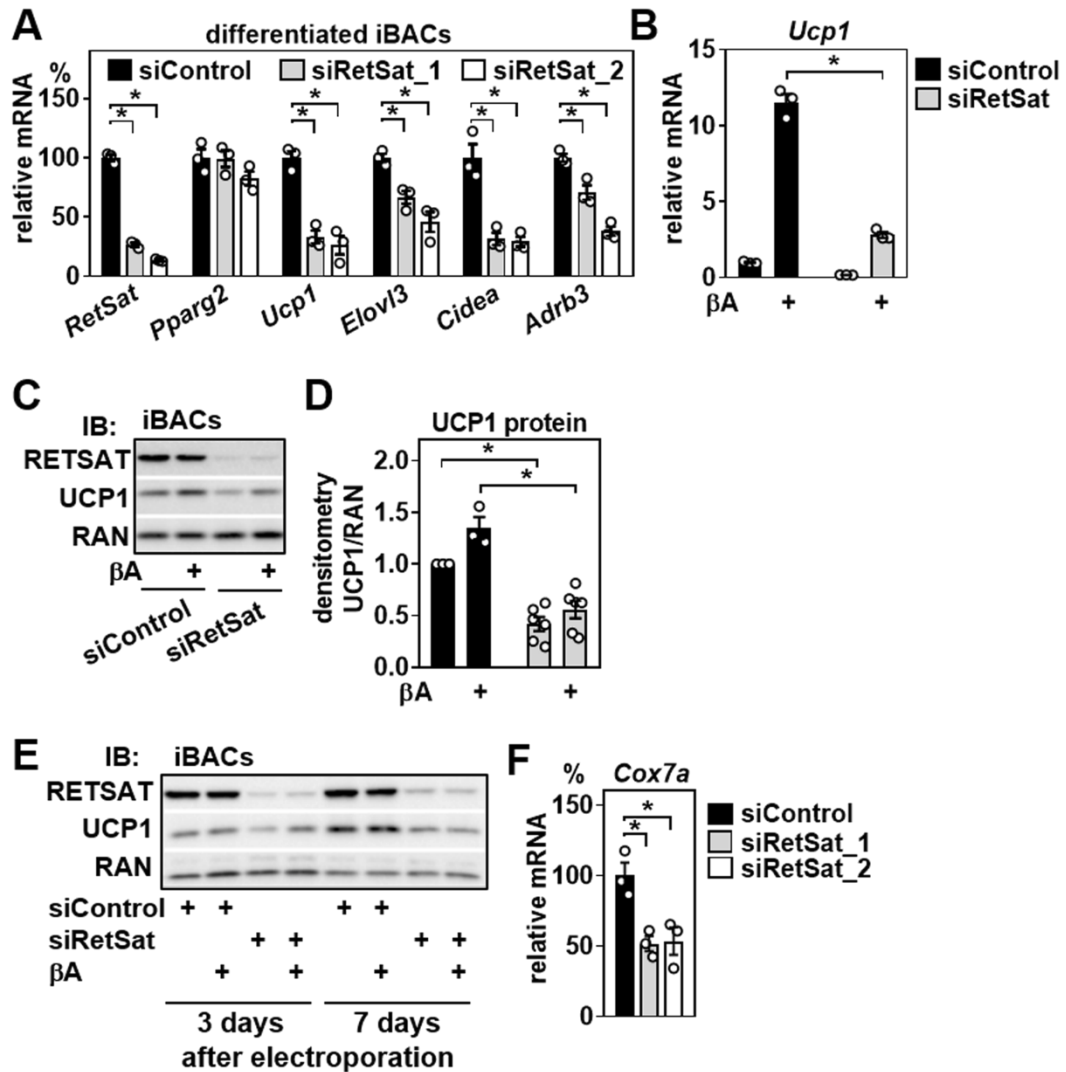


Figure 15. RetSat is required for thermogenic gene expression in immortalized brown adipocytes. A) Differentiated immortalized brown adipocytes (iBACs) were electroporated with indicated siRNA and mRNA expression of *RetSat*, *Pparg2*, and thermogenic genes was determined by qPCR. B) Differentiated iBACs were depleted of RetSat by siRNA and exposed to 10 μ M of the pan- β A Isoproterenol for 4 hours. *Ucp1* mRNA expression was analyzed by qPCR. C) RETSAT and UCP1 protein expression of cells described in B) was determined by immunoblotting. RAN served as loading control. D) Densitometric analysis of UCP1 protein shown in C). E) Differentiated immortalized brown adipocytes (iBACs) were electroporated with indicated siRNA. After indicated time, cells were exposed to the pan- β A isoproterenol for 4 hours and protein expression of RETSAT and UCP1 was determined by immunoblotting. RAN served as loading control. F) *Cox7a1* mRNA expression in iBACs

described in A) was analyzed by qPCR. Data are presented as individual data points and mean±sem, * P <0.05.

4.7 RetSat is required for thermogenesis gene expression in primary brown adipocytes

Since primary cell culture mimics the physiological state of cells *in vivo* more closely and generates more biologically relevant data, whether the reduction of thermogenesis genes led by RetSat depletion could be reproduced in cultured primary brown adipocytes was investigated. Although RetSat merely has slight effect on the brown adipocyte differentiation, in order to exclude its possible existed impairment on thermogenesis, SVF was isolated from the iBAT of RetSat flox/flox mice. Then primary preadipocytes, which take the highest percentage within SVF, were thoroughly differentiated into mature adipocytes. Subsequently, RetSat floxed primary brown adipocytes were infected with adenovirus Cre to knockout RetSat, infection with adenovirus GFP as control, and gene expression was compared after 96h. The fluorescence and morphology were observed on harvesting day, as shown in **upper panel of Figure 16A**, adenoviral GFP-infected primary brown adipocytes emitted green fluorescence upon blue light, and no fluorescence was found in primary brown adipocytes with adenovirus Cre. Moreover, adenovirus infection did not alter adipocyte morphology (**Figure 16A, lower panel**). The knockout efficiency was validated by immunoblotting in **Figure 16B**, RETSAT protein was almost not detectable in adenovirus Cre-infected primary brown adipocytes. RetSat ablation led to reduced *Ucp1* and *Elovl3* mRNA expression, and the decrease was also observed in Isoproterenol stress condition, namely, activated primary brown adipocytes (**Figure 16C**). These data further confirm the effect of RetSat depletion on the thermogenesis gene expression in brown adipocytes.

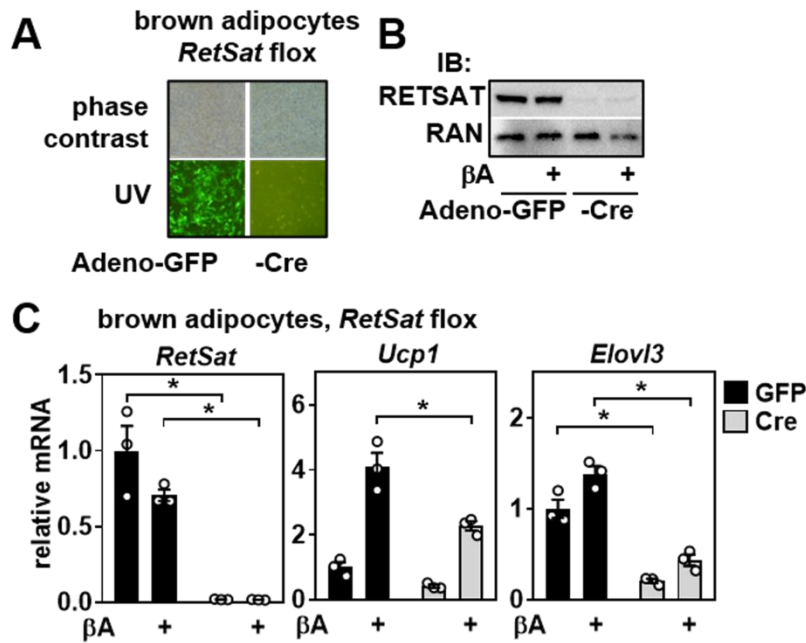


Figure 16. RetSat is required for thermogenic gene expression in primary brown adipocytes. A) Primary brown adipocytes with floxed *RetSat* alleles were infected with adenoviruses expressing Cre recombinase or GFP. 4 days later, fluorescence was recorded, then B) adipocytes were incubated with 10 μM βA for 4 hours and protein expression of RETSAT was determined by immunoblotting, RAN served as loading control. C) mRNA expression of *RetSat*, *Ucp1*, and *Elovl3* was analyzed by qPCR. Data are presented as individual data points and mean \pm sem, * $P < 0.05$.

4.8 RetSat ablation reduces mitochondrial respiration in primary brown adipocytes

Since RetSat depletion decreases UCP1 expression, which is located in mitochondrial inner membrane and produces heat by proton diffusion, the effect of RetSat on mitochondria function was investigated. As shown in **Figure 15F**, mitochondria gene *Cox7a1* mRNA was down-regulated in RetSat knocked down iBACs adipocytes, suggesting RetSat is required for mitochondrial gene expression in brown adipocytes. The respiration in mitochondria ensures the coupling of oxidative phosphorylation and ATP synthesis, thus, OCR of primary brown adipocytes with adenovirus-GFP or -Cre in basal condition was real-time monitored by Seahorse XF96 Flux Analyzer via sequential injection of Oligomycin, FCCP, and Antimycin A/Rotenone. Interestingly, RetSat ablation primary brown adipocytes showed significantly lower OCR, particularly after mitochondrial oxidative phosphorylation uncoupler FCCP injection (**Figure 17**,

left panel). As for calculated respiratory parameters, RetSat knockout resulted in a significant decrease in maximal respiration, and spare respiration capacity (**Figure 17, right panel**), suggesting RetSat ablation impairs mitochondria respiration in primary brown adipocytes.

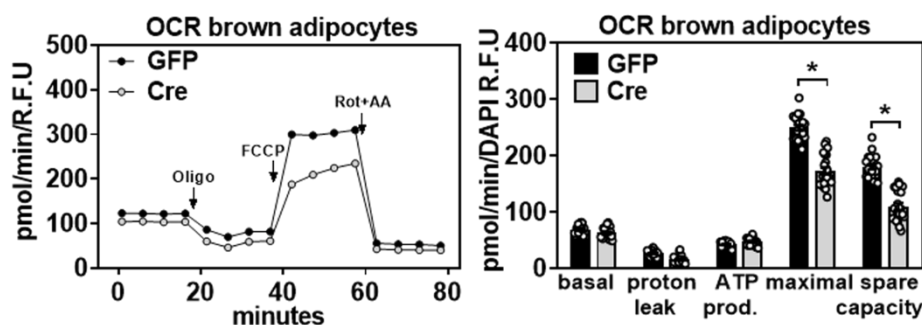


Figure 17. RetSat ablation reduces mitochondrial respiration in primary brown adipocytes. Oxygen consumption rate (OCR) of primary brown adipocytes with or without RetSat deletion was analyzed by Seahorse XF Analyzer (left panel) and evaluated stage-specifically (right panel). Data are presented as individual data points and mean \pm sem, * P <0.05.

4.9 RetSat is required for 3T3-L1 adipocytes browning

Since the effect of RetSat on the thermogenesis gene expression in brown adipocytes, the hypothesis that RetSat effects browning of 3T3-L1 adipocytes was made. Thereby, RetSat expression was interfered via two independent siRNA oligos in mature 3T3-L1 adipocytes by electroporation, followed by PPAR γ agonist Pioglitazone 72h incubation and additional β A Isoproterenol 6h stimulation to induce browning (**Figure 18A**). Pharmacological stimulation of PPAR γ and β -AR robustly elevated *Ucp1*, *Elovl3*, and *Cidea* mRNA expression in 3T3-L1 adipocytes, which resemble brown adipocytes thermogenetic phenotype. RetSat depletion resulted in a significant decrease in induced thermogenetic genes *Ucp1*, *Elovl3*, and *Cidea* mRNA upon browning induction (**Figure 18B**). As shown in **Figure 18C**, UCP1 protein expression was not detectable in 3T3-L1 adipocytes in basal or PPAR γ agonist stimulated conditions. In accordance with gene expression, RetSat knocked down 3T3-L1 adipocytes had weaker UCP1 protein expression upon thermogenic stimulators. Additionally, RetSat depletion led to down-regulated mitochondrial gene *Cox7a1* mRNA expression (**Figure 18D**).

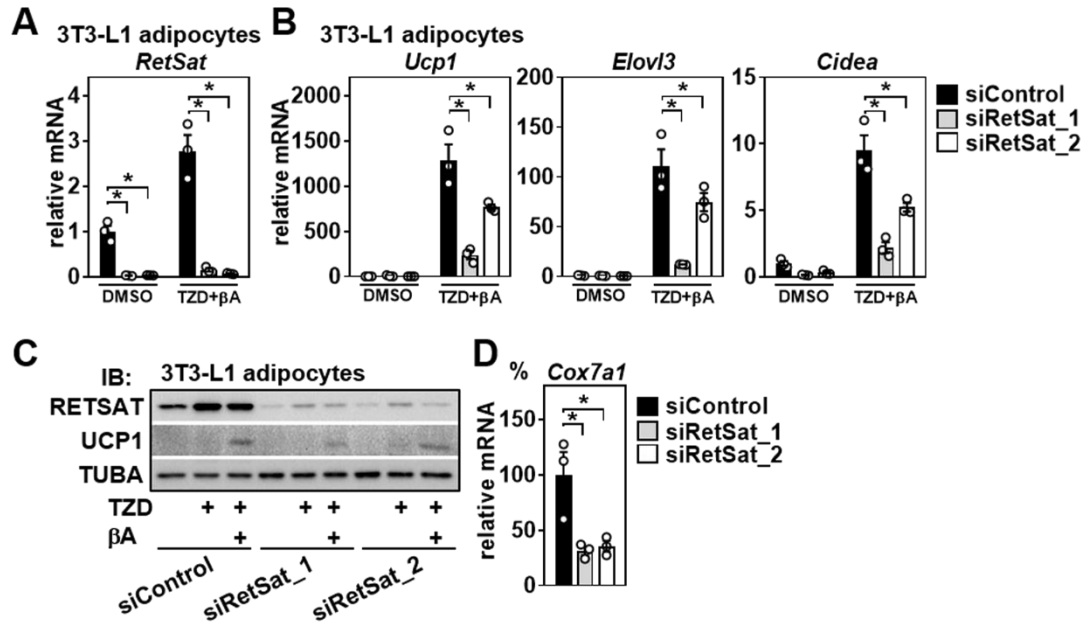


Figure 18. RetSat is required for browning of 3T3-L1 adipocytes. Differentiated 3T3-L1 adipocytes were electroporated with indicated siRNA, incubated with vehicle or the thiazolidinone (TZD) pioglitazone for 72 hours and pan-βA Isoproterenol for the final 6 hours, mRNA expression of A) RetSat and B) thermogenic genes determined by qPCR. C) Expression of RETSAT and UCP1 protein of cells described in A) was determined by immunoblotting. TUBA served as loading control. D) Differentiated 3T3-L1 adipocytes were electroporated with indicated siRNA, and mRNA expression of *Cox7a1* was analyzed by qPCR. Data are presented as individual data points and mean±sem, * $P < 0.05$.

4.10 RetSat depletion reduces mitochondrial respiration in 3T3-L1 adipocytes

To study effect of RetSat on mitochondrial respiration in basal 3T3-L1 adipocytes, OCR was determined by extracellular flux analysis. As shown in **left panel of Figure 19**, RetSat-depleted 3T3-L1 adipocytes had lower OCR during the whole process. Particularly, RetSat knockdown caused reduced basal respiration, maximal respiration, and spare respiration capacity, with a trend towards decreased OCR during ATP production (**Figure 19, right panel**), providing evidence that RetSat depletion reduces mitochondrial activity.

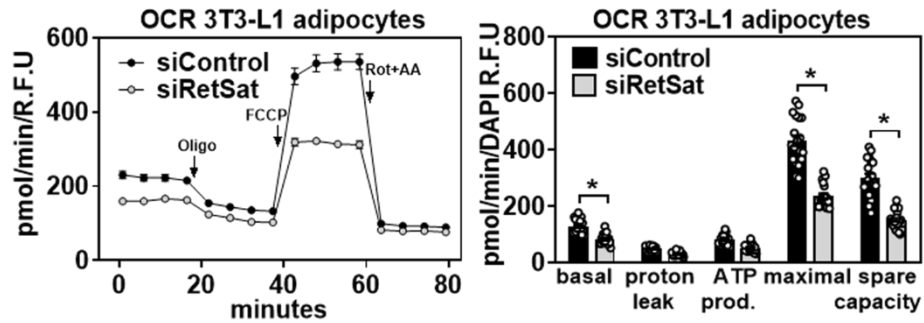


Figure 19. RetSat depletion reduces mitochondrial respiration in 3T3-L1 adipocytes. Oxygen consumption rate (OCR) of 3T3-L1 adipocytes with or without RetSat depletion was analyzed by Seahorse XF Analyzer (left panel) and evaluated stage-specifically (right panel). Data are presented as individual data points and mean±sem, * $P < 0.05$.

4.11 BAT-specific RetSat deletion mouse model construction and validation

To further validate Cre/LoxP system efficiency, RETSAT protein expression was detected by immunoblotting in multiple adipose tissues and liver tissue. As shown in **Figure 20A**, RETSAT protein was profoundly reduced in iBAT of Cre⁺ mice, however, RetSat deficiency did not result in any alteration in UCP1 protein expression. qPCR analysis confirmed *RetSat* mRNA was robustly decreased in iBAT of Cre⁺ mice, which showed comparable *Ucp1*, *Cidea*, *Adrb3*, and *Elovl3* mRNA expression (**Figure 20B**), revealing RetSat is not mandatory for thermogenesis gene expression in BAT. Meanwhile, ingWAT, pgWAT, and liver had stable RETSAT protein expression between Cre⁻ and Cre⁺ mice (**Figure 20C, D, and E**), indicating RetSat was specifically ablated in BAT, and BAT-specific RetSat deletion mouse model was established successfully for following applications.

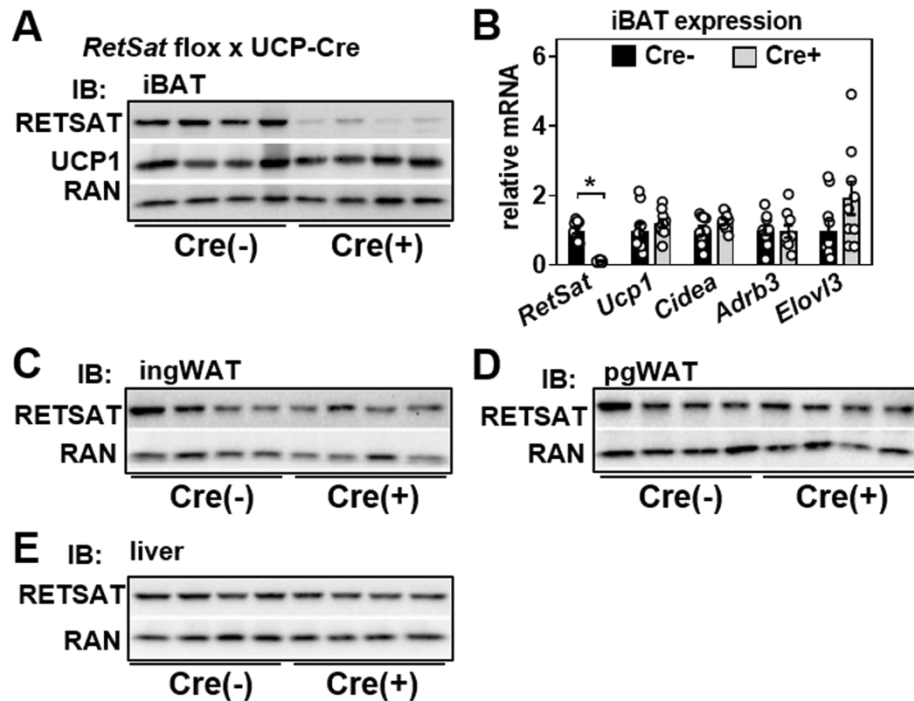


Figure 20. BAT-specific *RetSat* deletion mouse model construction and validation. A) Protein expression of RETSAT and UCP1 in iBAT of 3 months old, male mice of the indicated genotypes was determined by immunoblotting, RAN served as loading control. B) mRNA expression of indicated genes in mice described in A) was determined by qPCR. Protein expression of RETSAT in Cre- and Cre+ mice in C) inguinal-, D) perigonadal white adipose tissue (ing/pgWAT), and E) liver was determined by immunoblotting. RAN served as loading control. Data are presented as individual data points and mean \pm sem, * P <0.05.

4.12 *RetSat* deletion in brown adipose tissue of mice impairs acute cold tolerance

The *in vivo* effect of *RetSat* ablation was first explored in the mice fed normal chow. Histological analysis revealed similar lipid accumulation and adipocyte morphology in iBAT between genotypes (**Figure 21A**). Cre+ mice did not differ from Cre- mice in body weight, with the comparable food intake after a 12-week normal chow diet (**Figure 21B and C**). At the age of 22 weeks, the Cre+ mice had similar adipose tissue mass ratio, accompanied by no altered body composition (**Figure 21D and E**).

The core body temperature of mice was measured at the rectum. As shown in **Figure 21F**, at 0h, Cre+ mice showed lower but not significant body temperature relative to

Cre- mice at room temperature. To assess thermogenetic capacity, mice were subjected to cold exposure. The environmental temperature was switched from 21 °C to 4 °C, and Cre- mice had higher body temperature than Cre+ mice. However, unexpectedly, after being housed for 3h, the body temperature of Cre+ mice stopped decreasing, and was even comparable with that of Cre- mice. During long term cold exposure for 14 days, Cre+ mice showed similar body temperature to Cre- mice (**Figure 21G**). These cold tolerance data indicate that RetSat deficiency in BAT leads to impaired thermogenetic capacity upon acute cold exposure.

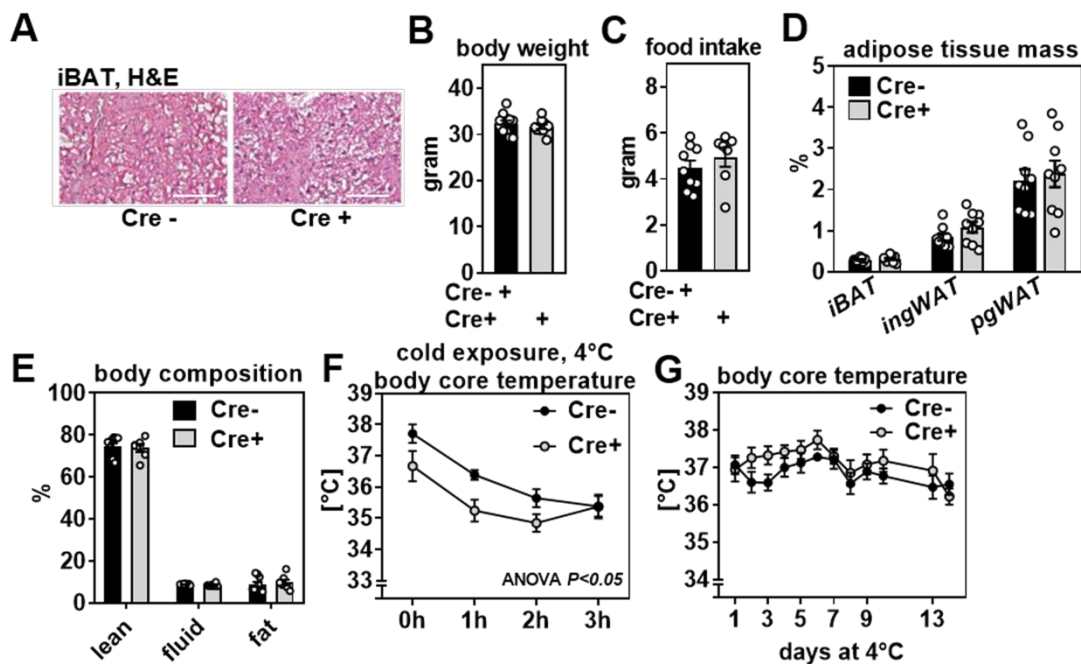


Figure 21. RetSat deletion in brown adipose tissue of mice impairs acute cold tolerance. A) iBAT morphology of Cre- and Cre+ mice was analyzed by hematoxylin & eosin staining (H&E, scale bar=50 μm). B) Body weights and C) 24 hours food intake of mice described in Figure 11 A. D) Relative adipose tissue mass of iBAT and inguinal/perigonadal white adipose tissue (ing/pgWAT) in Cre- and Cre+ mice. E) Body composition of Cre- and Cre+ mice before cold exposure. F) Cre- and Cre+ mice were exposed to 4 °C and core body temperature was determined by a rectal probe at indicated time points. G) Cre- and Cre+ mice were exposed to 4 °C and core body temperature was determined by a rectal probe at indicated time points. Data are presented as individual data points and mean±sem, * $P < 0.05$.

4.13 RetSat deletion in brown adipose tissue of mice does not promote diet-induced obesity

To investigate effect of RetSat on diet induced obesity, Cre- and Cre+ mice received 12-week HFD challenge. As shown in **Figure 22A**, Cre+ mice had comparable body weight on HFD compared with Cre- mice, accompanied by unchanged ratio of body weight gain. Moreover, after HFD induction, there was no change in body composition as well as adipose tissue mass ratio between genotypes (**Figure 22B and C**). These results suggest RetSat deletion in BAT of mice does not promote diet-induced obesity.

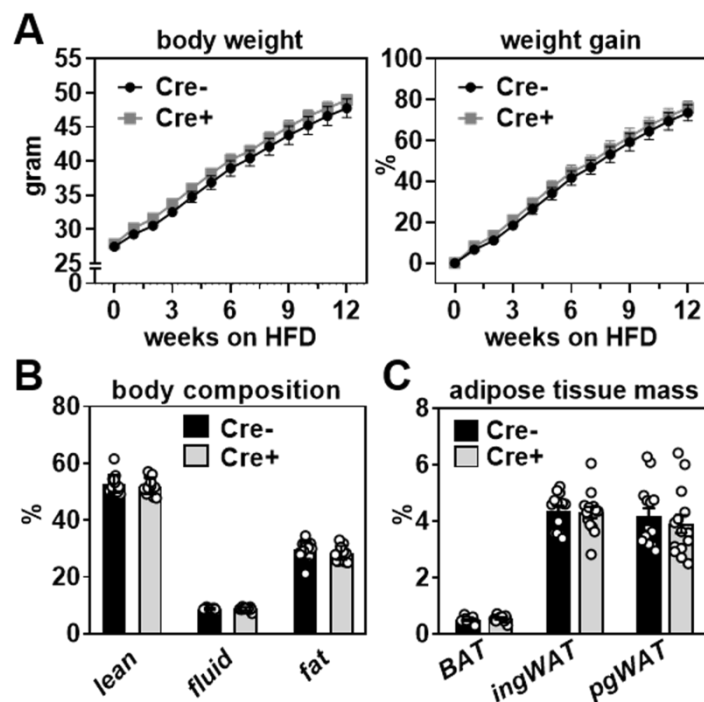


Figure 22. BAT-specific RetSat knockout mice maintained adiposity upon HFD. Male mice of the indicated genotypes were fed high-fat diet (HFD, 60% kcal/fat) for 12 weeks, starting at an age of 10 weeks, A) Body weights and weight gain were determined. B) Body composition of Cre- and Cre+ mice after HFD-feeding was determined by NMR. C) Adipose tissue mass of indicated depots was weighed in Cre- and Cre+ mice fed HFD. Data are presented as individual data points and mean \pm sem, * P <0.05.

4.14 BAT-specific RetSat deletion mice had slightly weakened glucose disposal capacity

After mice were challenged with HFD, glucose level was determined. Although there was no alteration in blood glucose between genotypes upon fed *ad libitum*, after 16 h starving, both groups of mice showed decreased blood glucose level, notably, obese Cre+ mice had significantly higher glucose content in blood relative to Cre- mice (**Figure 23A**). To further examine whether RetSat effects glucose disposal capacity of mice, glucose tolerance test was conducted. After glucose burden of 30 min, Cre+ mice showed an enhanced trend in glucose excursions with a higher area under the curve (**Figure 23B**). Subsequently, mice received insulin tolerance test, however, no difference in blood glucose level was observed during insulin burden (**Figure 23C**), suggesting that BAT-specific deletion of RetSat does not impair insulin sensitivity.

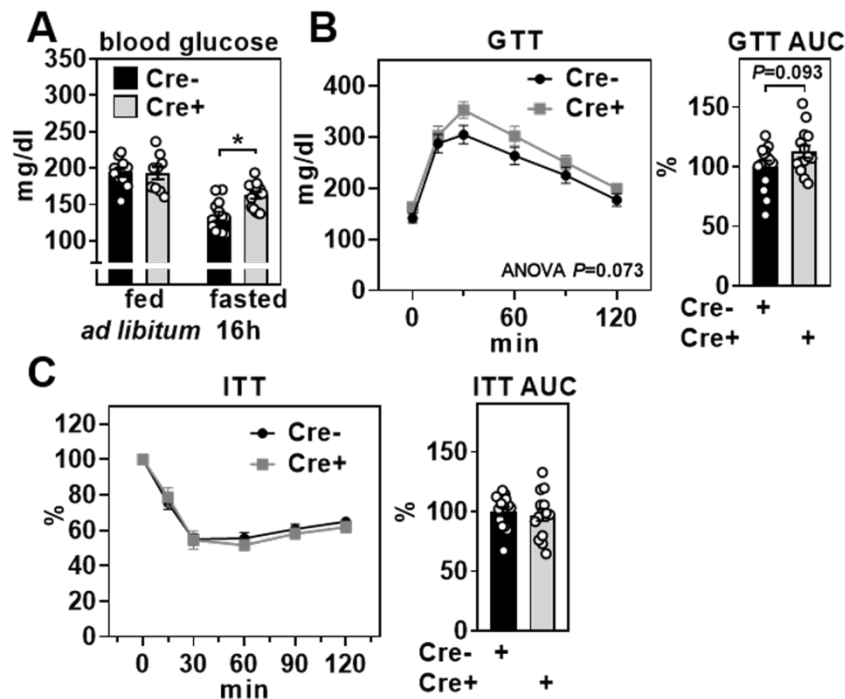


Figure 23. BAT-specific RetSat knockout slightly impaired glucose disposal capacity of mice upon HFD. A) Blood glucose levels of Cre- and Cre+ mice. B) Glucose and C) insulin tolerance of HFD-fed mice with indicated genotype. Data are presented as individual data points and mean \pm sem, * $P<0.05$ vs. Cre- mice.

4.15 RetSat deletion in BAT downregulates mitochondrially encoded and protein-folding associated genes

The cumulative data displays the important role of RetSat in thermogenic capacity of adipocytes, to explore the potential mechanism underlying this effect, iBAT from 5x Cre⁻ mice and 5x Cre⁺ mice were sent to bulk RNA sequencing. Compared to Cre⁻ mice, 162 down-regulated and 142 up-regulated genes were identified in iBAT of Cre⁺ mice (**Figure 24A**). In Kyoto Encyclopedia of Genes and Genomes (KEGG) pathway enrichments, the most impacted pathway of down-regulated genes is thermogenesis (**Figure 24B**), in accordance with *in vitro* and *in vivo* data. In line with reduced mitochondrial respiration and *Cox7a1* mRNA, the expression of 13 protein-encoding genes from mitochondrial genome decreased in iBAT of Cre⁺ mice (**Figure 24C**), supporting the effect of RetSat on mitochondria function. In Gene Ontology (GO) TERM Biological Process (BP) analysis, results showed that the down-regulated genes strongly took part in protein folding process (**Figure 24D**), consistently, protein process in endoplasmic reticulum (ER) is the secondary most impacted pathway in KEGG pathway, suggesting RetSat is mainly involved in proteostasis of ER. Accordingly, the selected protein folding associated genes were suppressive in the iBAT of Cre⁺ mice (**Figure 24E**).

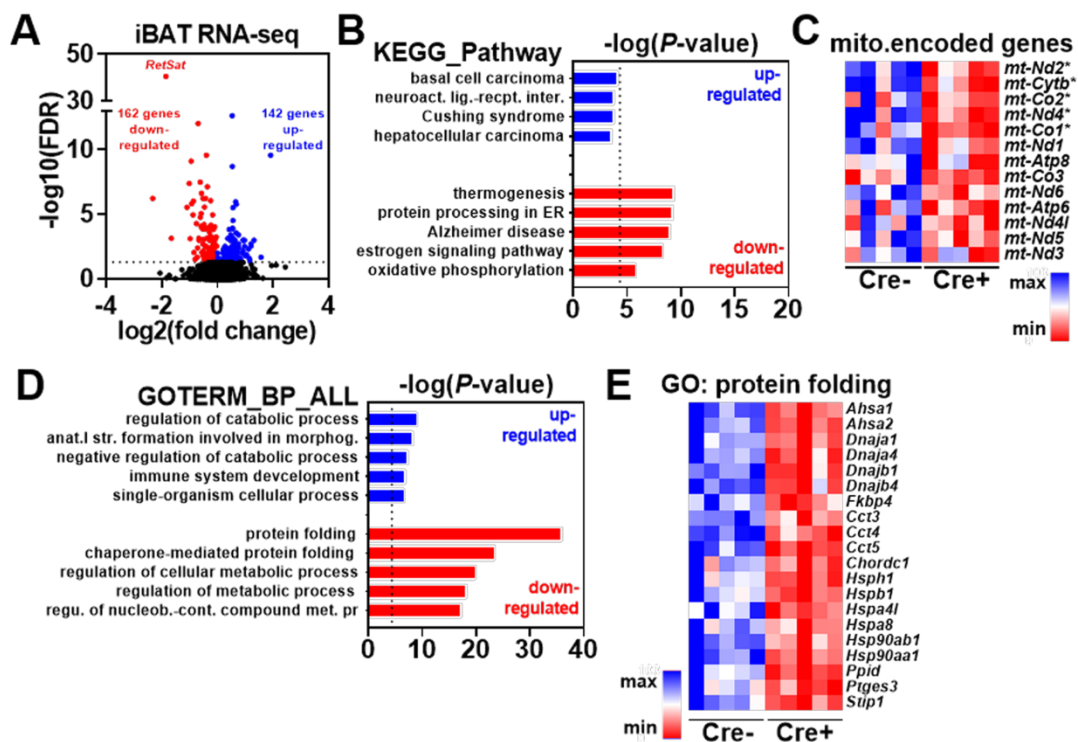


Figure 24. RetSat deletion in BAT downregulates mitochondrially encoded and protein-folding associated genes. A) Significantly (FDR<5%) upregulated (blue dots) and downregulated (red dots) genes in interscapular brown adipose tissue (iBAT) of Cre⁺ mice. B) KEGG pathway enrichment in up- and down-regulated genes in iBAT of Cre⁺ mice. C) Heatmap of all detected mitochondrially encoded genes in iBAT of Cre⁻ and Cre⁺ mice. D) Enriched gene ontology (GO) terms of biological process (BP) in up- and down-regulated genes in BAT of Cre⁺ mice. E) Downregulated genes in iBAT of Cre⁺ mice associated with the GO term protein folding. In C), *FDR<5%.

5 Discussion

5.1 RetSat is highly expressed in adipose tissue and stimulated by β -AR activation

Based on prior reports, RetSat has been implicated in metabolic activities, particularly in liver and adipose tissue, and this project focuses on its function in BAT and thermogenesis. As in WAT, RetSat has a high expression in BAT of mice. Due to development and ambient changes, BAT in adult humans is degraded and difficult to check out, but high expression of RetSat is observed in human neck brown fat from limited studies (165). To avoid the side effects of β -AR on heart, specific β 3A was chosen to mimic SNS activity and norepinephrine signaling, the induced RetSat protein in iBAT and ingWAT which are innervated by SNS confirm the previous regulation by cold exposure (9). Since β 3-AR plays a predominant role in adipocytes, non-selective β -AR agonist was applied to stimulate, up-regulation of RetSat was found in primary and immortalized brown and white adipocytes. The activated β 3-AR enhances lipolysis in adipose tissue, and RetSat^{-/-} mice had hepatic lipid accumulation (6), thus RetSat is more likely required for lipid mobilization.

5.2 Dynamic expression of RetSat and its action in brown adipocyte differentiation

RetSat has a dynamic expression pattern in brown adipocyte differentiation, the same as in white adipocytes. More notably, unlike classical adipogenesis markers *Pparg2* and *Fabp4*, RetSat is obviously present in brown preadipocytes. The loss and gain of RetSat function studies were employed to investigate its action in brown adipocyte

differentiation. Unexpectedly, RetSat depletion does not impair adipogenesis, however, *Ucp1* and *Elovl3* mRNA decreased with or nearly to significance, implying a stronger effect of RetSat on thermogenic program in brown adipocytes. Since PPAR γ activation induced UCP1 (116), although the effect of ectopic expression is not so strong as in white adipocytes, the mildly enhanced adipogenesis and thermogenesis in brown adipocytes are at least partly due to PPAR γ transcriptional activity promoted by RetSat overexpression.

5.3 RetSat is required for thermogenesis gene expression in brown adipocytes and white adipocyte browning

RetSat depletion was evidenced to decrease thermogenesis gene expression in basal and activated/recruited conditions in brown and white adipocytes. Recruited/activated BAT contributes more benefits to combat metabolic disease with respect to basal condition (166). Cold inducible BAT recruitment resulted in decreased body fat mass in the humans with low BAT activity (167), and β 3-AR agonist Mirabegron specifically delivered to iBAT of obese mice improved glucose homeostasis and prevented diet-induced obesity (168). Particularly, because of tightly controlled by multiple regulatory layers, mitochondrial UCP1 therein needs to be activated to produce heat (169), thus this project also emphasizes the effect of RetSat on β -adrenergic stimulated adipocytes. Isoproterenol is used to activate brown adipocytes *in vitro* study, whereas, thermogenesis agent (β 3-AR agonist) and browning agent (PPAR γ agonist) are both required for white adipocytes browning program in culture (170). Similar to the effect early in adipogenesis, *Pparg2* mRNA expression did not change upon RetSat depletion in mature brown adipocytes, in line with white adipocytes which are primarily responsible for lipid storage and ablation of RetSat did not alter the expression of lipid metabolism-related genes (4). It is noteworthy that the profound effect of RetSat on UCP1 protein *in vitro*, which may allow for post-translated protein accumulation. PPAR γ is needed for β -adrenergic signaling-mediated induction of brown adipocytes (171), here the current data indicate its target gene RetSat effects brown-adipocyte-specific gene expression and inducibility.

5.4 Loss of RetSat function reduces mitochondrial respiration in adipocytes

Since heat generation derived by proton leak is dependent on mitochondria UCP1

(172), additionally, *Cox7a1* is a subunit of Cytochrome c oxidase located in terminal component of the ETC, catalyzing oxygen reduction (173). The down-regulated *Ucp1* and *Cox7a1* encouraged us to analyze the effect of RetSat on mitochondrial respiration in adipocytes. Loss of RetSat reduced basal respiration and induced oxygen consumption, and impaired the responsiveness to increased energy demand in adipocytes. Calorie restriction lowered the rate of ROS generation at mitochondria to remedy obesity and aging-associated diseases, and the decreased Cytochrome c oxidase IV (*COX4*) and *Ucp1* mRNA, key masters of oxidative phosphorylation and energy production, were found in BAT of calorie-restricted mice (174), where *RetSat* mRNA was also down-regulated (175). Thus, all these data suggest a vital role of RetSat in adipocytes mitochondrial respiration.

5.5 The effect of RetSat BAT depletion on metabolic profile of mice

To our best knowledge, this is the first tissue-specific knockout mouse model to dissect the role of RetSat in BAT. Due to the specificity of UCP1-Cre, RetSat was unaltered in WAT and liver, the latter has the strongest expression across the organs. However, in contrast to *in vitro* findings, when RetSat was abolished by ~90% in iBAT, UCP1 had unchanged expression, as other thermogenesis makers, *Cidea* and *Adrb3*. *Cidea* is thought to be a PPAR γ target gene (176), enhancing PPAR γ binding to a UCP1 enhancer element to drive UCP1 transcription, and its depletion inhibited browning and uncoupling in human adipocytes (177). It is worth noting that chronic and acute RetSat loss of function exhibited inverse effects in adipogenesis and hepatic lipid storage (5). Additionally, Tamoxifen inducible UCP1-ERCre derived BAT-specific PPAR γ knockout in fully developed and adult C57BL/6N mice caused reduced UCP1 expression (171). In current C57BL/6J mouse model, UCP1-Cre induced RetSat ablation initially happened in embryonic cells, hence the stable brown adipocyte markers appear to because of the compensatory effect may be derived by PPAR γ or its other targeted genes during development, and the effects of an acute RetSat deletion in BAT may differ.

PPAR γ loss of function in BAT of mice showed comparable body composition and weight phenotype, but smaller brown adipocyte size (171), and RetSat globally deleted mice had intact adipose tissue and mild body weight increase on diet (6, 8). Similar to its function in brown adipocyte differentiation, RetSat ablated in BAT did not effect adiposity and body weight with either normal chow or HFD. In accordance, lipotrophy

was not observed in the brown adipocytes of Cre⁺ mice. Consequently, RetSat has no alteration on BAT development *in vivo*, which might be due to the white adipose tissue and muscle are main components of body weight.

RetSat was the most frequently significant gene in an integrated analysis of 16 data sets which aimed to solve the common mechanisms in insulin homeostasis (178). RetSat whole-body knockout mice had similar responses to glucose and insulin burdens (8). However, lower blood glucose, improved glucose tolerance, and comparable insulin sensitivity were observed in acute liver-specific RetSat depletion mice (140). Global glucose metabolism is implicated in a complex interorgan network in body (140), and generally recognized that the contribution of adipose tissue is smaller than liver or skeletal muscle (179). Besides fatty acid, BAT utilizes glucose as substrate fuel to produce heat (180), and consumes far exceed liver and skeletal muscle capacity upon cold exposure (180). In current study, RetSat deletion in BAT resulted in an increased blood glucose level upon starvation, and slightly impaired glucose disposal, resembling the effect of RetSat germline lack, the compensatory effect might be from the liver to a certain degree.

5.6 RetSat is necessary for core body temperature maintenance upon acute cold exposure

Large mammals have a series of neural, vascular, and metabolic responses to cold exposure (181), and non-shivering thermogenesis, which occurs in BAT, was initially defined as a cold-induced increase in heat generation and not related to shivering activity of muscle (182). BAT-specific PPAR γ knockout mice had unaltered body temperature upon long term cold challenge but blunted β 3-adrenergic responsiveness (171). RetSat ablated in BAT resulted in impaired thermogenesis capacity upon acute cold exposure, the effect disappeared under the long-term cold environment, which might be interpreted by the following reasons: 1) BAT activity is completely controlled by sensory and SNS innervation (183), and the neuroanatomical study indicated thermogenesis is dependent on coordinated and multiple redundant control (184). 2) Lipolysis in BAT is regularly recognized to be necessary for cold-induced thermogenesis, however, WAT is the major organ for lipid storage, and Schreiber et al. reported fatty acid supply for energy consumption and cold-induced thermogenesis severely depends on ATGL in WAT, but not BAT (185). 3) When facing cold stress, adults have sufficiently developed skeletal muscle mass to preserve body temperature

through shivering thermogenesis which is the primary heat source, such as physical exercise (186). In obesity-resistant mice, upon the insufficient adrenergic non-shivering thermogenesis in BAT, non-shivering thermogenesis in skeletal muscle adaptively augmented, and mediated by sarcolipin-induced uncoupling of sarco(endo)plasmic reticulum calcium ATPase pump activity (187). Based on shivering and non-shivering thermogenic activities, BAT and muscle are both forceful sources to maintain body temperature, even skeletal muscle might contribute more. The relative contribution of BAT and compensation of other organs are matters worth to be considered. To address these hypotheses, the experiments could be repeated at thermoneutrality, where UCP1 expression and BAT activity are repressive, to exclude any compensatory effects (23). In particular, pan-adipose tissue specific RetSat depletion mouse model is meaningful to further study its effect in adipose tissue. Additionally, non-invasive infrared thermography is used to specifically and accurately detect UCP1-mediated BAT thermogenesis *in vivo* (188) and avoids the thermoregulation caused by thermoprobe insertion.

5.7 Potential mechanism of RetSat in BAT upon transcriptome analysis

Mitochondrial DNA is a small part of DNA located in eukaryotic cell mitochondria (189), and its molecular adaptation to meet high energy demand has been found in large mammals facing extreme energetic challenges (190). The cellular biogenesis process, specifically OXPHOS, is regulated by both mitochondrial and nuclear genomes (191), further, BAT thermogenesis is shaped by mitochondria–nuclear interactions (192). The reduced expression of some genes from the mitochondrial DNA which produces OXPHOS subunits is concomitant by the defective thermogenesis gene transcription in nuclear in BAT-specific RetSat knockout mice.

Some areas on the mitochondrial surface make close contact with the ER membrane, known as mitochondria-associated membranes (MAMs) which is the site of physical and functional communication, the mice lacking ER-associated protein degradation were more sensitive to cold with deficient mitochondria function (193). The unfolded protein response (UPR) is the cellular response to an accumulation of unfolded or misfolded proteins in the endoplasmic reticulum lumen and is activated in the BAT of cold-exposed mice (194). Interestingly, the subcellular location of RetSat is endoplasmic reticulum membrane, and its deficiency caused repressive expression of protein folding associated genes in iBAT. On the other hand, ER Stress stimulated

PPAR γ degradation and suppressed UCP1 expression in adipose tissue (195). These data imply RetSat might take a role in bridge between mitochondria and endoplasmic reticulum.

Reference

1. Moise, A. R., Kuksa, V., Imanishi, Y., and Palczewski, K. (2004) Identification of all-trans-retinol:all-trans-13,14-dihydroretinol saturase. *J Biol Chem* **279**, 50230-50242
2. Moise, A. R., von Lintig, J., and Palczewski, K. (2005) Related enzymes solve evolutionarily recurrent problems in the metabolism of carotenoids. *Trends Plant Sci* **10**, 178-186
3. Wu, C., Jin, X., Tsueng, G., Afrasiabi, C., and Su, A. I. (2016) BioGPS: building your own mash-up of gene annotations and expression profiles. *Nucleic Acids Res* **44**, D313-316
4. Schupp, M., Lefterova, M. I., Janke, J., Leitner, K., Cristancho, A. G., Mullican, S. E., Qatanani, M., Szwegold, N., Steger, D. J., Curtin, J. C., Kim, R. J., Suh, M. J., Albert, M. R., Engeli, S., Gudas, L. J., and Lazar, M. A. (2009) Retinol saturase promotes adipogenesis and is downregulated in obesity. *Proc Natl Acad Sci U S A* **106**, 1105-1110
5. Weber, P., Flores, R. E., Kiefer, M. F., and Schupp, M. (2020) Retinol Saturase: More than the Name Suggests. *Trends Pharmacol Sci* **41**, 418-427
6. Pang, X. Y., Wang, S., Jurczak, M. J., Shulman, G. I., and Moise, A. R. (2017) Retinol saturase modulates lipid metabolism and the production of reactive oxygen species. *Arch Biochem Biophys* **633**, 93-102
7. Tang, T., Li, L., Tang, J., Li, Y., Lin, W. Y., Martin, F., Grant, D., Solloway, M., Parker, L., Ye, W., Forrest, W., Ghilardi, N., Oravec, T., Platt, K. A., Rice, D. S., Hansen, G. M., Abuin, A., Eberhart, D. E., Godowski, P., Holt, K. H., Peterson, A., Zambrowicz, B. P., and de Sauvage, F. J. (2010) A mouse knockout library for secreted and transmembrane proteins. *Nat Biotechnol* **28**, 749-755
8. Moise, A. R., Lobo, G. P., Erokwu, B., Wilson, D. L., Peck, D., Alvarez, S., Domínguez, M., Alvarez, R., Flask, C. A., de Lera, A. R., von Lintig, J., and Palczewski, K. (2010) Increased adiposity in the retinol saturase-knockout mouse. *Faseb j* **24**, 1261-1270

9. Sustarsic, E. G., Ma, T., Lynes, M. D., Larsen, M., Karavaeva, I., Havelund, J. F., Nielsen, C. H., Jedrychowski, M. P., Moreno-Torres, M., Lundh, M., Plucinska, K., Jespersen, N. Z., Grevengoed, T. J., Kramar, B., Peics, J., Hansen, J. B., Shamsi, F., Forss, I., Neess, D., Keipert, S., Wang, J., Stohlmann, K., Brandslund, I., Christensen, C., Jørgensen, M. E., Linneberg, A., Pedersen, O., Kiebish, M. A., Qvortrup, K., Han, X., Pedersen, B. K., Jastroch, M., Mandrup, S., Kjær, A., Gygi, S. P., Hansen, T., Gillum, M. P., Grarup, N., Emanuelli, B., Nielsen, S., Scheele, C., Tseng, Y. H., Færgeman, N. J., and Gerhart-Hines, Z. (2018) Cardiolipin Synthesis in Brown and Beige Fat Mitochondria Is Essential for Systemic Energy Homeostasis. *Cell Metab* **28**, 159-174.e111
10. Sakers, A., De Siqueira, M. K., Seale, P., and Villanueva, C. J. (2022) Adipose-tissue plasticity in health and disease. *Cell* **185**, 419-446
11. Sanchez-Gurmaches, J., Hung, C. M., and Guertin, D. A. (2016) Emerging Complexities in Adipocyte Origins and Identity. *Trends Cell Biol* **26**, 313-326
12. Heinonen, S., Jokinen, R., Rissanen, A., and Pietiläinen, K. H. (2020) White adipose tissue mitochondrial metabolism in health and in obesity. *Obes Rev* **21**, e12958
13. Jung, S. M., Sanchez-Gurmaches, J., and Guertin, D. A. (2019) Brown Adipose Tissue Development and Metabolism. *Handb Exp Pharmacol* **251**, 3-36
14. Pilkington, A. C., Paz, H. A., and Wankhade, U. D. (2021) Beige Adipose Tissue Identification and Marker Specificity-Overview. *Front Endocrinol (Lausanne)* **12**, 599134
15. Seale, P., Bjork, B., Yang, W., Kajimura, S., Chin, S., Kuang, S., Scimè, A., Devarakonda, S., Conroe, H. M., Erdjument-Bromage, H., Tempst, P., Rudnicki, M. A., Beier, D. R., and Spiegelman, B. M. (2008) PRDM16 controls a brown fat/skeletal muscle switch. *Nature* **454**, 961-967
16. Timmons, J. A., Wennmalm, K., Larsson, O., Walden, T. B., Lassmann, T., Petrovic, N., Hamilton, D. L., Gimeno, R. E., Wahlestedt, C., Baar, K., Nedergaard, J., and Cannon, B. (2007) Myogenic gene expression signature establishes that brown and white adipocytes originate from distinct cell lineages. *Proc Natl Acad Sci U S A* **104**, 4401-4406
17. Gesta, S., Tseng, Y. H., and Kahn, C. R. (2007) Developmental origin of fat: tracking obesity to its source. *Cell* **131**, 242-256
18. Wang, T., Sharma, A. K., and Wolfrum, C. (2022) Novel insights into adipose tissue heterogeneity. *Rev Endocr Metab Disord* **23**, 5-12

19. Song, A., Dai, W., Jang, M. J., Medrano, L., Li, Z., Zhao, H., Shao, M., Tan, J., Li, A., Ning, T., Miller, M. M., Armstrong, B., Huss, J. M., Zhu, Y., Liu, Y., Gradinaru, V., Wu, X., Jiang, L., Scherer, P. E., and Wang, Q. A. (2020) Low- and high-thermogenic brown adipocyte subpopulations coexist in murine adipose tissue. *J Clin Invest* **130**, 247-257
20. Sun, W., Dong, H., Balaz, M., Slyper, M., Drokhyansky, E., Colleluori, G., Giordano, A., Kovanicova, Z., Stefanicka, P., Balazova, L., Ding, L., Husted, A. S., Rudofsky, G., Ukropec, J., Cinti, S., Schwartz, T. W., Regev, A., and Wolfrum, C. (2020) snRNA-seq reveals a subpopulation of adipocytes that regulates thermogenesis. *Nature* **587**, 98-102
21. Sun, W., Modica, S., Dong, H., and Wolfrum, C. (2021) Plasticity and heterogeneity of thermogenic adipose tissue. *Nat Metab* **3**, 751-761
22. Fischer, A. W., Schlein, C., Cannon, B., Heeren, J., and Nedergaard, J. (2019) Intact innervation is essential for diet-induced recruitment of brown adipose tissue. *Am J Physiol Endocrinol Metab* **316**, E487-e503
23. Feldmann, H. M., Golozoubova, V., Cannon, B., and Nedergaard, J. (2009) UCP1 ablation induces obesity and abolishes diet-induced thermogenesis in mice exempt from thermal stress by living at thermoneutrality. *Cell Metab* **9**, 203-209
24. von Essen, G., Lindsund, E., Cannon, B., and Nedergaard, J. (2017) Adaptive facultative diet-induced thermogenesis in wild-type but not in UCP1-ablated mice. *Am J Physiol Endocrinol Metab* **313**, E515-e527
25. Wu, M. V., Bikopoulos, G., Hung, S., and Cедdia, R. B. (2014) Thermogenic capacity is antagonistically regulated in classical brown and white subcutaneous fat depots by high fat diet and endurance training in rats: impact on whole-body energy expenditure. *J Biol Chem* **289**, 34129-34140
26. Stanford, K. I., Middelbeek, R. J., Townsend, K. L., Lee, M. Y., Takahashi, H., So, K., Hitchcox, K. M., Markan, K. R., Hellbach, K., Hirshman, M. F., Tseng, Y. H., and Goodyear, L. J. (2015) A novel role for subcutaneous adipose tissue in exercise-induced improvements in glucose homeostasis. *Diabetes* **64**, 2002-2014
27. Kotzbeck, P., Giordano, A., Mondini, E., Murano, I., Severi, I., Venema, W., Cecchini, M. P., Kershaw, E. E., Barbatelli, G., Haemmerle, G., Zechner, R., and Cinti, S. (2018) Brown adipose tissue whitening leads to brown adipocyte death and adipose tissue inflammation. *J Lipid Res* **59**, 784-794
28. Cannon, B., de Jong, J. M. A., Fischer, A. W., Nedergaard, J., and Petrovic, N. (2020) Human brown adipose tissue: Classical brown rather than brite/beige? *Exp*

Physiol **105**, 1191-1200

29. Schlein, C., Fischer, A. W., Sass, F., Worthmann, A., Tödter, K., Jaeckstein, M. Y., Behrens, J., Lynes, M. D., Kiebish, M. A., Narain, N. R., Bussberg, V., Darkwah, A., Jespersen, N. Z., Nielsen, S., Scheele, C., Schweizer, M., Braren, I., Bartelt, A., Tseng, Y. H., Heeren, J., and Scheja, L. (2021) Endogenous Fatty Acid Synthesis Drives Brown Adipose Tissue Involution. *Cell Rep* **34**, 108624
30. Valle, A., Guevara, R., García-Palmer, F. J., Roca, P., and Oliver, J. (2008) Caloric restriction retards the age-related decline in mitochondrial function of brown adipose tissue. *Rejuvenation Res* **11**, 597-604
31. Kindred, J. H., Tuulari, J. J., Simon, S., Luckasen, G. J., Bell, C., and Rudroff, T. (2016) Brown adipose and central nervous system glucose uptake is lower during cold exposure in older compared to young men: a preliminary PET study. *Aging Clin Exp Res* **28**, 557-560
32. Scarpace, P. J., Mooradian, A. D., and Morley, J. E. (1988) Age-associated decrease in beta-adrenergic receptors and adenylate cyclase activity in rat brown adipose tissue. *J Gerontol* **43**, B65-70
33. Tajima, K., Ikeda, K., Chang, H. Y., Chang, C. H., Yoneshiro, T., Oguri, Y., Jun, H., Wu, J., Ishihama, Y., and Kajimura, S. (2019) Mitochondrial lipoylation integrates age-associated decline in brown fat thermogenesis. *Nat Metab* **1**, 886-898
34. Deng, J., Schoeneman, S. E., Zhang, H., Kwon, S., Rigsby, C. K., Shore, R. M., and Josefsen, J. L. (2015) MRI characterization of brown adipose tissue in obese and normal-weight children. *Pediatr Radiol* **45**, 1682-1689
35. Shimizu, I., Aprahamian, T., Kikuchi, R., Shimizu, A., Papanicolaou, K. N., MacLauchlan, S., Maruyama, S., and Walsh, K. (2014) Vascular rarefaction mediates whitening of brown fat in obesity. *J Clin Invest* **124**, 2099-2112
36. Da Eira, D., Jani, S., and Ceddia, R. B. (2023) An obesogenic diet impairs uncoupled substrate oxidation and promotes whitening of the brown adipose tissue in rats. *J Physiol* **601**, 69-82
37. Rasmussen, A. T. (1923) The so-called hibernating gland. *Journal of Morphology* **38**, 147-205
38. Sheldon, E. F. (1924) The so-called hibernating gland in mammals: A form of adipose tissue. *The Anatomical Record* **28**, 331-347
39. Rylander, E., Pribylová, H., and Lind, J. (1972) A thermographic study of infants exposed to cold. *Acta Paediatr Scand* **61**, 42-48
40. Carter, B. W., and Schucany, W. G. (2008) Brown adipose tissue in a newborn.

Proc (Bayl Univ Med Cent) **21**, 328-330

41. van Marken Lichtenbelt, W. D., Vanhommel, J. W., Smulders, N. M., Drossaerts, J. M., Kemerink, G. J., Bouvy, N. D., Schrauwen, P., and Teule, G. J. (2009) Cold-activated brown adipose tissue in healthy men. *N Engl J Med* **360**, 1500-1508
42. Saito, M., Okamatsu-Ogura, Y., Matsushita, M., Watanabe, K., Yoneshiro, T., Nio-Kobayashi, J., Iwanaga, T., Miyagawa, M., Kameya, T., Nakada, K., Kawai, Y., and Tsujisaki, M. (2009) High incidence of metabolically active brown adipose tissue in healthy adult humans: effects of cold exposure and adiposity. *Diabetes* **58**, 1526-1531
43. Virtanen, K. A., Lidell, M. E., Orava, J., Heglind, M., Westergren, R., Niemi, T., Taittonen, M., Laine, J., Savisto, N. J., Enerbäck, S., and Nuutila, P. (2009) Functional brown adipose tissue in healthy adults. *N Engl J Med* **360**, 1518-1525
44. Cypess, A. M., Lehman, S., Williams, G., Tal, I., Rodman, D., Goldfine, A. B., Kuo, F. C., Palmer, E. L., Tseng, Y. H., Doria, A., Kolodny, G. M., and Kahn, C. R. (2009) Identification and importance of brown adipose tissue in adult humans. *N Engl J Med* **360**, 1509-1517
45. Tan, C. L., and Knight, Z. A. (2018) Regulation of Body Temperature by the Nervous System. *Neuron* **98**, 31-48
46. Reverte-Salisa, L., Sanyal, A., and Pfeifer, A. (2019) Role of cAMP and cGMP Signaling in Brown Fat. *Handb Exp Pharmacol* **251**, 161-182
47. Pagnon, J., Matzaris, M., Stark, R., Meex, R. C., Macaulay, S. L., Brown, W., O'Brien, P. E., Tiganis, T., and Watt, M. J. (2012) Identification and functional characterization of protein kinase A phosphorylation sites in the major lipolytic protein, adipose triglyceride lipase. *Endocrinology* **153**, 4278-4289
48. Seale, P. (2015) Transcriptional Regulatory Circuits Controlling Brown Fat Development and Activation. *Diabetes* **64**, 2369-2375
49. Bast-Habersbrunner, A., and Fromme, T. (2020) Purine Nucleotides in the Regulation of Brown Adipose Tissue Activity. *Front Endocrinol (Lausanne)* **11**, 118
50. Fedorenko, A., Lishko, P. V., and Kirichok, Y. (2012) Mechanism of fatty-acid-dependent UCP1 uncoupling in brown fat mitochondria. *Cell* **151**, 400-413
51. Bertholet, A. M., and Kirichok, Y. (2017) UCP1: A transporter for H(+) and fatty acid anions. *Biochimie* **134**, 28-34
52. Cannon, B., and Nedergaard, J. (2017) What Ignites UCP1? *Cell Metab* **26**, 697-698
53. Fromme, T., Kleigrew, K., Dunkel, A., Retzler, A., Li, Y., Maurer, S., Fischer, N., Diezko, R., Kanzleiter, T., Hirschberg, V., Hofmann, T., and Klingenspor, M. (2018)

Degradation of brown adipocyte purine nucleotides regulates uncoupling protein 1 activity. *Mol Metab* **8**, 77-85

54. Hatefi, Y. (1993) ATP synthesis in mitochondria. *Eur J Biochem* **218**, 759-767

55. Nolfi-Donagan, D., Braganza, A., and Shiva, S. (2020) Mitochondrial electron transport chain: Oxidative phosphorylation, oxidant production, and methods of measurement. *Redox Biol* **37**, 101674

56. Mitchell, P. (1961) Coupling of phosphorylation to electron and hydrogen transfer by a chemi-osmotic type of mechanism. *Nature* **191**, 144-148

57. Goldman, A. D., Weber, J. M., LaRowe, D. E., and Barge, L. M. (2023) Electron transport chains as a window into the earliest stages of evolution. *Proc Natl Acad Sci U S A* **120**, e2210924120

58. Smolina, N., Khudiakov, A., and Kostareva, A. (2023) Assaying Mitochondrial Respiration as an Indicator of Cellular Metabolism and Fitness. *Methods Mol Biol* **2644**, 3-14

59. Balaban, R. S. (1990) Regulation of oxidative phosphorylation in the mammalian cell. *Am J Physiol* **258**, C377-389

60. Tseng, Y. H., Cypess, A. M., and Kahn, C. R. (2010) Cellular bioenergetics as a target for obesity therapy. *Nat Rev Drug Discov* **9**, 465-482

61. Divakaruni, A. S., and Brand, M. D. (2011) The regulation and physiology of mitochondrial proton leak. *Physiology (Bethesda)* **26**, 192-205

62. Bertholet, A. M., Natale, A. M., Bisignano, P., Suzuki, J., Fedorenko, A., Hamilton, J., Brustovetsky, T., Kazak, L., Garrity, R., Chouchani, E. T., Brustovetsky, N., Grabe, M., and Kirichok, Y. (2022) Mitochondrial uncouplers induce proton leak by activating AAC and UCP1. *Nature* **606**, 180-187

63. Heytler, P. G., and Prichard, W. W. (1962) A new class of uncoupling agents--carbonyl cyanide phenylhydrazones. *Biochem Biophys Res Commun* **7**, 272-275

64. Li, N., Ragheb, K., Lawler, G., Sturgis, J., Rajwa, B., Melendez, J. A., and Robinson, J. P. (2003) Mitochondrial complex I inhibitor rotenone induces apoptosis through enhancing mitochondrial reactive oxygen species production. *J Biol Chem* **278**, 8516-8525

65. Kim, H., Esser, L., Hossain, M. B., Xia, D., Yu, C.-A., Rizo, J., van der Helm, D., and Deisenhofer, J. (1999) Structure of Antimycin A1, a Specific Electron Transfer Inhibitor of Ubiquinol-Cytochrome c Oxidoreductase. *Journal of the American Chemical Society* **121**, 4902-4903

66. Hauck, A. K., Huang, Y., Hertzler, A. V., and Bernlohr, D. A. (2019) Adipose

- oxidative stress and protein carbonylation. *J Biol Chem* **294**, 1083-1088
67. Chenna, S., Koopman, W. J. H., Prehn, J. H. M., and Connolly, N. M. C. (2022) Mechanisms and mathematical modeling of ROS production by the mitochondrial electron transport chain. *Am J Physiol Cell Physiol* **323**, C69-c83
68. Jastroch, M., Divakaruni, A. S., Mookerjee, S., Treberg, J. R., and Brand, M. D. (2010) Mitochondrial proton and electron leaks. *Essays Biochem* **47**, 53-67
69. Emorine, L. J., Marullo, S., Briand-Sutren, M. M., Patey, G., Tate, K., Delavier-Klutchko, C., and Strosberg, A. D. (1989) Molecular characterization of the human beta 3-adrenergic receptor. *Science* **245**, 1118-1121
70. Cero, C., Lea, H. J., Zhu, K. Y., Shamsi, F., Tseng, Y. H., and Cypess, A. M. (2021) β 3-Adrenergic receptors regulate human brown/beige adipocyte lipolysis and thermogenesis. *JCI Insight* **6**
71. Riis-Vestergaard, M. J., Richelsen, B., Bruun, J. M., Li, W., Hansen, J. B., and Pedersen, S. B. (2020) Beta-1 and Not Beta-3 Adrenergic Receptors May Be the Primary Regulator of Human Brown Adipocyte Metabolism. *J Clin Endocrinol Metab* **105**
72. Blondin, D. P., Nielsen, S., Kuipers, E. N., Severinsen, M. C., Jensen, V. H., Miard, S., Jespersen, N. Z., Kooijman, S., Boon, M. R., Fortin, M., Phoenix, S., Frisch, F., Guérin, B., Turcotte É, E., Haman, F., Richard, D., Picard, F., Rensen, P. C. N., Scheele, C., and Carpentier, A. C. (2020) Human Brown Adipocyte Thermogenesis Is Driven by β 2-AR Stimulation. *Cell Metab* **32**, 287-300.e287
73. Miller, C. N., Yang, J. Y., England, E., Yin, A., Baile, C. A., and Rayalam, S. (2015) Isoproterenol Increases Uncoupling, Glycolysis, and Markers of Beiging in Mature 3T3-L1 Adipocytes. *PLoS One* **10**, e0138344
74. Bloom, J. D., Dutia, M. D., Johnson, B. D., Wissner, A., Burns, M. G., Largis, E. E., Dolan, J. A., and Claus, T. H. (1992) Disodium (R,R)-5-[2-[[2-(3-chlorophenyl)-2-hydroxyethyl]-amino] propyl]-1,3-benzodioxole-2,2-dicarboxylate (CL 316,243). A potent beta-adrenergic agonist virtually specific for beta 3 receptors. A promising antidiabetic and antiobesity agent. *J Med Chem* **35**, 3081-3084
75. Himms-Hagen, J., Cui, J., Danforth, E., Jr., Taatjes, D. J., Lang, S. S., Waters, B. L., and Claus, T. H. (1994) Effect of CL-316,243, a thermogenic beta 3-agonist, on energy balance and brown and white adipose tissues in rats. *Am J Physiol* **266**, R1371-1382
76. Warner, A., Kjellstedt, A., Carreras, A., Böttcher, G., Peng, X. R., Seale, P., Oakes, N., and Lindén, D. (2016) Activation of β 3-adrenoceptors increases in vivo free fatty

acid uptake and utilization in brown but not white fat depots in high-fat-fed rats. *Am J Physiol Endocrinol Metab* **311**, E901-e910

77. Fujimoto, Y., Hashimoto, O., Shindo, D., Sugiyama, M., Tomonaga, S., Murakami, M., Matsui, T., and Funaba, M. (2019) Metabolic changes in adipose tissues in response to $\beta(3)$ -adrenergic receptor activation in mice. *J Cell Biochem* **120**, 821-835

78. Deeks, E. D. (2018) Mirabegron: A Review in Overactive Bladder Syndrome. *Drugs* **78**, 833-844

79. Baskin, A. S., Linderman, J. D., Brychta, R. J., McGehee, S., Anflück-Chames, E., Cero, C., Johnson, J. W., O'Mara, A. E., Fletcher, L. A., Leitner, B. P., Duckworth, C. J., Huang, S., Cai, H., Garraffo, H. M., Millo, C. M., Dieckmann, W., Tolstikov, V., Chen, E. Y., Gao, F., Narain, N. R., Kiebish, M. A., Walter, P. J., Herscovitch, P., Chen, K. Y., and Cypess, A. M. (2018) Regulation of Human Adipose Tissue Activation, Gallbladder Size, and Bile Acid Metabolism by a $\beta(3)$ -Adrenergic Receptor Agonist. *Diabetes* **67**, 2113-2125

80. Cypess, A. M., Weiner, L. S., Roberts-Toler, C., Franquet Elía, E., Kessler, S. H., Kahn, P. A., English, J., Chatman, K., Trauger, S. A., Doria, A., and Kolodny, G. M. (2015) Activation of human brown adipose tissue by a $\beta(3)$ -adrenergic receptor agonist. *Cell Metab* **21**, 33-38

81. O'Mara, A. E., Johnson, J. W., Linderman, J. D., Brychta, R. J., McGehee, S., Fletcher, L. A., Fink, Y. A., Kapuria, D., Cassimatis, T. M., Kelsey, N., Cero, C., Sater, Z. A., Piccinini, F., Baskin, A. S., Leitner, B. P., Cai, H., Millo, C. M., Dieckmann, W., Walter, M., Javitt, N. B., Rotman, Y., Walter, P. J., Ader, M., Bergman, R. N., Herscovitch, P., Chen, K. Y., and Cypess, A. M. (2020) Chronic mirabegron treatment increases human brown fat, HDL cholesterol, and insulin sensitivity. *J Clin Invest* **130**, 2209-2219

82. Finlin, B. S., Memetimin, H., Zhu, B., Confides, A. L., Vekaria, H. J., El Khouli, R. H., Johnson, Z. R., Westgate, P. M., Chen, J., Morris, A. J., Sullivan, P. G., Dupont-Versteegden, E. E., and Kern, P. A. (2020) The $\beta(3)$ -adrenergic receptor agonist mirabegron improves glucose homeostasis in obese humans. *J Clin Invest* **130**, 2319-2331

83. Finlin, B. S., Memetimin, H., Confides, A. L., Kasza, I., Zhu, B., Vekaria, H. J., Harfmann, B., Jones, K. A., Johnson, Z. R., Westgate, P. M., Alexander, C. M., Sullivan, P. G., Dupont-Versteegden, E. E., and Kern, P. A. (2018) Human adipose beigeing in response to cold and mirabegron. *JCI Insight* **3**

84. Schoonjans, K., and Auwerx, J. (2000) Thiazolidinediones: an update. *Lancet* **355**, 1008-1010

85. Tontonoz, P., and Spiegelman, B. M. (2008) Fat and beyond: the diverse biology of PPARgamma. *Annu Rev Biochem* **77**, 289-312
86. Barak, Y., Nelson, M. C., Ong, E. S., Jones, Y. Z., Ruiz-Lozano, P., Chien, K. R., Koder, A., and Evans, R. M. (1999) PPAR gamma is required for placental, cardiac, and adipose tissue development. *Mol Cell* **4**, 585-595
87. Shibata, Y., Eguchi, J., and Wada, J. (2023) Brown Adipose Tissue PPAR γ Is Required for the Insulin-Sensitizing Action of Thiazolidinediones. *Acta Med Okayama* **77**, 243-254
88. Tai, T. A., Jennermann, C., Brown, K. K., Oliver, B. B., MacGinnitie, M. A., Wilkison, W. O., Brown, H. R., Lehmann, J. M., Kliewer, S. A., Morris, D. C., and Graves, R. A. (1996) Activation of the nuclear receptor peroxisome proliferator-activated receptor gamma promotes brown adipocyte differentiation. *J Biol Chem* **271**, 29909-29914
89. Merlin, J., Sato, M., Nowell, C., Pakzad, M., Fahey, R., Gao, J., Dehvari, N., Summers, R. J., Bengtsson, T., Evans, B. A., and Hutchinson, D. S. (2018) The PPAR γ agonist rosiglitazone promotes the induction of brite adipocytes, increasing β -adrenoceptor-mediated mitochondrial function and glucose uptake. *Cell Signal* **42**, 54-66
90. Kelly, L. J., Vicario, P. P., Thompson, G. M., Candelore, M. R., Doebber, T. W., Ventre, J., Wu, M. S., Meurer, R., Forrest, M. J., Conner, M. W., Cascieri, M. A., and Moller, D. E. (1998) Peroxisome proliferator-activated receptors gamma and alpha mediate in vivo regulation of uncoupling protein (UCP-1, UCP-2, UCP-3) gene expression. *Endocrinology* **139**, 4920-4927
91. Petrovic, N., Walden, T. B., Shabalina, I. G., Timmons, J. A., Cannon, B., and Nedergaard, J. (2010) Chronic peroxisome proliferator-activated receptor gamma (PPARgamma) activation of epididymally derived white adipocyte cultures reveals a population of thermogenically competent, UCP1-containing adipocytes molecularly distinct from classic brown adipocytes. *J Biol Chem* **285**, 7153-7164
92. Festuccia, W. T., Blanchard, P. G., Turcotte, V., Laplante, M., Sariahmetoglu, M., Brindley, D. N., Richard, D., and Deshaies, Y. (2009) The PPARgamma agonist rosiglitazone enhances rat brown adipose tissue lipogenesis from glucose without altering glucose uptake. *Am J Physiol Regul Integr Comp Physiol* **296**, R1327-1335
93. Chandra, V., Huang, P., Hamuro, Y., Raghuram, S., Wang, Y., Burris, T. P., and Rastinejad, F. (2008) Structure of the intact PPAR-gamma-RXR- nuclear receptor complex on DNA. *Nature* **456**, 350-356
94. Barbera, M. J., Schluter, A., Pedraza, N., Iglesias, R., Villarroya, F., and Giralt, M.

- (2001) Peroxisome proliferator-activated receptor alpha activates transcription of the brown fat uncoupling protein-1 gene. A link between regulation of the thermogenic and lipid oxidation pathways in the brown fat cell. *J Biol Chem* **276**, 1486-1493
95. Qiang, L., Wang, L., Kon, N., Zhao, W., Lee, S., Zhang, Y., Rosenbaum, M., Zhao, Y., Gu, W., Farmer, S. R., and Accili, D. (2012) Brown remodeling of white adipose tissue by SirT1-dependent deacetylation of Ppar γ . *Cell* **150**, 620-632
96. Ohno, H., Shinoda, K., Spiegelman, B. M., and Kajimura, S. (2012) PPAR γ agonists induce a white-to-brown fat conversion through stabilization of PRDM16 protein. *Cell Metab* **15**, 395-404
97. Esterson, Y. B., Zhang, K., Koppaka, S., Kehlenbrink, S., Kishore, P., Raghavan, P., Maginley, S. R., Carey, M., and Hawkins, M. (2013) Insulin sensitizing and anti-inflammatory effects of thiazolidinediones are heightened in obese patients. *J Investig Med* **61**, 1152-1160
98. Walter, M. H., and Strack, D. (2011) Carotenoids and their cleavage products: biosynthesis and functions. *Nat Prod Rep* **28**, 663-692
99. Kumar, M. V., Sunvold, G. D., and Scarpace, P. J. (1999) Dietary vitamin A supplementation in rats: suppression of leptin and induction of UCP1 mRNA. *J Lipid Res* **40**, 824-829
100. Jeyakumar, S. M., Vajreswari, A., and Giridharan, N. V. (2006) Chronic dietary vitamin A supplementation regulates obesity in an obese mutant WNIN/Ob rat model. *Obesity (Silver Spring)* **14**, 52-59
101. Bonet, M. L., Oliver, J., Picó, C., Felipe, F., Ribot, J., Cinti, S., and Palou, A. (2000) Opposite effects of feeding a vitamin A-deficient diet and retinoic acid treatment on brown adipose tissue uncoupling protein 1 (UCP1), UCP2 and leptin expression. *J Endocrinol* **166**, 511-517
102. Fenzl, A., Kulterer, O. C., Spirk, K., Mitulović, G., Marculescu, R., Bilban, M., Baumgartner-Parzer, S., Kautzky-Willer, A., Kenner, L., Plutzky, J., Quadro, L., and Kiefer, F. W. (2020) Intact vitamin A transport is critical for cold-mediated adipose tissue browning and thermogenesis. *Mol Metab* **42**, 101088
103. Mercader, J., Ribot, J., Murano, I., Felipe, F., Cinti, S., Bonet, M. L., and Palou, A. (2006) Remodeling of white adipose tissue after retinoic acid administration in mice. *Endocrinology* **147**, 5325-5332
104. Puigserver, P., Vázquez, F., Bonet, M. L., Picó, C., and Palou, A. (1996) In vitro and in vivo induction of brown adipocyte uncoupling protein (thermogenin) by retinoic acid. *Biochem J* **317** (Pt 3), 827-833

105. Kumar, M. V., and Scarpace, P. J. (1998) Differential effects of retinoic acid on uncoupling protein-1 and leptin gene expression. *J Endocrinol* **157**, 237-243
106. Murholm, M., Isidor, M. S., Basse, A. L., Winther, S., Sørensen, C., Skovgaard-Petersen, J., Nielsen, M. M., Hansen, A. S., Quistorff, B., and Hansen, J. B. (2013) Retinoic acid has different effects on UCP1 expression in mouse and human adipocytes. *BMC Cell Biol* **14**, 41
107. Allenby, G., Bocquel, M. T., Saunders, M., Kazmer, S., Speck, J., Rosenberger, M., Lovey, A., Kastner, P., Grippo, J. F., Chambon, P., and et al. (1993) Retinoic acid receptors and retinoid X receptors: interactions with endogenous retinoic acids. *Proc Natl Acad Sci U S A* **90**, 30-34
108. Alvarez, R., de Andrés, J., Yubero, P., Viñas, O., Mampel, T., Iglesias, R., Giralt, M., and Villarroya, F. (1995) A novel regulatory pathway of brown fat thermogenesis. Retinoic acid is a transcriptional activator of the mitochondrial uncoupling protein gene. *J Biol Chem* **270**, 5666-5673
109. Bonet, M. L., Puigserver, P., Serra, F., Ribot, J., Vázquez, F., Pico, C., and Palou, A. (1997) Retinoic acid modulates retinoid X receptor alpha and retinoic acid receptor alpha levels of cultured brown adipocytes. *FEBS Lett* **406**, 196-200
110. Alvarez, R., Checa, M., Brun, S., Viñas, O., Mampel, T., Iglesias, R., Giralt, M., and Villarroya, F. (2000) Both retinoic-acid-receptor- and retinoid-X-receptor-dependent signalling pathways mediate the induction of the brown-adipose-tissue-uncoupling-protein-1 gene by retinoids. *Biochem J* **345 Pt 1**, 91-97
111. Ribot, J., Felipe, F., Bonet, M. L., and Palou, A. (2004) Retinoic acid administration and vitamin A status modulate retinoid X receptor alpha and retinoic acid receptor alpha levels in mouse brown adipose tissue. *Mol Cell Biochem* **266**, 25-30
112. Rial, E., González-Barroso, M., Fleury, C., Iturrizaga, S., Sanchis, D., Jiménez-Jiménez, J., Ricquier, D., Goubert, M., and Bouillaud, F. (1999) Retinoids activate proton transport by the uncoupling proteins UCP1 and UCP2. *Embo j* **18**, 5827-5833
113. Klingenberg, M., and Huang, S. G. (1999) Structure and function of the uncoupling protein from brown adipose tissue. *Biochim Biophys Acta* **1415**, 271-296
114. Tomás, P., Jiménez-Jiménez, J., Zaragoza, P., Vuligonda, V., Chandraratna, R. A., and Rial, E. (2004) Activation by retinoids of the uncoupling protein UCP1. *Biochim Biophys Acta* **1658**, 157-164
115. Suzuki, M., Chen, H. J., Tomonaga, S., Hashimoto, O., Kawada, T., Matsui, T., and Funaba, M. (2019) Chronic retinoic acid treatment induces differentiation and changes in the metabolite levels of brown (pre)adipocytes. *Cell Biochem Funct* **37**, 377-384

116. Teruel, T., Hernandez, R., Benito, M., and Lorenzo, M. (2003) Rosiglitazone and retinoic acid induce uncoupling protein-1 (UCP-1) in a p38 mitogen-activated protein kinase-dependent manner in fetal primary brown adipocytes. *J Biol Chem* **278**, 263-269
117. Bartelt, A., and Heeren, J. (2014) Adipose tissue browning and metabolic health. *Nat Rev Endocrinol* **10**, 24-36
118. Ziqubu, K., Dlodla, P. V., Mthembu, S. X. H., Nkambule, B. B., Mabhida, S. E., Jack, B. U., Nyambuya, T. M., and Mazibuko-Mbeje, S. E. (2023) An insight into brown/beige adipose tissue whitening, a metabolic complication of obesity with the multifactorial origin. *Front Endocrinol (Lausanne)* **14**, 1114767
119. Au-Yong, I. T., Thorn, N., Ganatra, R., Perkins, A. C., and Symonds, M. E. (2009) Brown adipose tissue and seasonal variation in humans. *Diabetes* **58**, 2583-2587
120. Yoneshiro, T., Matsushita, M., Nakae, S., Kameya, T., Sugie, H., Tanaka, S., and Saito, M. (2016) Brown adipose tissue is involved in the seasonal variation of cold-induced thermogenesis in humans. *Am J Physiol Regul Integr Comp Physiol* **310**, R999-r1009
121. Yoneshiro, T., Aita, S., Matsushita, M., Okamatsu-Ogura, Y., Kameya, T., Kawai, Y., Miyagawa, M., Tsujisaki, M., and Saito, M. (2011) Age-related decrease in cold-activated brown adipose tissue and accumulation of body fat in healthy humans. *Obesity (Silver Spring)* **19**, 1755-1760
122. Pfannenberg, C., Werner, M. K., Ripkens, S., Stef, I., Deckert, A., Schmadl, M., Reimold, M., Häring, H. U., Claussen, C. D., and Stefan, N. (2010) Impact of age on the relationships of brown adipose tissue with sex and adiposity in humans. *Diabetes* **59**, 1789-1793
123. Leitner, B. P., Huang, S., Brychta, R. J., Duckworth, C. J., Baskin, A. S., McGehee, S., Tal, I., Dieckmann, W., Gupta, G., Kolodny, G. M., Pacak, K., Herscovitch, P., Cypess, A. M., and Chen, K. Y. (2017) Mapping of human brown adipose tissue in lean and obese young men. *Proc Natl Acad Sci U S A* **114**, 8649-8654
124. Ouellet, V., Routhier-Labadie, A., Bellemare, W., Lakhil-Chaieb, L., Turcotte, E., Carpentier, A. C., and Richard, D. (2011) Outdoor temperature, age, sex, body mass index, and diabetic status determine the prevalence, mass, and glucose-uptake activity of 18F-FDG-detected BAT in humans. *J Clin Endocrinol Metab* **96**, 192-199
125. Lee, P., Greenfield, J. R., Ho, K. K., and Fulham, M. J. (2010) A critical appraisal of the prevalence and metabolic significance of brown adipose tissue in adult humans. *Am J Physiol Endocrinol Metab* **299**, E601-606

126. Heymsfield, S. B., and Wadden, T. A. (2017) Mechanisms, Pathophysiology, and Management of Obesity. *N Engl J Med* **376**, 254-266
127. Lee, P., Swarbrick, M. M., and Ho, K. K. (2013) Brown adipose tissue in adult humans: a metabolic renaissance. *Endocr Rev* **34**, 413-438
128. Vijgen, G. H., Bouvy, N. D., Teule, G. J., Brans, B., Hoeks, J., Schrauwen, P., and van Marken Lichtenbelt, W. D. (2012) Increase in brown adipose tissue activity after weight loss in morbidly obese subjects. *J Clin Endocrinol Metab* **97**, E1229-1233
129. van der Lans, A. A., Hoeks, J., Brans, B., Vijgen, G. H., Visser, M. G., Vosselman, M. J., Hansen, J., Jörgensen, J. A., Wu, J., Mottaghy, F. M., Schrauwen, P., and van Marken Lichtenbelt, W. D. (2013) Cold acclimation recruits human brown fat and increases nonshivering thermogenesis. *J Clin Invest* **123**, 3395-3403
130. Liu, X., Wang, S., You, Y., Meng, M., Zheng, Z., Dong, M., Lin, J., Zhao, Q., Zhang, C., Yuan, X., Hu, T., Liu, L., Huang, Y., Zhang, L., Wang, D., Zhan, J., Jong Lee, H., Speakman, J. R., and Jin, W. (2015) Brown Adipose Tissue Transplantation Reverses Obesity in Ob/Ob Mice. *Endocrinology* **156**, 2461-2469
131. Liu, X., Zheng, Z., Zhu, X., Meng, M., Li, L., Shen, Y., Chi, Q., Wang, D., Zhang, Z., Li, C., Li, Y., Xue, Y., Speakman, J. R., and Jin, W. (2013) Brown adipose tissue transplantation improves whole-body energy metabolism. *Cell Res* **23**, 851-854
132. Zhu, Z., Spicer, E. G., Gavini, C. K., Goudjo-Ako, A. J., Novak, C. M., and Shi, H. (2014) Enhanced sympathetic activity in mice with brown adipose tissue transplantation (transBATation). *Physiol Behav* **125**, 21-29
133. Gloyn, A. L., and Drucker, D. J. (2018) Precision medicine in the management of type 2 diabetes. *Lancet Diabetes Endocrinol* **6**, 891-900
134. Chondronikola, M., Volpi, E., Børsheim, E., Porter, C., Annamalai, P., Enerbäck, S., Lidell, M. E., Saraf, M. K., Labbe, S. M., Hurren, N. M., Yfanti, C., Chao, T., Andersen, C. R., Cesani, F., Hawkins, H., and Sidossis, L. S. (2014) Brown adipose tissue improves whole-body glucose homeostasis and insulin sensitivity in humans. *Diabetes* **63**, 4089-4099
135. Orava, J., Nuutila, P., Lidell, M. E., Oikonen, V., Nojonen, T., Viljanen, T., Scheinin, M., Taittonen, M., Niemi, T., Enerbäck, S., and Virtanen, K. A. (2011) Different metabolic responses of human brown adipose tissue to activation by cold and insulin. *Cell Metab* **14**, 272-279
136. Hanssen, M. J., Hoeks, J., Brans, B., van der Lans, A. A., Schaart, G., van den Driessche, J. J., Jörgensen, J. A., Boekschoten, M. V., Hesselink, M. K., Havekes, B., Kersten, S., Mottaghy, F. M., van Marken Lichtenbelt, W. D., and Schrauwen, P.

- (2015) Short-term cold acclimation improves insulin sensitivity in patients with type 2 diabetes mellitus. *Nat Med* **21**, 863-865
137. Wang, Z., Ning, T., Song, A., Rutter, J., Wang, Q. A., and Jiang, L. (2020) Chronic cold exposure enhances glucose oxidation in brown adipose tissue. *EMBO Rep* **21**, e50085
138. Stanford, K. I., Middelbeek, R. J., Townsend, K. L., An, D., Nygaard, E. B., Hitchcox, K. M., Markan, K. R., Nakano, K., Hirshman, M. F., Tseng, Y. H., and Goodyear, L. J. (2013) Brown adipose tissue regulates glucose homeostasis and insulin sensitivity. *J Clin Invest* **123**, 215-223
139. Olsen, J. M., Sato, M., Dallner, O. S., Sandström, A. L., Pisani, D. F., Chambard, J. C., Amri, E. Z., Hutchinson, D. S., and Bengtsson, T. (2014) Glucose uptake in brown fat cells is dependent on mTOR complex 2-promoted GLUT1 translocation. *J Cell Biol* **207**, 365-374
140. Heidenreich, S., Witte, N., Weber, P., Goehring, I., Tolkachov, A., von Loeffelholz, C., Döcke, S., Bauer, M., Stockmann, M., Pfeiffer, A. F. H., Birkenfeld, A. L., Pietzke, M., Kempa, S., Muenzner, M., and Schupp, M. (2017) Retinol saturase coordinates liver metabolism by regulating ChREBP activity. *Nat Commun* **8**, 384
141. Harms, M. J., Ishibashi, J., Wang, W., Lim, H. W., Goyama, S., Sato, T., Kurokawa, M., Won, K. J., and Seale, P. (2014) Prdm16 is required for the maintenance of brown adipocyte identity and function in adult mice. *Cell Metab* **19**, 593-604
142. Green, H., and Meuth, M. (1974) An established pre-adipose cell line and its differentiation in culture. *Cell* **3**, 127-133
143. Prokesch, A., Pelzmann, H. J., Pessentheiner, A. R., Huber, K., Madreiter-Sokolowski, C. T., Drougard, A., Schittmayer, M., Kolb, D., Magnes, C., Trausinger, G., Graier, W. F., Birner-Gruenberger, R., Pospisilik, J. A., and Bogner-Strauss, J. G. (2016) N-acetylaspartate catabolism determines cytosolic acetyl-CoA levels and histone acetylation in brown adipocytes. *Sci Rep* **6**, 23723
144. Schupp, M., Janke, J., Clasen, R., Unger, T., and Kintscher, U. (2004) Angiotensin type 1 receptor blockers induce peroxisome proliferator-activated receptor-gamma activity. *Circulation* **109**, 2054-2057
145. Nguyen, A., Guo, J., Banyard, D. A., Fadavi, D., Toranto, J. D., Wirth, G. A., Paydar, K. Z., Evans, G. R., and Widgerow, A. D. (2016) Stromal vascular fraction: A regenerative reality? Part 1: Current concepts and review of the literature. *J Plast Reconstr Aesthet Surg* **69**, 170-179
146. Kim, T. K., and Eberwine, J. H. (2010) Mammalian cell transfection: the

- present and the future. *Anal Bioanal Chem* **397**, 3173-3178
147. Milhavet, O., Gary, D. S., and Mattson, M. P. (2003) RNA interference in biology and medicine. *Pharmacol Rev* **55**, 629-648
148. Manoharan, M. (2004) RNA interference and chemically modified small interfering RNAs. *Curr Opin Chem Biol* **8**, 570-579
149. Gehl, J. (2003) Electroporation: theory and methods, perspectives for drug delivery, gene therapy and research. *Acta Physiol Scand* **177**, 437-447
150. Wasungu, L., and Hoekstra, D. (2006) Cationic lipids, lipoplexes and intracellular delivery of genes. *J Control Release* **116**, 255-264
151. Isidor, M. S., Winther, S., Basse, A. L., Petersen, M. C., Cannon, B., Nedergaard, J., and Hansen, J. B. (2016) An siRNA-based method for efficient silencing of gene expression in mature brown adipocytes. *Adipocyte* **5**, 175-185
152. Bulcha, J. T., Wang, Y., Ma, H., Tai, P. W. L., and Gao, G. (2021) Viral vector platforms within the gene therapy landscape. *Signal Transduct Target Ther* **6**, 53
153. Cepko, C., and Pear, W. (2001) Overview of the retrovirus transduction system. *Curr Protoc Mol Biol* **Chapter 9**, Unit9.9
154. Van Duyne, G. D. (2015) Cre Recombinase. *Microbiol Spectr* **3**, Mdna3-0014-2014
155. de Martin, R., Raidl, M., Hofer, E., and Binder, B. R. (1997) Adenovirus-mediated expression of green fluorescent protein. *Gene Ther* **4**, 493-495
156. Orlicky, D. J., and Schaack, J. (2001) Adenovirus transduction of 3T3-L1 cells. *J Lipid Res* **42**, 460-466
157. Kraus, N. A., Ehebauer, F., Zapp, B., Rudolphi, B., Kraus, B. J., and Kraus, D. (2016) Quantitative assessment of adipocyte differentiation in cell culture. *Adipocyte* **5**, 351-358
158. Wu, M., Neilson, A., Swift, A. L., Moran, R., Tamagnine, J., Parslow, D., Armistead, S., Lemire, K., Orrell, J., Teich, J., Chomicz, S., and Ferrick, D. A. (2007) Multiparameter metabolic analysis reveals a close link between attenuated mitochondrial bioenergetic function and enhanced glycolysis dependency in human tumor cells. *Am J Physiol Cell Physiol* **292**, C125-136
159. Gohlke, S., Zagoriy, V., Cuadros Inostroza, A., Méret, M., Mancini, C., Japtok, L., Schumacher, F., Kuhlmann, D., Graja, A., Stephanowitz, H., Jähnert, M., Krause, E., Wernitz, A., Petzke, K. J., Schürmann, A., Kleuser, B., and Schulz, T. J. (2019) Identification of functional lipid metabolism biomarkers of brown adipose tissue aging. *Mol Metab* **24**, 1-17

160. Kong, X., Banks, A., Liu, T., Kazak, L., Rao, R. R., Cohen, P., Wang, X., Yu, S., Lo, J. C., Tseng, Y. H., Cypess, A. M., Xue, R., Kleiner, S., Kang, S., Spiegelman, B. M., and Rosen, E. D. (2014) IRF4 is a key thermogenic transcriptional partner of PGC-1 α . *Cell* **158**, 69-83
161. Schneider, C. A., Rasband, W. S., and Eliceiri, K. W. (2012) NIH Image to ImageJ: 25 years of image analysis. *Nat Methods* **9**, 671-675
162. Dennis, G., Jr., Sherman, B. T., Hosack, D. A., Yang, J., Gao, W., Lane, H. C., and Lempicki, R. A. (2003) DAVID: Database for Annotation, Visualization, and Integrated Discovery. *Genome Biol* **4**, P3
163. Barrett, T., Wilhite, S. E., Ledoux, P., Evangelista, C., Kim, I. F., Tomashevsky, M., Marshall, K. A., Phillippy, K. H., Sherman, P. M., Holko, M., Yefanov, A., Lee, H., Zhang, N., Robertson, C. L., Serova, N., Davis, S., and Soboleva, A. (2013) NCBI GEO: archive for functional genomics data sets--update. *Nucleic Acids Res* **41**, D991-995
164. Maurer, S. F., Fromme, T., Grossman, L. I., Hüttemann, M., and Klingenspor, M. (2015) The brown and brite adipocyte marker Cox7a1 is not required for non-shivering thermogenesis in mice. *Sci Rep* **5**, 17704
165. Xue, R., Lynes, M. D., Dreyfuss, J. M., Shamsi, F., Schulz, T. J., Zhang, H., Huang, T. L., Townsend, K. L., Li, Y., Takahashi, H., Weiner, L. S., White, A. P., Lynes, M. S., Rubin, L. L., Goodyear, L. J., Cypess, A. M., and Tseng, Y. H. (2015) Clonal analyses and gene profiling identify genetic biomarkers of the thermogenic potential of human brown and white preadipocytes. *Nat Med* **21**, 760-768
166. Harms, M., and Seale, P. (2013) Brown and beige fat: development, function and therapeutic potential. *Nat Med* **19**, 1252-1263
167. Yoneshiro, T., Aita, S., Matsushita, M., Kayahara, T., Kameya, T., Kawai, Y., Iwanaga, T., and Saito, M. (2013) Recruited brown adipose tissue as an antiobesity agent in humans. *J Clin Invest* **123**, 3404-3408
168. Hao, L., Scott, S., Abbasi, M., Zu, Y., Khan, M. S. H., Yang, Y., Wu, D., Zhao, L., and Wang, S. (2019) Beneficial Metabolic Effects of Mirabegron In Vitro and in High-Fat Diet-Induced Obese Mice. *J Pharmacol Exp Ther* **369**, 419-427
169. Li, Y., and Fromme, T. (2022) Uncoupling Protein 1 Does Not Produce Heat without Activation. *Int J Mol Sci* **23**
170. Merlin, J., Sato, M., Chia, L. Y., Fahey, R., Pakzad, M., Nowell, C. J., Summers, R. J., Bengtsson, T., Evans, B. A., and Hutchinson, D. S. (2018) Rosiglitazone and a $\beta(3)$ -Adrenoceptor Agonist Are Both Required for Functional Browning of White Adipocytes in Culture. *Front Endocrinol (Lausanne)* **9**, 249

171. Lasar, D., Rosenwald, M., Kiehlmann, E., Balaz, M., Tall, B., Opitz, L., Lidell, M. E., Zamboni, N., Krznar, P., Sun, W., Varga, L., Stefanicka, P., Ukropec, J., Nuutila, P., Virtanen, K., Amri, E. Z., Enerbäck, S., Wahli, W., and Wolfrum, C. (2018) Peroxisome Proliferator Activated Receptor Gamma Controls Mature Brown Adipocyte Inducibility through Glycerol Kinase. *Cell Rep* **22**, 760-773
172. Cannon, B., and Nedergaard, J. (2004) Brown adipose tissue: function and physiological significance. *Physiol Rev* **84**, 277-359
173. Kadenbach, B., and Hüttemann, M. (2015) The subunit composition and function of mammalian cytochrome c oxidase. *Mitochondrion* **24**, 64-76
174. Okita, N., Hayashida, Y., Kojima, Y., Fukushima, M., Yuguchi, K., Mikami, K., Yamauchi, A., Watanabe, K., Noguchi, M., Nakamura, M., Toda, T., and Higami, Y. (2012) Differential responses of white adipose tissue and brown adipose tissue to caloric restriction in rats. *Mech Ageing Dev* **133**, 255-266
175. Boutant, M., Kulkarni, S. S., Joffraud, M., Raymond, F., Métaïron, S., Descombes, P., and Cantó, C. (2016) SIRT1 Gain of Function Does Not Mimic or Enhance the Adaptations to Intermittent Fasting. *Cell Rep* **14**, 2068-2075
176. Viswakarma, N., Yu, S., Naik, S., Kashireddy, P., Matsumoto, K., Sarkar, J., Surapureddi, S., Jia, Y., Rao, M. S., and Reddy, J. K. (2007) Transcriptional regulation of Cidea, mitochondrial cell death-inducing DNA fragmentation factor alpha-like effector A, in mouse liver by peroxisome proliferator-activated receptor alpha and gamma. *J Biol Chem* **282**, 18613-18624
177. Jash, S., Banerjee, S., Lee, M. J., Farmer, S. R., and Puri, V. (2019) CIDEA Transcriptionally Regulates UCP1 for Britening and Thermogenesis in Human Fat Cells. *iScience* **20**, 73-89
178. Park, P. J., Kong, S. W., Tebaldi, T., Lai, W. R., Kasif, S., and Kohane, I. S. (2009) Integration of heterogeneous expression data sets extends the role of the retinol pathway in diabetes and insulin resistance. *Bioinformatics* **25**, 3121-3127
179. DeFronzo, R. A., Gunnarsson, R., Björkman, O., Olsson, M., and Wahren, J. (1985) Effects of insulin on peripheral and splanchnic glucose metabolism in noninsulin-dependent (type II) diabetes mellitus. *J Clin Invest* **76**, 149-155
180. Lee, P., Bova, R., Schofield, L., Bryant, W., Dieckmann, W., Slattery, A., Govendir, M. A., Emmett, L., and Greenfield, J. R. (2016) Brown Adipose Tissue Exhibits a Glucose-Responsive Thermogenic Biorhythm in Humans. *Cell Metab* **23**, 602-609
181. Mäkinen, T. M. (2007) Human cold exposure, adaptation, and performance in

- high latitude environments. *Am J Hum Biol* **19**, 155-164
182. Himms-Hagen, J. (1984) Nonshivering thermogenesis. *Brain Res Bull* **12**, 151-160
183. Bartness, T. J., Vaughan, C. H., and Song, C. K. (2010) Sympathetic and sensory innervation of brown adipose tissue. *Int J Obes (Lond)* **34 Suppl 1**, S36-42
184. Ryu, V., Garretson, J. T., Liu, Y., Vaughan, C. H., and Bartness, T. J. (2015) Brown adipose tissue has sympathetic-sensory feedback circuits. *J Neurosci* **35**, 2181-2190
185. Schreiber, R., Diwoky, C., Schoiswohl, G., Feiler, U., Wongsiriroj, N., Abdellatif, M., Kolb, D., Hoeks, J., Kershaw, E. E., Sedej, S., Schrauwen, P., Haemmerle, G., and Zechner, R. (2017) Cold-Induced Thermogenesis Depends on ATGL-Mediated Lipolysis in Cardiac Muscle, but Not Brown Adipose Tissue. *Cell Metab* **26**, 753-763.e757
186. Blondin, D. P., and Haman, F. (2018) Shivering and nonshivering thermogenesis in skeletal muscles. *Handb Clin Neurol* **156**, 153-173
187. Janovska, P., Zouhar, P., Bardova, K., Otahal, J., Vrbacky, M., Mracek, T., Adamcova, K., Lenkova, L., Funda, J., Cajka, T., Drahota, Z., Stanic, S., Rustan, A. C., Horakova, O., Houstek, J., Rossmeisl, M., and Kopecky, J. (2023) Impairment of adrenergically-regulated thermogenesis in brown fat of obesity-resistant mice is compensated by non-shivering thermogenesis in skeletal muscle. *Mol Metab* **69**, 101683
188. Crane, J. D., Mottillo, E. P., Farncombe, T. H., Morrison, K. M., and Steinberg, G. R. (2014) A standardized infrared imaging technique that specifically detects UCP1-mediated thermogenesis in vivo. *Mol Metab* **3**, 490-494
189. Basu, U., Bostwick, A. M., Das, K., Dittenhafer-Reed, K. E., and Patel, S. S. (2020) Structure, mechanism, and regulation of mitochondrial DNA transcription initiation. *J Biol Chem* **295**, 18406-18425
190. Boore, J. L. (1999) Animal mitochondrial genomes. *Nucleic Acids Res* **27**, 1767-1780
191. Zhang, F., and Broughton, R. E. (2013) Mitochondrial-nuclear interactions: compensatory evolution or variable functional constraint among vertebrate oxidative phosphorylation genes? *Genome Biol Evol* **5**, 1781-1791
192. Bize, P., Lowe, I., Lehto Hürlimann, M., and Heckel, G. (2018) Effects of the Mitochondrial and Nuclear Genomes on Nonshivering Thermogenesis in a Wild Derived Rodent. *Integr Comp Biol* **58**, 532-543

193. Zhou, Z., Torres, M., Sha, H., Halbrook, C. J., Van den Bergh, F., Reinert, R. B., Yamada, T., Wang, S., Luo, Y., Hunter, A. H., Wang, C., Sanderson, T. H., Liu, M., Taylor, A., Sesaki, H., Lyssiotis, C. A., Wu, J., Kersten, S., Beard, D. A., and Qi, L. (2020) Endoplasmic reticulum-associated degradation regulates mitochondrial dynamics in brown adipocytes. *Science* **368**, 54-60
194. Asada, R., Kanemoto, S., Matsuhisa, K., Hino, K., Cui, M., Cui, X., Kaneko, M., and Imaizumi, K. (2015) IRE1 α -XBP1 is a novel branch in the transcriptional regulation of Ucp1 in brown adipocytes. *Sci Rep* **5**, 16580
195. Yuliana, A., Daijo, A., Jheng, H. F., Kwon, J., Nomura, W., Takahashi, H., Ara, T., Kawada, T., and Goto, T. (2019) Endoplasmic Reticulum Stress Impaired Uncoupling Protein 1 Expression via the Suppression of Peroxisome Proliferator-Activated Receptor γ Binding Activity in Mice Beige Adipocytes. *Int J Mol Sci* **20**

List of Figures

Figure 1. RetSat catalyzed saturation reaction of 13, 14 double bond of all- <i>trans</i> retinol.....	8
Figure 2. Regulation of RetSat expression and effect of RetSat in adipocytes....	9
Figure 3. The morphology comparison of brown adipocyte, beige adipocyte, and white adipocyte.	12
Figure 4. UCP1-mediated uncoupling in mitochondria of brown adipocytes.....	16
Figure 5. Pharmacological approaches to activate brown adipocytes and induce white adipocytes browning.	18
Figure 6. Preadipocyte differentiation process.....	37
Figure 7. Seahorse mitochondria stress test profile.....	42
Figure 8. Cre-induced recombination of floxed allele.....	43
Figure 9. Experimental scheme for establishing RetSat flox/flox UCP1 Cre mice.	44
Figure 10. RetSat is highly expressed in brown adipose tissue.	54
Figure 11. RetSat is induced by β -adrenergic stimulation.	55
Figure 12. RetSat is up-regulated during differentiation of brown adipocytes....	56
Figure 13. RetSat depletion does not impair brown adipocyte differentiation. ...	57
Figure 14. RetSat over-expression slightly enhances brown adipocyte differentiation.	59
Figure 15. RetSat is required for thermogenic gene expression in immortalized brown adipocytes.	60
Figure 16. RetSat is required for thermogenic gene expression in primary brown adipocytes.....	62
Figure 17. RetSat ablation reduces mitochondrial respiration in primary brown adipocytes.....	63
Figure 18. RetSat is required for browning of 3T3-L1 adipocytes.	64
Figure 19. RetSat depletion reduces mitochondrial respiration in 3T3-L1 adipocytes.....	65
Figure 20. BAT-specific RetSat deletion mouse model construction and validation.	66
Figure 21. RetSat deletion in brown adipose tissue of mice impairs acute cold tolerance.	67
Figure 22. BAT-specific RetSat knockout mice maintained adiposity upon HFD.	68

Figure 23. BAT-specific RetSat knockout slightly impaired glucose disposal capacity of mice upon HFD. 69

Figure 24. RetSat deletion in BAT downregulates mitochondrially encoded and protein-folding associated genes..... 71

List of Tables

Table 1. Comparison of features among classical brown, white, and beige adipocytes.....	12
Table 2. Chemicals and reagents	23
Table 3. Kits	29
Table 4. Primary antibodies for immunoblotting	29
Table 5. Secondary antibodies for immunoblotting	30
Table 6. Primers for real-time quantitative polymerase chain reaction	30
Table 7. siRNA oligonucleotides sequences	31
Table 8. Primers for mouse genotyping	32
Table 9. List of Mouse diet.....	32
Table 10. Main equipments.....	33
Table 11. Consumables	33
Table 12. Growth media composition.....	36
Table 13. Maintenance media composition.....	36
Table 14. Induction media composition.....	36
Table 15. Mitochondria stress test stepped commands	40
Table 16. PCR mastermix.....	45
Table 17. PCR program.....	45
Table 18. Reverse transcriptase master mix.....	49
Table 19. RT-qPCR master mix	49
Table 20. RT-qPCR program	50
Table 21. Sodium Dodecyl Sulfate-Polyacrylamide 1.5 mm thick gel composition	51
Table 22. DNase I reaction mix.....	53

Acknowledgement

Thanks to my supervisor Prof. Dr. Michael Schupp (Charité - Universitätsmedizin Berlin) for his guidance and patience in this project, especially the latter is much more important to me.

Thanks to Prof. Dr. Nan Ma (Free University of Berlin & Helmholtz-Zentrum Hereon) for help in enrollment and encouragement during project.

Thanks to my colleague Manuela Sommerfeld for help in the histology work, Roberto E. Flores for guidance in Seahorse assay, and Dr. Sylvia J. Wowro for application of primary cells experiment.

Thanks to Prof. Dr. Tim J. Schulz (German Institute of Human Nutrition Potsdam-Rehbrücke) and his group members Dr. Sabrina Gohlke and Anneke Johanna Heida for the help in cold exposure assay.

Thanks to Prof. Dr. Holger Scholz (Charité - Universitätsmedizin Berlin) for guidance in SVF isolation.

Thanks to hundreds of adult and newborn mice, which contributed data to *in vivo* and primary adipocyte studies.

Thanks to the supports from my parents.